MULTIPLE-PROXY RECORDS OF DELTA EVOLUTION AND DISPERSAL SYSTEM BEHAVIOR: FLUVIAL AND COASTAL BOREHOLE EVIDENCE FROM THE BENGAL BASIN, BANGLADESH

By

Russell David Pate

Thesis

Submitted to the Faculty of the

Graduate School of Vanderbilt University

in partial fulfillment of the requirements

for the degree of

MASTER OF SCIENCE

in

Earth and Environmental Sciences

December, 2008

Nashville, Tennessee

Approved:

Professor Steven L. Goodbred Jr.

Professor David J. Furbish

Professor Kaye S. Savage

CONTENTS

LIST OF TABLES

LIST OF FIGURES

ACKNOWLEDGMENT

I would like to extend sincere thanks to my advisor, Steve Goodbred, for his continued support throughout my graduate career. I have greatly appreciated Steve's enthusiasm and thoughtful insight during the thesis process. He has been a fundamental contributor to my research and has graciously provided me the freedom to pursue my own ideas. Without Steve, I would not have had the opportunity to experience the amazing people and culture of Bangladesh. I would also like to thank my committee and the rest of the Earth and Environmental Sciences faculty at Vanderbilt University for their invaluable insight and guidance during my brief two years in the department. I would like to extend a special thanks to Mike Ramirez for his positive presence and hours of lab work that were critical to this study. I would also like to thank Dr. Warner Cribb for his patience and assistance with XRF analyses at Middle Tennessee State University.

I would also like to thank the faculty of Geology and Geophysics at the University of Missouri-Rolla for helping me to develop a solid background in geology and providing me with multiple opportunites to travel the world and experience new things. Finally, I wish to thank my parents, without whom my success would not be possible. They have always encouraged me to pursue my passion and offer their unconditional love and support.

CHAPTER I

INTRODUCTION

I.1 Introduction

The tectonically active Ganges-Brahmaputra (G-B) delta system is responsible for the highest sediment discharge to the global ocean of any of the world's river systems (Milliman and Syvitski, 1992). It was not until recently that subaerial and submarine delta processes were linked in a systems-view interpretation of Late Quaternary delta development. Several studies have described the volume and distribution of sediment flux during key stages of delta development, (ie: Kuehl et al., 1989; Weber et al., 1997b; Goodbred and Kuehl, 1999, 2000a) and several studies have discussed preliminary concepts of delta stratigraphy and evolution (ie: Goodbred and Kuehl, 2000b; Goodbred et al., 2003; Heroy et al., 2003; Allison et al., 2003). Much work remains to further unravel processes and mechanisms responsible for the depositional history of the G-B margin in relation to river position, sediment flux, and sediment provenance.

I present detailed stratigraphic, paleoenvironmental, and provenance data for two deep boreholes from the Bengal Basin using a multiple-proxy approach to better understand critical processes and mechanisms responsible for Late Quaternary G-B delta evolution. In addition to a traditional stratigraphic and facies approach, I use down-core trends in sediment geochemistry and magnetic susceptibility to further develop paleoenvironmental and provenance interpretations. This study is a part of

an overarching effort to determine how changing source areas, weathering patterns, and delivery of sediment have influenced development of the Bengal Basin under the control of shifting monsoon regimes.

The country of Bangladesh is situated within the G-B delta system and is one of the most densely populated regions of the world. The majority of land is at or slightly above sea-level, and the population is exposed to frequent flooding and unpredictable land loss and gain. Modern climate change and sea-level rise have the potential to significantly alter delta dynamics, therefore it is critical to understand prior response of the delta system during changes in climate, global sea-level, and sediment flux throughout the Late Quaternary.

I.2 Study Area

The G-B delta system is fed by the Ganges and Brahmaputra rivers and represents the world's largest subaerial delta system, with a surface area of over 100,000 km^2 comprised of riverine channel, floodplain, and delta-plain environments (Goodbred et al., 2003). The modern delta extends offshore 125 km across the continental shelf as a prograding clinoform and stretches 250 km along shelf from the eastern coast of Bangladesh to the "Swatch of No Ground" submarine canyon. The total combined area of the subaerial and submarine delta is approximately 140,000 km^2 (Kuehl et al., 2005).

The G-B delta has several significant differences from other large delta systems of the world (Goodbred and Kuehl, 1999, 2000b), including:

- Initial development of the G-B delta began 2,000-3,000 years earlier than most of the world's delta systems,
- relative shoreline stability during rapid early Holocene sea-level rise,
- trapping of a significant portion of the sediment load to inland tectonic basins.

Recent studies of the G-B delta system suggest that tectonics, sediment supply, and sea-level have contributed roughly equably to Late Quaternary margin and delta development (Goodbred and Kuehl, 2000a,b; Goodbred et al., 2003). Long-term variability of the regional climate system, driven by the South Asian monsoon, is a critical overarching control on delta development. The major controls acting on the G-B delta system are intimately linked and respond to local, regional, and global processes.

I.2.1 Tectonic Setting

The G-B delta system lies within the tectonically active setting of the South Asian continental collision. In addition to external tectonic forcing, locally active basin-scale processes contribute to delta development including overthrusting, compression, strike-slip, and normal faulting. The Bengal Basin formed seaward of the subsiding Himalayan Foredeep following the onset of the Asian-Indian plate collision beginning in the Eocene (Figure I.1). The Bengal Basin is a classic tectonically active trailing-edge margin that exhibits regional subsidence and uplift patterns that reflect underlying structural troughs and active faults (Allison et al., 2003). The Precambrian Shillong Massif and Indian Shield bound the basin to the north and

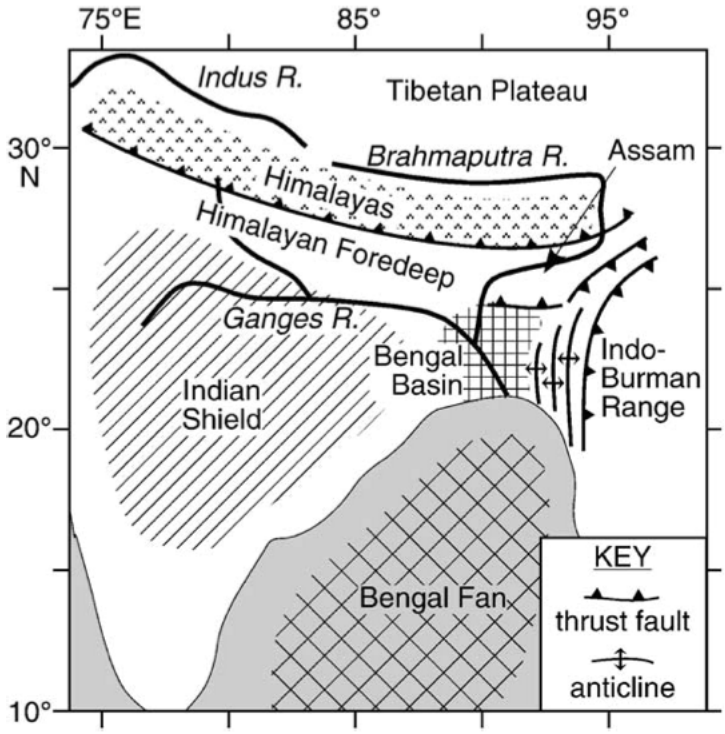

Figure I.1: Tectono-sedimentary map of the Indo-Asian collision. The Bengal Basin is the primary depocenter for the Ganges and Brahmaputra rivers and is situated along a tectonically active trailing-edge margin bounded by the Indian craton, Himalayan foredeep, and Indo-Burman fold belt (from Goodbred, 2003).

west, and the Neogene Tripura Fold Belt in the Burmese highlands bounds the basin to the east (Figure I.2).

The Bengal Basin is partitioned into several sub-basins isolated by uplifted Pleistocene alluvial deposits, the Madhupur Terrace and Barind Tract, and neotectonic uplift on the Comilla Terrace (Figure I.3) (Goodbred and Kuehl, 2000b). Uplifted regions are, in part, responsible for controlling channel migration and course avulsion over historic and geologic timescales. Channel avulsions for the Brahmaputra, and the smaller Tista, river have been documented on historical timescales as recently as 200 yr B.P (Fergusson, 1863).

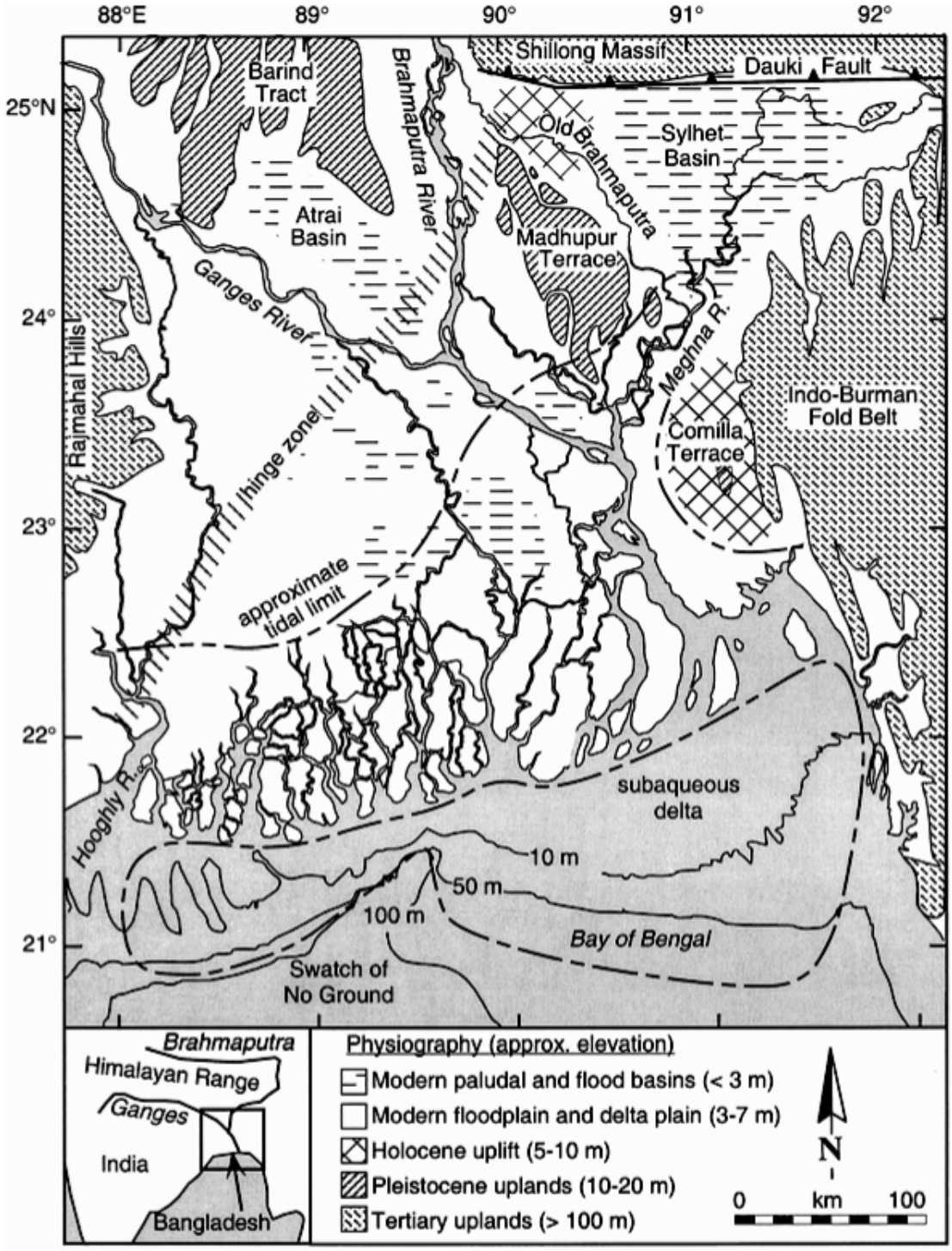

Figure I.2: Regional map of the Bengal Basin showing the physiography and geology of the Ganges-Brahmaputra delta and surrounding area (from Goodbred, 2003).

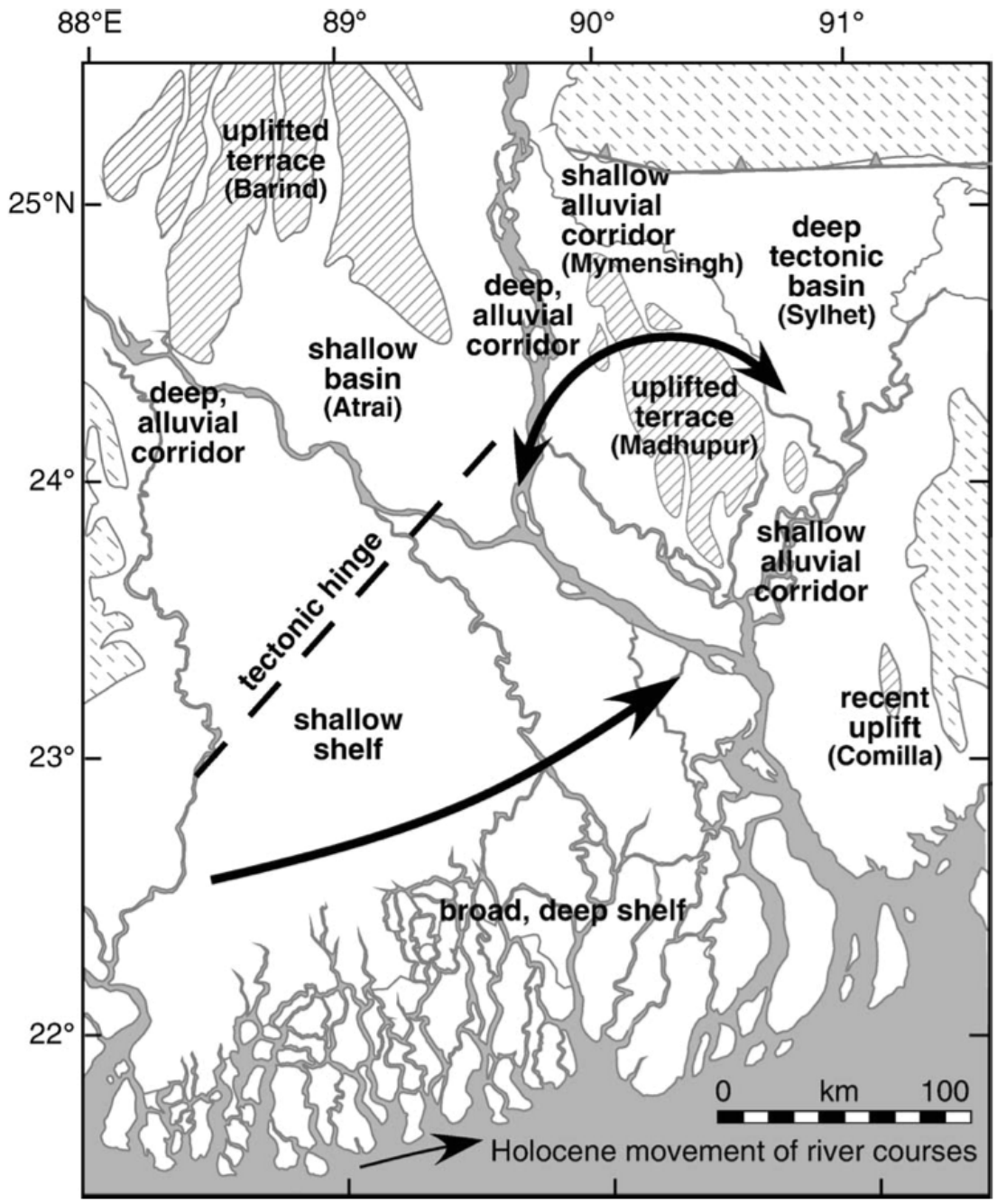

Figure I.3: Map of the tectonomorphic features and controls on the G-B delta system. Areas of uplift partition the delta into numerous sub-basins with unique sedimentation and stratigraphic preservation potential. The large arrows show general Holocene pathways for the major river channels. The Ganges has migrated to the east during the Holocene and the Brahmaputra has avulsed between its modern course and the modern Meghna river valley east of the Madhupur terrace (from Goodbred, 2003).

I.2.2 The Ganges Watershed

The Ganges watershed spans more than 1 x 10^6 km^2 and flows a distance of approximately 2,500 km from its headwaters to the confluence with the Brahmaputra river in Bangladesh. The Ganges river originates from several glacier-fed highland streams on the southern slopes of the Himalaya. The main trunk of the Ganges flows east along the Himalayan foreland basin and receives input from tributaries to the north from the Himalaya and southern tributaries from the Indian shield (Singh, 1996). Contributions to water discharge are approximately 60% from the Himalayan tributaries and 40% from the southern rivers (Singh, 2001), although geochemical studies of the rivers indicate that the Himalayan rivers contribute the dominant dissolved and particulate load to the Ganges (Galy and France-Lanord, 1999, 2001). South of their confluence in Bangladesh, the Ganges and Brahmaputra rivers ultimately debouch into the Bay of Bengal.

Himalayan tributaries and southern tributaries of the Ganges drain unique lithologies (Figure I.4). Tributaries from the southern slope of the Himalaya primarily drain Precambrian metamorphic rocks, with some input from Paleozoic-Mesozoic sedimentary sequences and Pleistocene alluvium. Lowland Ganges tributaries drain Mesozoic-Tertiary flood basalts, Precambrian metamorphics, and Archean granites and gneisses (Kuehl et al., 2005). The Ganges and Brahmaputra watersheds drain distinctly different lithologies, thus imparting potentially diagnostic characteristics within their sediment load such as mineralogy, detrital zircon age population distribution, and geochemical composition.

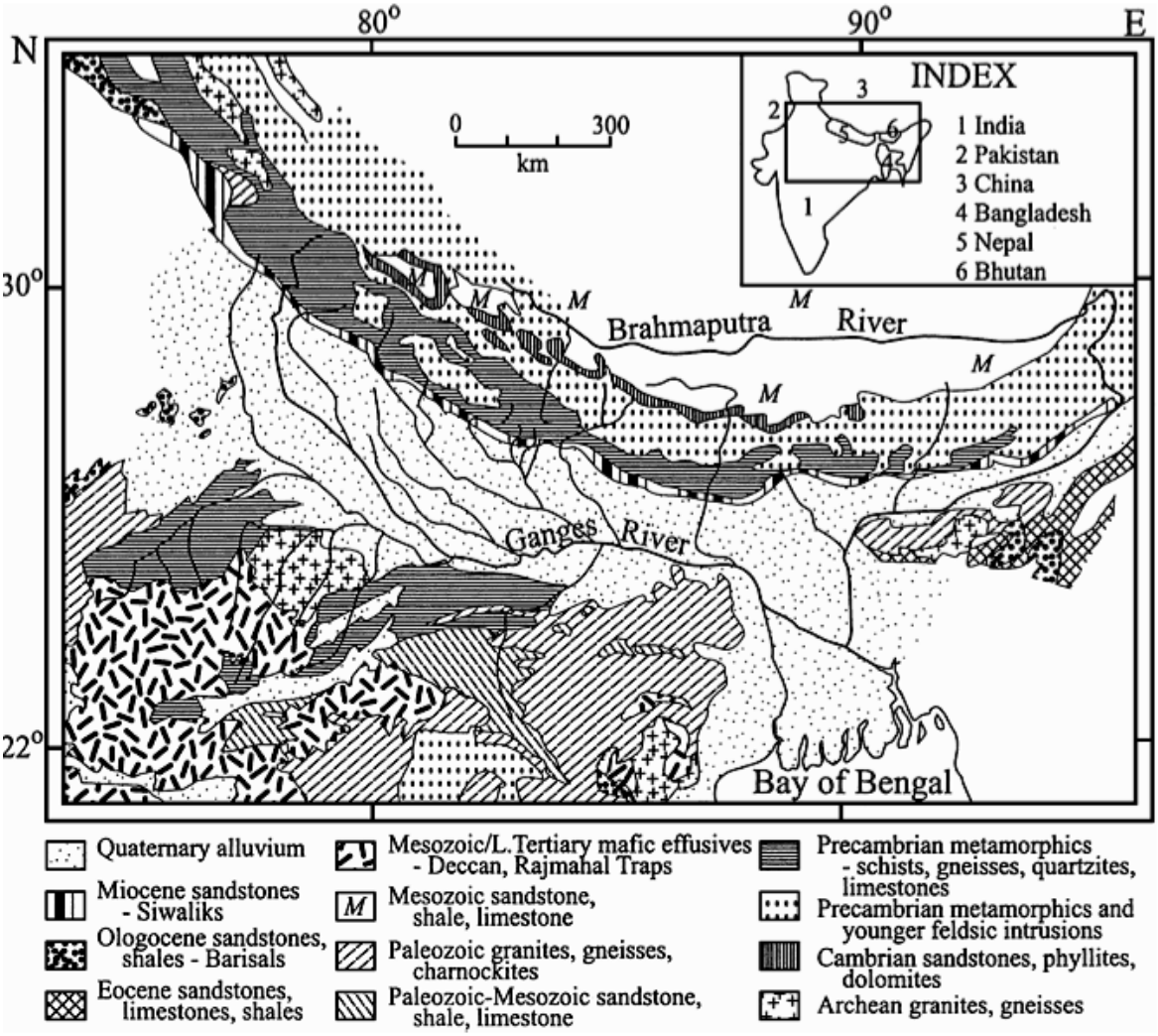

Figure I.4: Geologic map of the Ganges and Brahmaputra drainage basins. Unique lithologies drained by each river impart variations in mineralogy, detrital zircon age populations, and elemental signatures. The Ganges drains the Indian shield and the southern slope of the Himalaya and receives input primarily from Himalayan-type lithologies and Indian subcontinent lithologies. The Brahmaputra drains the northern slope of the Himalaya and receives input primarily from the Tibetan-type lithologies and some Himalayan-type lithologies (from Kuehl et al., 2005).

I.2.3 The Brahmaputra Watershed

The Brahmaputra watershed covers 630,000 km^2 and flows a distance of 2,800 km. The Brahmaputra river originates in a large glacier field on the northern slopes of the Himalaya at an elevation of approximately 5,200 m. It flows eastward as the Tsangpo river through Tibet along the Indus-Tsangpo Suture. Following a short reach in the northeast direction, the Tsangpo turns sharply around Namche Barwa, then continues on a southwesterly course into India as the Siang or Dihang river (Singh and France-Lanord, 2002). The river then cuts southeast through the Lesser Himalaya and Sub-Himalaya before entering the Brahmaputra (Assam) Plain at an elevation of 170 meters (Singh and France-Lanord, 2002). It flows south through Bangladesh as the Brahmaputra before converging with the Ganges and debouching into the Bay of Bengal.

The geology of the Brahmaputra drainage basin is dominated by Mesozoic sandstone, shale, and limestone, with some input from Precambrian igneous and Cambrian sedimentary rocks (Figure I.4). Tibetan lithologies contribute the primary distinguishing characteristics between Brahmaputra and Ganges sediments and represent the major source of sediment (Singh and France-Lanord, 2002; Singh et al., 2006). Despite traversing a shorter arc within the Himalaya, the Brahmaputra river consistently has a greater sediment flux than the Ganges.

Over the course of the river, the Brahmaputra experiences a significant range of elevation and slope. The path of the river through the Tsangpo Basin in Tibet is relatively flat and has an average elevation greater than 4,700 m (Singh and France-Lanord, 2002). The abrupt turn around Namche Barwa through the Himalaya creates

a dramatic increase in slope as the path of the river drops approximately 2,000 m in elevation over less than 200 km distance. Across the alluvial plain in Assam and Bangladesh, the Brahmaputra experiences only 150 m of elevation drop from eastern Assam to the confluence with the Ganges (Singh and France-Lanord, 2002). Besides significant variability in slope and lithology, the path of the Brahmaputra traverses extremely variable regional climates. Extremes in precipitation range from cold, arid conditions in Tibet to the monsoon dominated Himalaya and alluvial plain.

I.2.4 Regional Climate

Fluvial systems of South Asia are strongly influenced by acute climatic seasonality and long-term climatic variability. The South Asian southwest summer monsoon is the primary control on precipitation for the region occupied by the G-B delta. As a result of the southwest monsoon, warm, humid air is advected from the Indian Ocean towards the Himalayan range, thus having a significant impact on fluvial hydrology and sediment dispersal. Sediment dispersal within the G-B delta system exhibits an acute and rapid response to South Asian climate change (Goodbred and Kuehl, 2000a). The G-B delta system is largely driven by runoff from the southwest summer monsoon, during which the G-B rivers deliver the majority of water and sediment load to the margin. The Ganges river discharges 80-90% of its water and 95% of its sediment during the summer monsoon months of June through November. The Brahmaputra river discharges 95% of its water during May through November. An intensely wet summer monsoon coupled with dry winter monsoon conditions further enhances strong coupling of the G-B fluvial systems with summer monsoon strength (Goodbred, 2003).

Strength of the southwest summer monsoon has varied significantly during the past 150 ky and has greatly impacted precipitation distribution and intensity, glacial activity, and sediment flux within the G-B system. Prell and Kutzbach (1987) suggest strength of the southwest monsoon is intimately related to Milankovitch-tuned variations in summer insolation. Prell and Kutzbach (1987) found that, in conjunction with Milankovitch variations, global boundary conditions such as atmospheric CO_2, sea level, ice sheet extent, and sea surface temperature also modulate insolation-driven variability and have profound impacts on monsoon intensity.

I.2.5 Sediment Supply and Delta Evolution

The Ganges and Brahmaputra rivers originate in the Himalaya and are responsible for transporting a combined one billion tons (10^9) of sediment annually to the Bengal Basin. Sediment budget analysis by Goodbred and Kuehl (2000a) suggests the Ganges and Brahmaputra rivers transported more than double the present amount of sediment to the margin during strengthened monsoon conditions from 11-7 ka B.P. Figure I.5 from Goodbred and Kuehl (2000a) shows the distribution of sediment storage within the G-B delta system over the past 18 ky B.P. plotted with eustatic sea level and the South Asia aridity index. Deposition began on the canyon and fan system before initial delta development at 11 ka yr B.P. Since the last glacial maximum (LGM), the G-B system has evolved from an alluvial-valley complex to a coastal marine delta front and prograding subaerial delta plain. Goodbred et al. (2003) suggest immense sediment supply, not the rate of sea-level rise, was responsible for initial delta development at 11 ka yr B.P. and delta stability under conditions of rapid eustatic rise.

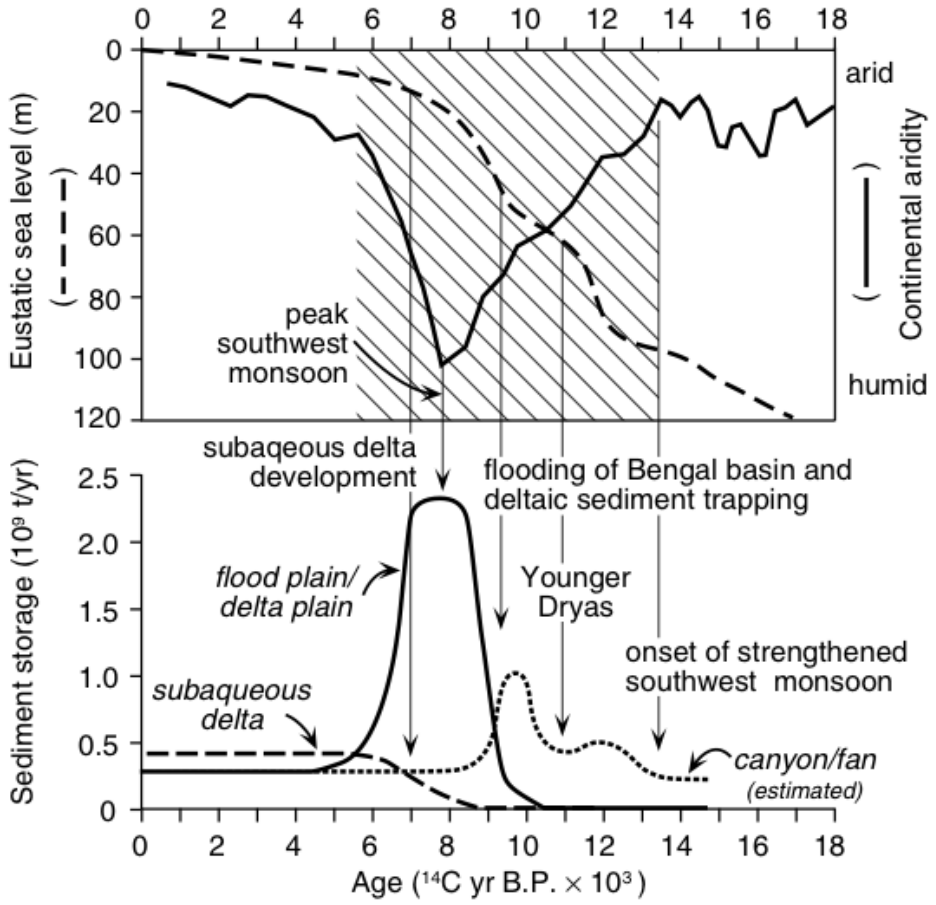

Figure I.5: Plots of eustatic sea level (Bard et al., 1996; Fairbanks, 1989), South Asia aridity index (Prins and Postma, 2000), and G-B sediment storage (Goodbred and Kuehl, 2000a, 1999; Weber et al., 1997a). Hachured area shows period of high regional insolation (Colin et al., 1999) and vertical arrows and annotations highlight correlations between climate, sea level, and events within the G-B system (from Goodbred and Kuehl, 2000a).

During the LGM, low insolation and strong glacial boundary conditions resulted in a weakened summer monsoon and significantly reduced regional precipitation (Cullen, 1981; Gasse et al., 1991). Off-shore seismic studies show an absence of sedimentation on the Bengal fan as river discharge was greatly reduced during the LGM (Weber et al., 1997b). By 15 ky B.P. active sedimentation began on the Bengal fan and increased gradually for the next several thousands years, indicating

that sediment flux to the margin increased but bypassed the shelf directly to the canyon-fan system (Weber et al., 1997b). Increased insolation during the early Holocene reinvigorated summer monsoon strength and regional precipitation (Figure I.5). Several studies provide evidence for warmer and wetter regional conditions during the early Holocene, including evidence from Tibetan lacustrine records (Gasse et al., 1991), Arabian Sea ^{18}O records (Sirocko et al., 1993), eolian deposits (Prins and Postma, 2000), pollen and lake stratigraphy (Van Campo, 1986; Swain et al., 1983; Dill, 2003), and salinity records (Cullen, 1981) and clay mineralogy records (Chauhan et al., 1993; Colin et al., 1999) from the Bay of Bengal.

Rising sea level after 11 ky B.P. spurred a significant drop in fan sedimentation (Weber et al., 1997b) as the major depocenter shifted to the newly flooded Bengal margin (Goodbred and Kuehl, 2000a). Immense, long-term sediment output during the early Holocene (11-7 ky B.P.) described by Goodbred and Kuehl (2000a) is believed to be directly related to a long-term (10^3 yr) intensification of the southwest monsoon, which was brought about by a peak in regional insolation at 9 ky B.P. (COHMAP, 1988; Gasse et al., 1991). Between 11-7 ky B.P., margin sediment flux was sufficient to keep pace with rapid sea-level rise and producing significant vertical aggradation (Goodbred and Kuehl, 2000b). Less rapid sea-level rise changed the G-B delta from an aggradational to progradational system after 7 ky B.P., which allowed for subaerial delta progradation and subaqueous delta development on the shelf. Goodbred and Kuehl (1999) suggest during the past 7 ky of relative sea-level highstand, G-B sediments have been equally partitioned across the subaerial delta, subaqueous delta, and canyon-fan system.

The Holocene G-B delta has prograded seaward creating a 380 km wide delta front bounded by the Hoogly River to the west and the active Tripura Fold Belt to the east. Based on clay mineralogy and radiocarbon ages from the lower delta plain, Allison et al. (2003) proposed lower delta plain progradation following maximum transgression occurred in several phases beginning in the west and gradually shifting east towards the modern delta. The western region of the delta is likely replenished through tidal reworking of sediment transported alongshore towards the "Swatch of No Ground" submarine canyon. Prior to modern land use practices the lower delta plain region was reported to be mangrove dominated, similar to the modern Sunderbans region.

I.2.6 Strontium

Strontium has been recognized as a potential provenance indicator as early as the 1950s (Turekian and Kulp, 1956). Global marine Sr studies reveal increasing $^{87}Sr/^{86}Sr$ values during the Cenozoic (ie: Burke et al., 1982; Palmer and Edmond, 1989; Richter et al., 1992). The Sr flux from major watersheds around the world was examined in order to determine the mechanism responsible for increasing global marine $^{87}Sr/^{86}Sr$ values.

Studies within the Ganges and Brahmaputra watersheds found high Sr concentration and high $^{87}Sr/^{86}Sr$ values compared to other major rivers of the world (ie: Krishnaswami et al., 1992; Palmer and Edmond, 1989, 1992). Significant input of Sr with high $^{87}Sr/^{86}Sr$ values from Himalayan rivers followed uplift and exhumation of the Himalayan-Tibetan orogen and is directly linked to the global increase in oceanic $^{87}Sr/^{86}Sr$ over the past 40 Ma. Enhanced silicate weathering has been cited as the

dominant source of radiogenic Sr from the Himalaya (Singh et al., 1998; Dalai et al., 2003; Bickle et al., 2003, 2005), although it has been suggested that metamorphosed carbonates are also an important source (Singh et al., 1998; Galy and France-Lanord, 1999; Bickle et al., 2001).

Geochemically distinct source lithologies combined with a rapid source-to-sink response of the G-B delta system provides a unique opportunity for sediment provenance study. Results from $^{87}Sr/^{86}Sr$ studies within Ganges and Brahmaputra watersheds inspired provenance and weathering studies using $^{87}Sr/^{86}Sr$ values for G-B margin sediments (Singh and France-Lanord, 2002; Tripathi et al., 2007; Clift et al., 2008). Sediments eroded from the Brahmaputra watershed are less radiogenic than Ganges sediments because of significant Sr contribution from Tibetan lithologies with low $^{87}Sr/^{86}Sr$ values (Derry and France-Lanord, 1997; Singh et al., 2006). Brahmaputra sediments typically have $^{87}Sr/^{86}Sr$ values in the range of 0.72 to 0.74, while Ganges sediments have significantly higher $^{87}Sr/^{86}Sr$ values approaching 0.80, because of sediment flux dominated by more radiogenic Himalayan lithologies.

Traditionally, $^{87}Sr/^{86}Sr$ values have been used as provenance indicators. I suggest Sr concentration is also a useful provenance indicator because it preserves the geochemical fingerprint imparted by unique catchment lithologies within the Himalaya. This is an important relationship because Sr concentration data can be generated inexpensively using X-ray fluorescence (XRF), while $^{87}Sr/^{86}Sr$ values require a much more labor intensive and time consuming elemental extraction approach. A well-defined correlation between Sr concentration and sediment provenance for G-B delta sediments will significantly enhance our understanding of delta development by

producing comprehensive and relatively inexpensive geochemical datasets throughout the Bengal Basin.

Figure I.6 shows $^{87}Sr/^{86}Sr$ values plotted against Sr concentration for Tibetan samples (ie: Brahmaputra) and Himalayan samples (ie: Ganges). Data are from direct sampling of Brahmaputra and Ganges bank and suspended sediments as well as borehole sediments from Goodbred et al. (unpublished) believed to receive primarily Ganges or Brahmaputra sediment based on their physiographic locations. Tibetan sediments have markedly higher Sr concentrations and lower (less radiogenic) $^{87}Sr/^{86}Sr$ values. Himalayan sediments are more variable, but generally have higher $^{87}Sr/^{86}Sr$ values and lower Sr concentrations. These data suggest a Sr concentration cutoff of approximately 150 ppm between Tibetan and Himalayan lithologies. Additional Sr data from several boreholes from Youngs et al. (unpublished) show possible river avulsions and provenance shifts based on abrupt changes in downcore $^{87}Sr/^{86}Sr$ values.

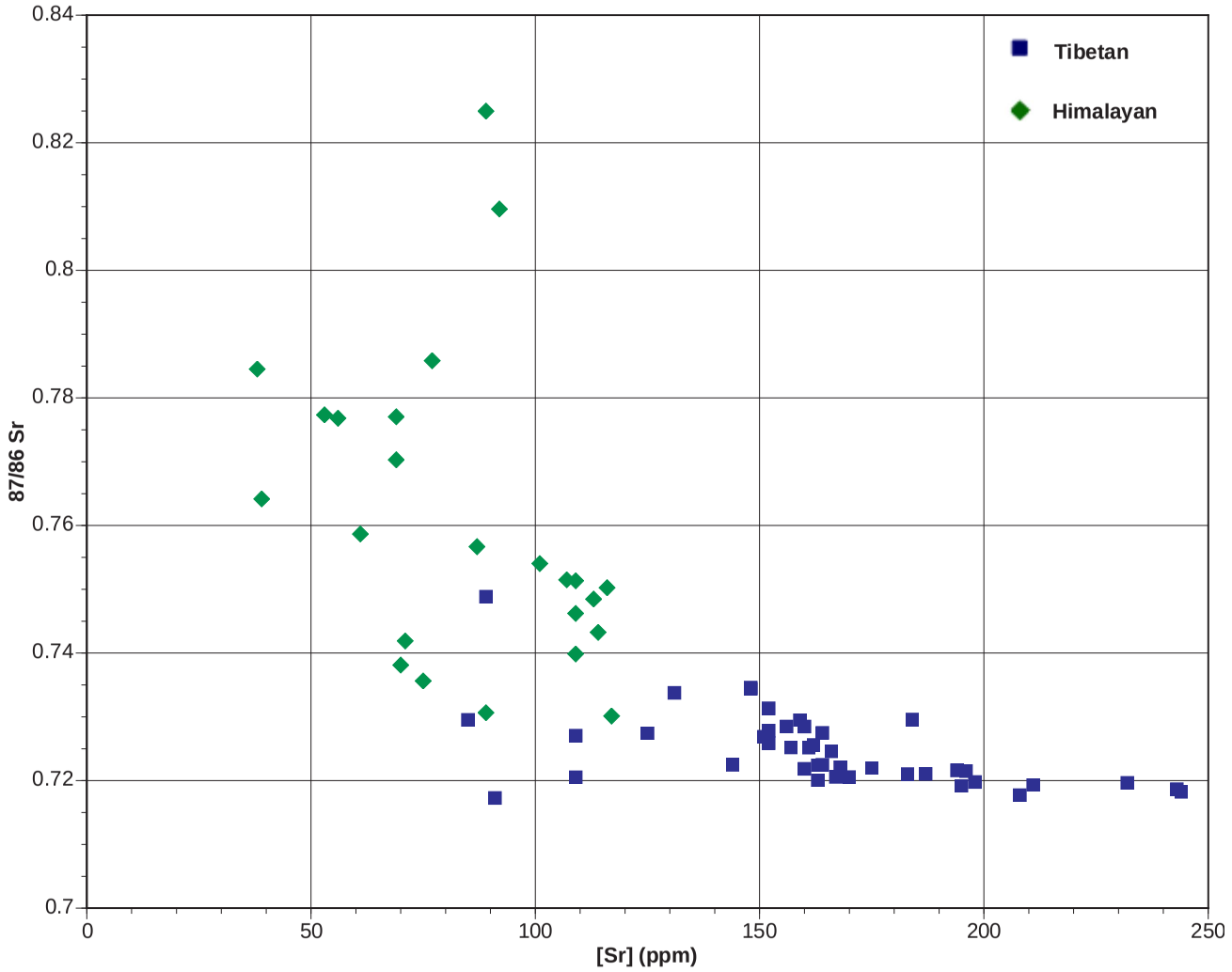

Figure I.6: Plot of $^{87}Sr/^{86}Sr$ values versus Sr concentration for Bengal Basin borehole data. "Tibetan" were sampled directly from Brahmaputra bank and suspended sediments as well as borehole samples from known Brahmaputra sediments in the Sylhet Basin. Data labeled "Himalayan" were sampled directly from Ganges bank and suspended sediments as well as known Ganges sediment from borehole samples in the western region of the delta. Data from Youngs et al., unpublished and Singh et al., 2006.

CHAPTER II

METHODS

II.1 Field Work

Two sample locations, near Magura and Raipur, Bangladesh, were selected as part of National Science Foundation (NSF) grant EAR 0309536. The borehole collected near Magura, Bangladesh is located within the Jessore basin southwest of the modern confluence of the Ganges and Brahmaputra Rivers. The borehole collected near Raipur, Bangladesh is located along the modern rivermouth estuary in the southeastern region of the delta. See Figure II.1 and Table A.1 for borehole locations.

Boreholes were continuously sampled using a reverse-circulating hollow-stem auger with a lined split-spoon sampler. Sections of core were preserved in one-half meter sections of polyvinyl chloride (PVC) sealed with wax at each end. Approximately two hundred and eighty sections of core from two boreholes were packaged and shipped from Bangladesh to Vanderbilt University.

Natural gamma and conductivity downhole electric logs were also collected utilizing a three-coil slim hole induction tool in PVC-cased tubewells located next to the boreholes to a depth of approximately 150 m. Natural gamma-ray logs record a continuous reading of natural gamma radiation emanating from sediments penetrated by the borehole. Conductivity logs measure the electrical conductivity of sediment surrounding the borehole.

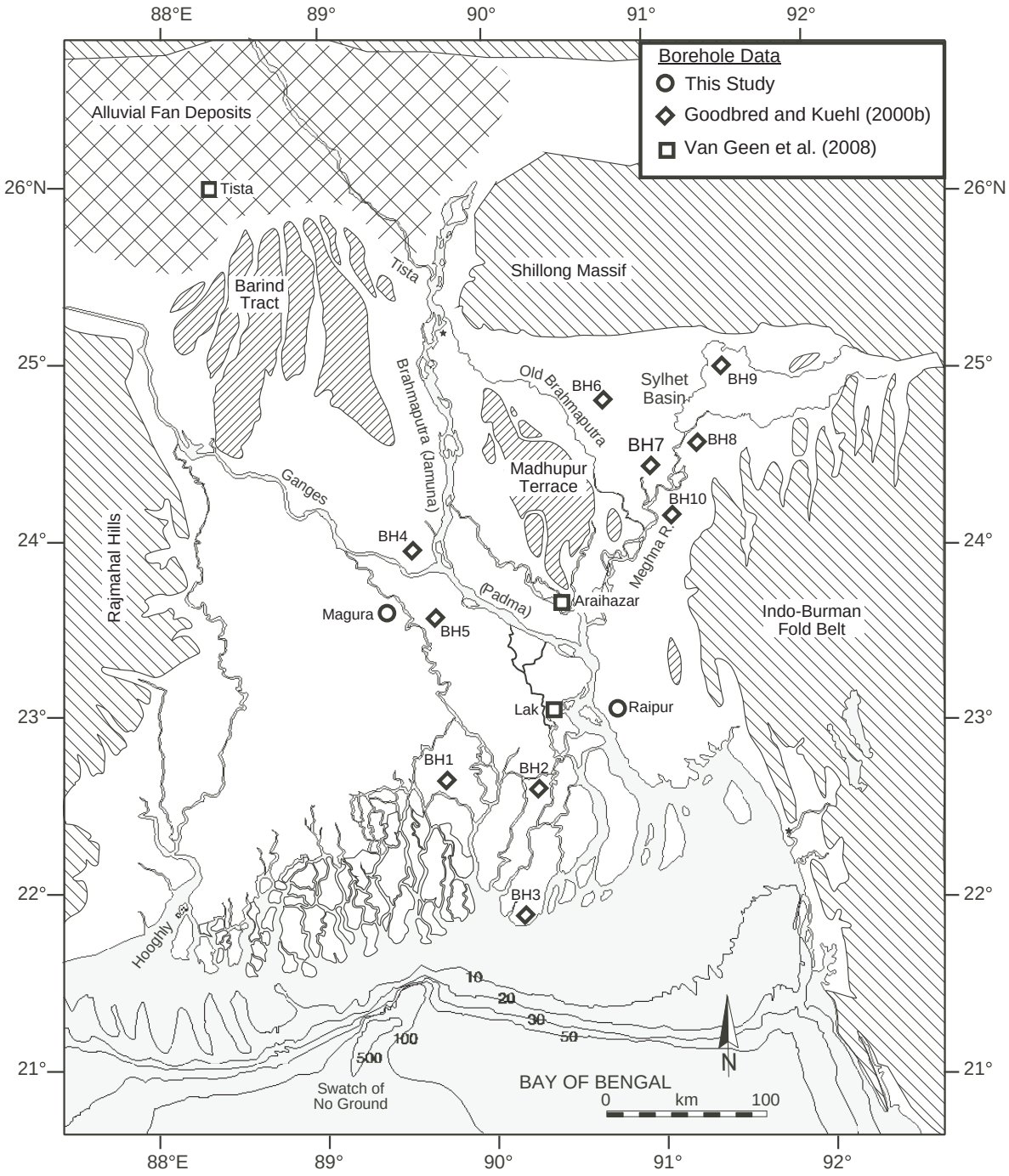

Figure II.1: Borehole locations from this study, Goodbred and Kuehl, 2000b, and Van Geen et al., 2008. The modern and historical courses of the Brahmaputra river are separated by the uplifted Madhurpur Terrace. The Ganges river has migrated east from the Hooghly to its present course during the Late Quaternary. The Tista river has avulsed between the Ganges and Brahmaputra rivers, and historical paths traversed through the Barind Tract (modified from Goodbred and Kuehl, 2000b.

II.2 Laboratory Work

II.2.1 Core Logger

The use of the GeoTek Multi-Sensor Core Logger (MSCL) has been widely applied to sediment core analysis (Weber et al., 1997a). The MSCL at Vanderbilt University is equipped to analyze whole-core and split-core properties for gamma ray attenuation porosity estimate (GRAPE) using a ^{137}Cs source, magnetic susceptibility (MS) using Bartington loop and point sensors, and a high-resolution linescan digital camera.

Whole-core sections were analyzed for a continuous bulk density porosity estimate (GRAPE) using a ^{137}Cs source. Whole-core MS was measured using a Bartington magnetic loop sensor set to sample at 1 cm intervals. Split-core sections were analyzed for magnetic susceptibility using a high-resolution Bartington point counter set to sample at 0.5 cm intervals. Each core section was imaged using a high-resolution linescan digital camera.

Individual PVC-cased sections of core were scored on opposite sides using a table saw with a fixed blade height. A handheld utility knife equipped with a hook blade was used for final separation of individual pre-scored PVC sections. A thin metal wire was passed through each section of split core to produce two identical halves of sediment-filled PVC. Half of each core was sealed and archived using a tabletop polybag impulse sealer. Un-archived halves were described and subsampled for additonal analysis.

II.2.2 Grain Size

Grain-size analysis was performed at Vanderbilt University using a Malvern Mastersizer 2000 laser-diffraction particle-size analyzer. Each core section was sub-sampled for grain size analysis based on downcore lithology and facies variations. Reported grain size data was generated from an average of three consecutive grain size analyses for each sub-sample (Tables A.10 and A.12).

II.2.3 Sediment Geochemistry

Elemental analysis was primarily performed at Middle Tennessee State University (MTSU) using an Oxford Instruments MDX 1080+ multi-dispersive X-ray fluorescence spectrometer. Additional elemental analysis was performed by the Washington State University Geoanalytical Laboratory on a ThermoARL Advant'XP+ sequential X-ray fluorescence spectrometer. Major element results were normalized to 100% and minor element results were not normalized and reported in ppm. Samples analyzed at the Washington State University Geoanalytical Laboratory were not decarbonated, while samples analyzed at MTSU were decarbonated. Ganges river sediment contains several percent carbonate, while the carbonate content of Brahmaputra sediments is minimal. Samples from Ganges river sediments containing carbonates generally had higher Sr concentrations prior to decarbonation, probably due to substitution of Sr for Ca in carbonate minerals. Brahmaputra sediments were less effected by the decarbonation process because of minimal carbonate content. The overall trends in Sr concentrations are robust and not affected by the decarbonation process. The following procedure was used for decarbonation.

Samples were combusted at 600 degrees Celsius for 72 hours and treated with a 15% acetic acid leach to remove carbonate material. Samples which reacted strongly to the acetic acid leach were noted to contain a significant fraction of carbonate material. Samples were then repeatedly rinsed with deionized water to remove excess acetic acid. Following an acetic acid leach, samples were crushed into a fine powder using an alumina ceramic shatterbox. Finally, samples were pressed into pellets for XRF analysis using a hydraulic press set at 11,000 psi for approximately ten minutes. Major and minor elemental analyses were performed for each pelleted sample.

II.2.4 Radiocarbon Dating

Five samples were sent to the National Ocean Sciences Accelerator Mass Spectrometry Facility (NOSAMS) for radiocarbon dating. Two samples were analyzed from the Magura borehole and three samples from the Raipur borehole (Table III.6). Reported results from NOSAMS were converted to calendar ages (2 sigma range) using Calib 5.0.2 software using the terrestrial IntCal04 calibration dataset.

II.2.5 Detrital Zircon Geochronology

Detrital zircon geochronology was conducted on two samples from a third sediment core, BH8, collected near Ajmiriganj, Bangladesh within the tectonically subsiding Sylhet Basin in the northeast region of the G-B Delta (Figure II.1). Detrital zircon grains were isolated and analyzed from sediment samples collected at depths of 92 m (AZ300) and 99 m (AZ325) using the following procedure.

Sediment samples were dry-sieved to remove large lithic fragments and subjected

to a hand-held magnet to remove strongly magnetic minerals such as magnetite. A heavy liquid separation process was used to remove grains with a specific gravity greater than the heavy liquid. Zircon grains were recovered from the light fraction following heavy liquid separation. The remaining mixture of heavy liquid and sediment was passed through filter paper to isolate the light fraction containing the individual zircon grains. The remaining material was subjected to a Frantz magnetic separator to remove remaining magnetic minerals. Finally, zircon grains were handpicked from the remaining light fraction using a binocular microscope. Sample AZ300 yielded 36 zircon grains, and sample AZ325 yielded 31 zircon grains.

Following separation procedures, detrital zircon grains were mounted in epoxy, polished, and carbon coated. Carbon coated mounts were analyzed under a scanning electron microscope and analyzed with energy dispersion spectroscopy (EDS) to distinguish zircon from non-zircon grains. Images were not taken because of a malfunctioning electron backscatter unit. Individual zircon grains were analyzed using a Perkin Elmer Elan 6100 DRC Laser Ablation Inductively Coupled Plasma Mass Spectrometer (LA-ICPMS) at Vanderbilt University. Individual zircon grains were subjected to a high-intensity laser, and the ablated material was passed through a mass spectrometer. Raw data was reduced using the Glitter software package (van Achterbergh et al., 1996) to determine individual zircon ages from uranium and lead isotope ratios.

CHAPTER III

RESULTS

III.1 Grain Size

High-resolution, down-core sand grain-size data was collected for Magura and Raipur. This study focuses on the sand-sized fraction because it has been found to be a more robust geochemical provenance indicator compared to silt and clay-sized fractions (Goodbred, personal communications). Fine sand is the predominant grain size for Magura sediments. Borehole sediments from Raipur exhibit a more variable grain size distribution, and fine sand is predominant within the sand-sized fraction. Coarse sand and gravel are present at Magura and Raipur within discrete, pulsed intervals.

Sand grain-size data from Magura and Raipur plotted on a ternary diagram (Figure III.1) reveal distinctly different sand-sized populations for the two boreholes. Data from Magura plot together as a continuum with <40% coarse sand, while data from Raipur plot as two discrete populations, >40% coarse sand and <20% coarse sand. Raipur samples with >40% coarse sand represent a unique facies and are further described in following section. Note that the coarsest samples from Raipur are coarser than those from Magura despite Raipur's being closer to the coast than Magura, which is more than 150 km upstream and closer to the Himalayan sediment source.

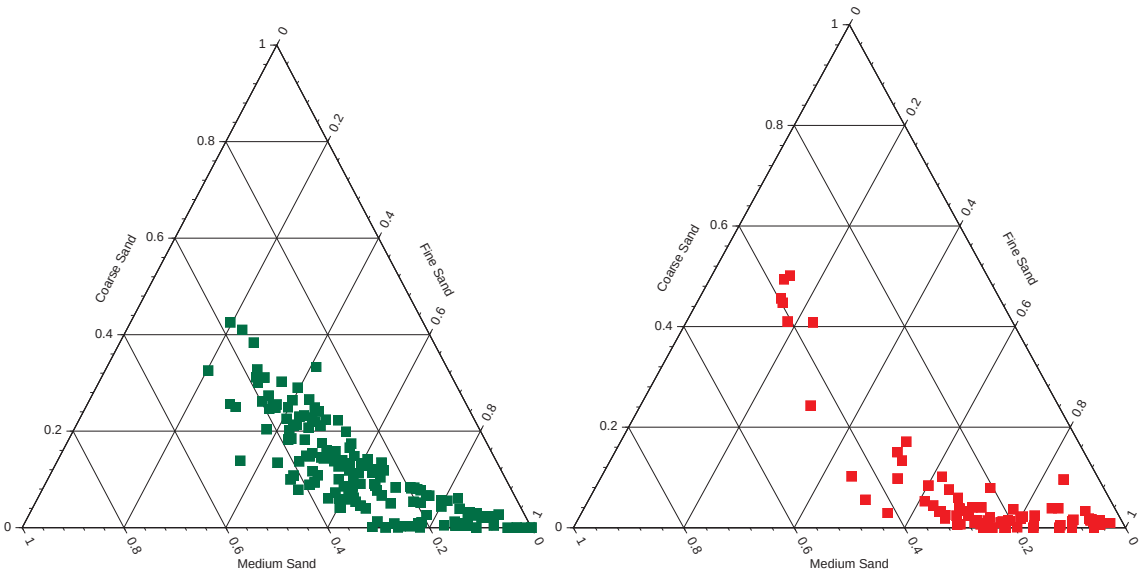

(a) Magura

(b) Raipur

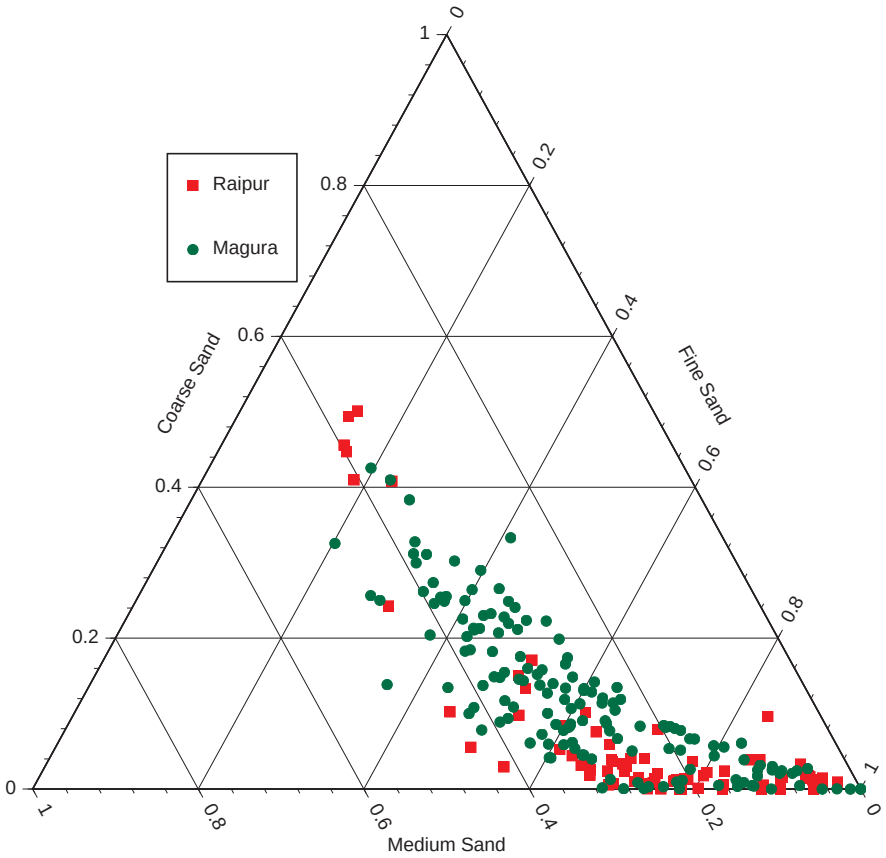

(c) Magura and Raipur

Figure III.1: Ternary diagrams for Magura and Raipur sand grain size distribution. Note two discrete sand grain-size populations for Raipur, >40% coarse sand and <20% coarse sand, except for one sample.

III.2 Facies Analysis

Downcore changes in sediment characteristics (i.e., grain size, color, sedimentary structure, MS) were used to develop a sedimentary facies scheme for boreholes collected near Magura and Raipur, Bangladesh. Raipur contains all six sedimentary facies described below, while Magura contains facies B and E. All facies are summarized in Table III.1. Figures III.2 and III.3 show examples from each facies found at Magura and Raipur. Where applicable, this facies scheme is correlated with facies descriptions from previous investigations (i.e. Goodbred and Kuehl, 2000b). Stiff, reddish-yellow to yellowish-red highly weathered sediments from Magura and Raipur are interpreted as weathered paleosols of the Late Pleistocene lowstand and are used primarily for stratigraphic interpretation and are not assigned to a separate "oxidized" facies as previously used in Goodbred and Kuehl (2000b).

III.2.1 Facies A

Facies A consists of dark gray to black stiff clay rich in disseminated organic material and root fragments. Sedimentary structures are not preserved within the clay, and, when present, facies A is less than 5 m thick.

III.2.1.1 Interpretation

Facies A is interpreted as muddy coastal plain deposits. Large mangrove roots found within the unit are characteristic of a muddy coastal plain setting such as the modern Sunderbans region. Facies A, within the overall stratigraphic section at Raipur, is positioned at the base of two coarsening upwards sequences that transition from a coastal, tidally influenced environment towards a more fluvial dominated

environment. Radiocarbon dates (Table III.6) at Raipur from the Holocene indicate rapid accretion rates of 1 cm/yr for facies A and C.

III.2.2 Facies B

Facies B comprises of brown silt-dominated sediments and can be further divided into subfacies B1 and B2 based on the presence of sedimentary structure. Where present, facies B is less than 10 m thick.

- Facies B1 contains millimeter-scale planar bedded brown and tan silts with occasional cross-bedding.
- Facies B2 contains brown silt-dominated sediments with an absence of preserved sedimentary structures.

III.2.2.1 Interpretation

Facies B is interpreted as proximal floodplain and overbank deposits commonly found throughout the G-B delta. Deposition of facies B is associated with slack or slow-water deposition from overbank floodwaters of a nearby channel, often in response to channel migration and river avulsion. Facies B as described here corresponds with the "Thin Mud" facies from Goodbred and Kuehl (2000b).

III.2.3 Facies C

Facies C consists of gray to brown silt-dominated sediments. Sedimentary structures include frequently inter-laminated (<1 cm thick) gray to brown silty clay and mm-scale tan to light gray silt to fine sand beds. Root fragments up to several

cm in length are found within the unit. Facies C always directly overlies facies A and underlies facies D.

III.2.3.1 Interpretation

Facies C is interpreted as tidal rhythmite deposits. Regularly inter-bedded silty clay and silty sand layers are indicative of coastal environments exposed to regular tidal influence. Deposition of facies C lies directly above facies A, which is interpreted as coastal-plain mud deposits, and directly below facies D, which is interpreted as muddy estuarine or river mouth sands. The contact between facies A and facies C reflects gradational shifting from clay to silt-dominated sediments to interbedded silty clay and silty sand.

III.2.4 Facies D

Facies D is typically a dark gray to brown, muddy, fine sand. Facies D has little preserved bedding and frequent evidence of bioturbation. At Raipur, facies D can be distinguished from facies E by its higher silt and mud fraction and an absence of coarse sand.

III.2.4.1 Interpretation

Facies D is interpreted as estuarine/distributary-mouth channel deposition, and is interpreted to represent changes from vertical aggradation to horizontal distributary-mouth progradation across the coastal plain and nearshore environment. Compared with facies E, facies D is generally finer grained and more poorly sorted with a higher fraction of mud (20%) and a sand fraction skewed towards fine-grained.

Facies D as described here corresponds with the "Muddy Sand" facies from Goodbred and Kuehl (2000b).

III.2.5 Facies E

Facies E is a gray, tan, or brown sand with a range of size distributions from fine to coarse. Facies E is common throughout the G-B delta. A detailed description of facies E for Raipur and Magura are provided below.

Within the Raipur borehole, facies E is typically a light gray fine sand. Gray to black millimeter scale laminae are commonly interbedded within the light gray sands. Micas are common throughout facies E and occasionally group to form thin layers. At Raipur, facies E can be distinguished from facies D by its generally lower mud fraction and higher coarse sand fraction.

Within the Magura borehole, facies E can be subdivided into four subfacies:

E1 Subfacies E1 consists of interbedded tan and brown fine sands with abundant, well-developed cross-bedding.

E2 Subfacies E2 consists of gray and tan fine sands with no preserved sedimentary structures and infrequent evidence of bioturbation.

E3 Subfacies E3 consists of gray and tan medium to coarse sands with a lack of preserved sedimentary structures.

E4 Facies E4 is similar to subfacies E3 with the addition of large lithic gravel-sized fragments scattered within medium to coarse sand.

III.2.5.1 Interpretation

Facies E is interpreted as alluvial valley and river channel fill. Deposition of facies B overlying multiple sequences of facies E along with multiple weathering horizons within facies E indicates successive channel avulsions and channel reoccupation during the Pleistocene and Holocene. Facies E as described here corresponds with the "Sand" facies from Goodbred and Kuehl (2000a).

At Magura, sub-facies E1 is interpreted as secondary channel fill based on the flow regime necessary to deposit very fine to fine sand at millimeter scale bedding. Facies E2 and E3 are interpreted as main fluvial channel fill. Facies E4 is also interpreted as main channel fill, but with the addition of gravel input.

III.2.6 Facies F

Facies F consists of tan to brown coarse sand and gravel. Sand grain size distribution is generally >40% coarse, >40% medium, and <20% fine sand, which is strikingly different from the fine sands commonly seen within facies D and E. The sand is poorly sorted, lacks bedding, and contains abundant lithic fragments and small gravel. Deposition of facies F occurs as discrete, pulsed inputs within tidal facies C.

III.2.6.1 Interpretation

Based on the following evidence, Facies F is interpreted as the product of high-energy floods, perhaps from glacial or tectonic lake bursts.

- proximity of coarse grained sediments to the coast,
- lack of a local source for coarse sands and gravels,

- interbedded nature of coarse material within fine-grained tidal rhythmite deposits (facies C),
- unique geochemical data that suggests a non-Ganges and non-Brahmaputra sediment source,
- downcore $^{87}Sr/^{86}Sr$ values and detrital zircon age populations which suggest the Tibetan source to the Brahmaputra was shut off, allowing Eastern Himalayan tributaries (ie: Tista) to dominate sediment provenance,
- geomorphological field evidence from Montgomery et al. (2004) that documents Himalayan glacial lakes, which may have blocked the path of the Brahmaputra, and associated burst floods.

Table III.1: Summary table of stratigraphic facies and interpretation.

Facies	Lithology	Color	Sedimentary Structure	Organic Material	Interpretation
A	clay- to silt-dominated muds	dark gray to black	none	disseminated organics, mangrove roots up to several cm	muddy coastal plain
B	silty-mud to silts with very fine sand	brown (reddish yellow to yellowish red where oxidized)	mm-scale planar laminae with occasional cross-bedding	uncommon disseminated organics	floodplain and overbank deposits
C	alternating silty muds and silty fine sands	gray to brown	clay interbedded with silt to fine sand	mangrove root fragments up to several cm	tidal rhythmites
D	muddy fine to medium sand	dark gray to brown	none	none	muddy estuarine to river mouth sands
E	clean fine, medium, and coarse sands	light gray (reddish yellow to yellowish red where oxidized)	occasional interbedded mm-scale dark laminae	none	valley and river channel fill
F	coarse sand (>40%) with lithic gravel	tan to brown	none	none	outburst flood event?

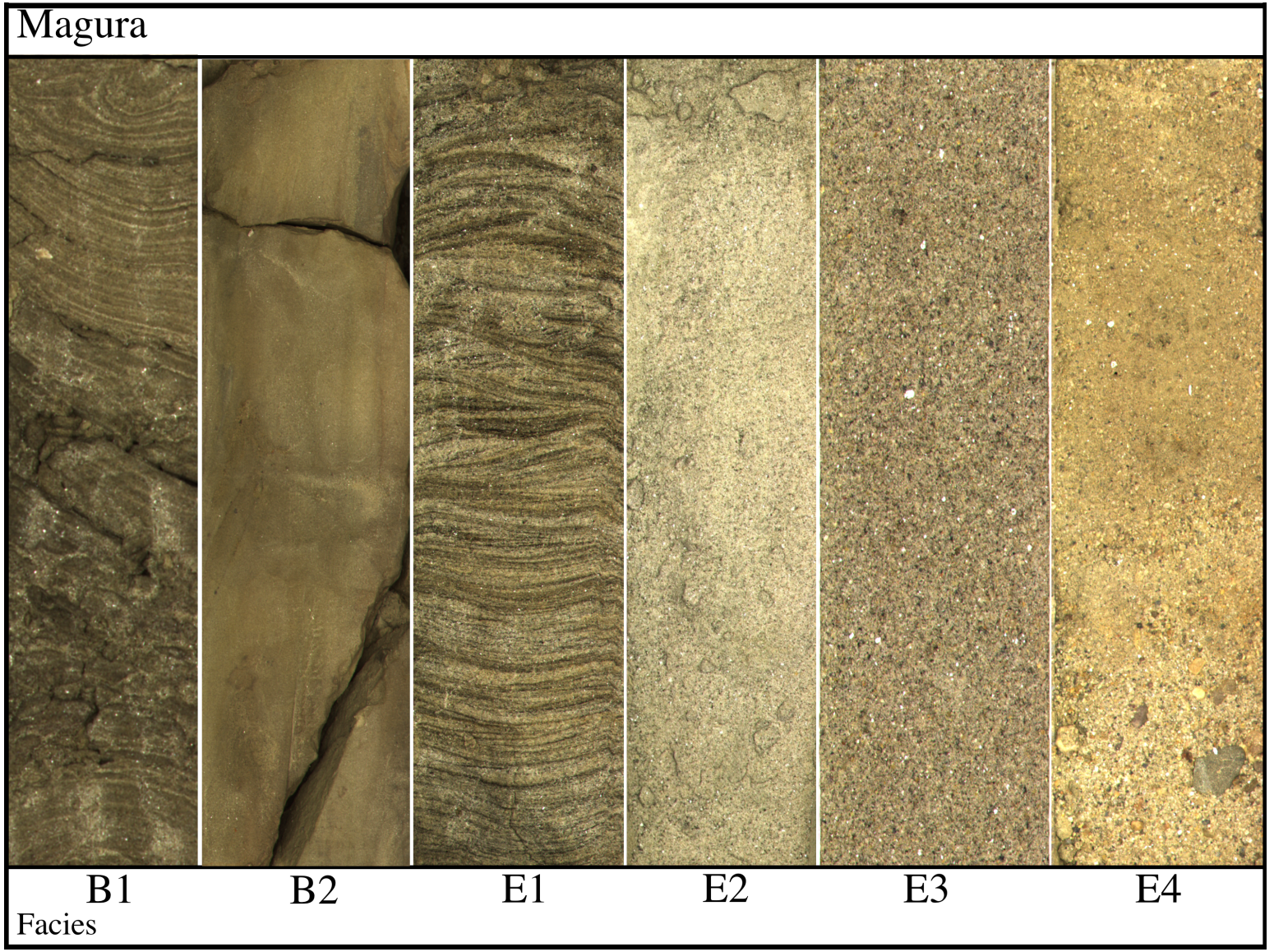

Figure III.2: Digital images of sample facies found at Magura.

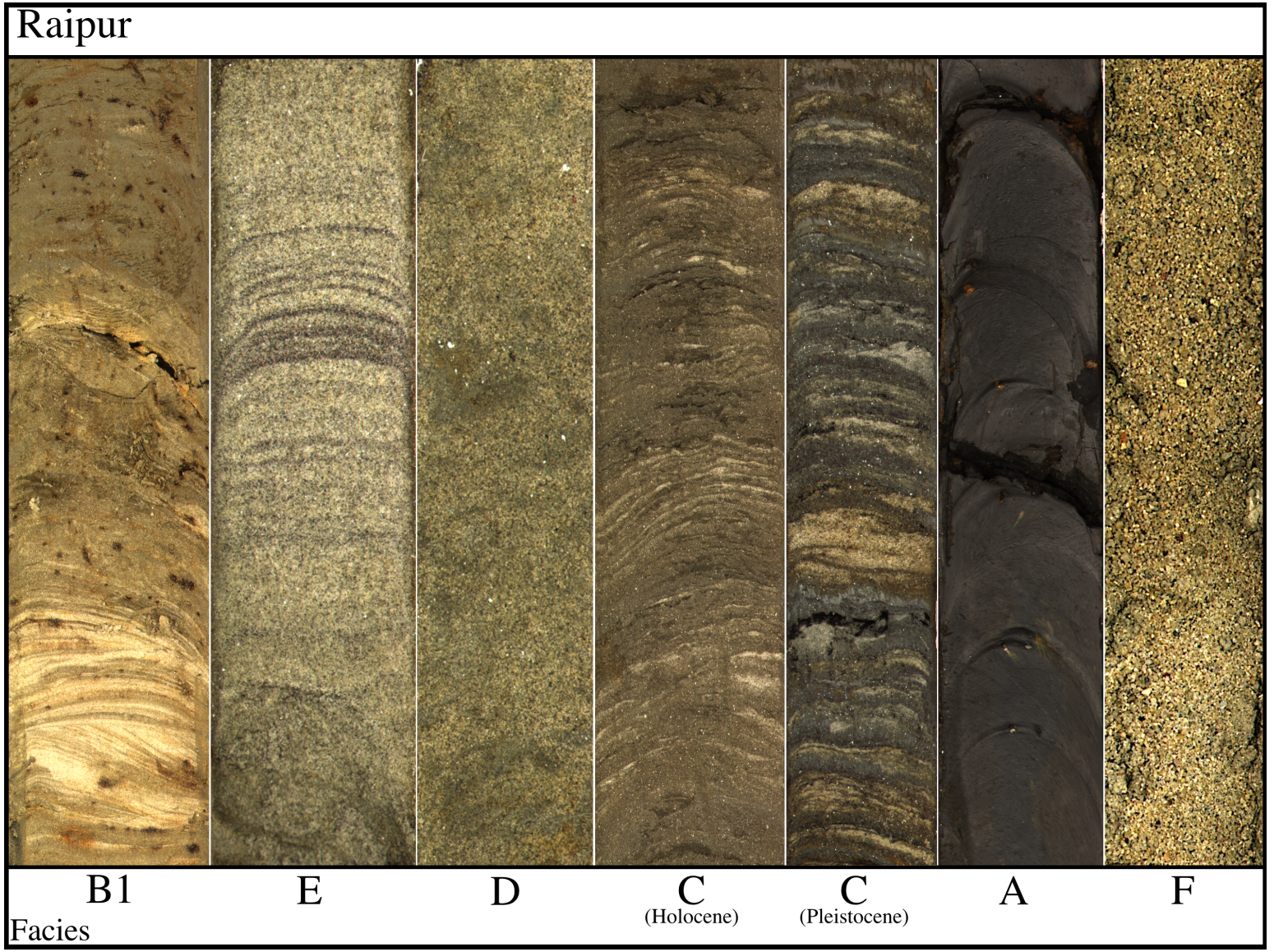

Figure III.3: Digital images of sample facies found at Raipur.

III.3 Sediment Geochemistry

III.3.1 Magnetic Susceptibility

MS is a measure of the degree of magnetization of material in response to an external magnetic field. The inherent ability of sediment to respond to an applied external magnetic field largely depends on the presence of iron oxides (ferromagnetic and antiferromagnetic), and, if present in high enough quantities, other paramagnetic and diamagnetic minerals (Sangode et al., 2007). Environmental magnetism has primarily been applied to provenance and correlation studies in lake sediments (ie: Oldfield, 1991), deep-sea sedimentary cores (ie: Bloemendal et al., 1988), and loess deposits (ie: Jones and Beavers, 1964; Fang et al., 1999). Magnetic susceptibility of sedimentary deposits has been successfully applied as a reliable indicator of changing depositional processes, climate change, sediment provenance, and post-depositional alteration (Verosub and Roberts, 1995). Under the driving forces of climate and tectonics, potential sources of magnetic minerals include source, erosion, transport, depositional processes, depositional components, and post-depositional processes (Verosub and Roberts, 1995).

MS has not previously been applied to G-B delta sediments. Downcore trend in MS for borehole sediments from Magura and Raipur show intervals with significantly increased MS values compared to typical background values of <100 SI. Very high (>1,000 SI) and high (>300 SI) MS values occur in borehole sediments that exhibit little to no discernible variations in color or lithology when compared to adjacent sediments with background values. High MS values occur in weathered sediments

from the Pleistocene lowstand exposure surface. Trends in MS closely follow trends in down-core electric logs as well as proposed stratigraphic and facies analysis.

Table III.2: Range of MS values and classifications.

MS value (SI)	Classification
<100	Background
>300	High
>1,000	Very High

III.3.1.1 Magura

Holocene sediments at Magura exhibit background MS values (>100 SI). A minimal increase in MS occurs between 9-12 and 23-26 m depth associated with fluvial sand facies E2, probably due to mm-scale horizons of heavy minerals commonly caused by hydraulic sorting. High (>300 SI) and very high (>1,000 SI) MS values occur within Pleistocene lowstand exposure sediments. Weathering and exposure leaches major elements, primarily Na, K, and Ca, and enriches sediments in iron oxides, thus producing high MS values within weathered horizons. Two additional MS peaks occur at 50 and 71 m depth within a 63 m sequence of continuous sand facies E. These MS peaks are not visible to the unaided eye when looking at the sediments, and are interpreted as subtle weathering horizons that are also distinguishable using elemental data discussed in the following section. Downcore MS trends allow for increased resolution for stratigraphic analysis of seemingly continuous sand deposition, and can apparently help to identify phases of river abandonment and avulsion where the floodplain cap has not been preserved.

Table III.3: Down-core MS trends for Magura.

Depth (m)	Facies	MS (SI)	Comments
0-26	E1, E2, B1, B2	<100	Slightly elevated MS values within facies E2
26-31	B2, E2	>300	Pleistocene lowstand exposure surface, MS peaks within facies E2
31-120	E2, E3, E4	<100	MS values generally at background levels, high MS peaks at 50 and 71 m represent weathering horizons

III.3.1.2 Raipur

Magnetic susceptibility data for Raipur show strikingly different trends than at Magura. Holocene sediments from 0-40 m have the most variable MS signature, predominantly within facies E and D. Magnetic susceptibility peaks within this interval generally oscillate between 50 and 300 SI, although there are several peaks >300 SI. The highly variable MS signature of Holocene sands at Raipur is possibly the result of preferential bedload deposition at the fluvial mouth, particularly for facies D. As a river enters the fluvial mouth and estuarine environment, it is no longer able to transport heavy minerals within its bedload. As the bedload is deposited, heavy minerals are concentrated within mm-scale horizons by hydraulic sorting. Horizons of dark, mm-scale heavy mineral deposits are more prevalent within facies D and E at Raipur than Magura, and may explain the variable nature of MS data for Raipur Holocene sediments. An alternative explanation for high MS values at Raipur is diagenetic formation of Fe-rich magnetic minerals in coastal environments in the Bengal Basin described by Sangode et al. (2007). Based on elemental data, MS

peaks within facies E and D are likely not subtle weathering horizons as described in Magura.

The Pleistocene lowstand exposure surface has a surprisingly low MS signature despite visibly weathered red and orange sediments. Below the Pleistocene lowstand exposure surface, facies D exhibits a similarly variable MS signature as facies D in the Holocene. For Holocene and Pleistocene sediments, MS values are significantly higher within sand facies than muddy facies. Pleistocene occurrences of facies A and C have MS values which closely resemble MS values within Holocene facies A and C.

Table III.4: Down-core MS trends for Raipur.

Depth (m)	Facies	MS (SI)	Comments
0-40	B1, E, D	50-300	Variable MS values, generally between 50-300 SI, associated with mineralogy of facies E and D.
40-56	C, A	<100	Facies C slightly higher MS values than facies A, possibly caused by the presence of cm-scale interbedded fine sands
56-67	B, E	<100	Pleistocene lowstand exposure surface, MS values surprisingly at background levels except for isolated values around 200 SI
67-78	D	50-300	Variable MS values, generally between 50-300 SI, closely resembles Holocene facies D.
78-120	C, F, A	<100	MS values generally at background values, closely resembles Holocene facies A and C, isolated peaks infrequent within facies F.

III.3.2 Elemental Analysis

A complete compilation of down-core elemental analysis of Magura and Raipur sediments can be found in Appendix A. Sediments with unusually high MS peaks typically exhibit distinctly different elemental composition compared to sediments with background MS values. Geochemical differences are attributed to either:

1. weathering horizons, which are typically enriched in Fe-oxides and depleted in Ca, Na, and K (relative to Al),
2. a hydraulic sorting effect concentrating dense, and often magnetic minerals, into a "placer" like deposit.

Weathering horizons can either be easily recognizable (ie: Pleistocene lowstand exposure surface) or subtle and indistinguishable without supporting data. Weathered sediments are typically enriched in Fe and commonly depleted in Ca, Na, and K, relative to Al. This relationship is complicated by the fact that different source rocks feeding sediment to the G-B margin have different initial concentrations for these major elements, thus making it difficult to determine the degree of weathering simply by direct comparison between samples. Geochemical analysis was performed on four samples from MS peaks at 50 and 71 m. A sample was collected directly from sediments yielding the high MS peaks (samples 73A and 91A), and another from adjacent sediments with background values of MS (samples 73B and 91B). Proposed weathering horizons within facies E at Magura are supported by peaks in MS values, high Fe concentrations, and generally depleted Ca, Na, and K concentrations. Figure III.4 shows the down-core relationship between FeO, Cr, and Zr associated with weathering horizons. See Appendix A for complete geochemical data.

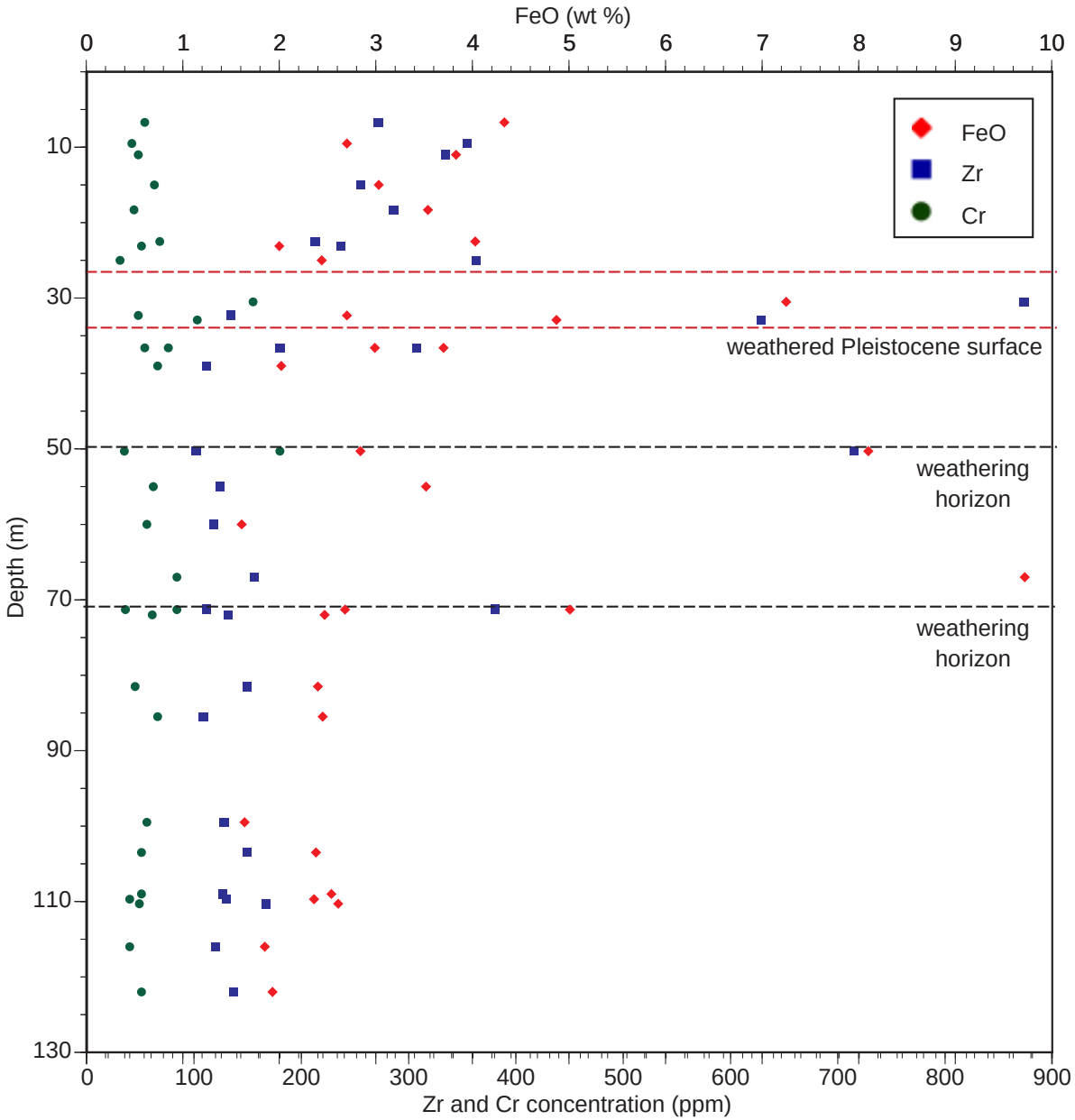

Figure III.4: Down-core FeO, Zr, and Cr concentrations for Magura. Black dashed lines represent apparent weathering horizons at 50 and 71 m based on elemental and MS data. The Pleistocene lowstand and weathering horizon is between 26 to 31 m as represented by the red dashed lines. FeO, Cr, and Zr values generally increase within weathering horizons. Weathering effects tend to enrich sediments in FeO, Cr, and Zr while depleting Ca, Na, and K.

Evidence for "placer" like deposits can be seen in elemental data. Enrichment of Zr is a potential indicator for "placer" like deposits for G-B delta sediments. Zircon grains, containing significant Zr, have a higher specific gravity than sand and feldspar grains, and are typically abundant within horizons concentrated in heavy minerals via hydraulic sorting. It is important to note that weathering can also enrich sediment in Zr as less resistant minerals such as feldspars are depleted while zircon grains are resistant to weathering. Supporting geochemical data is used to identify MS peaks as stratigraphic weathering horizons or simply the effect of hydraulic sorting. Sediments that have undergone a "placer" type influence are typically not depleted in Na, K, and Ca and are typically enriched in Zr, Ni, and Cr. Additionally, "placer" type deposits usually have very high MS values (>1,000 SI) while weathering horizons are generally between 300 and 700 SI. Facies D at Raipur provides the best evidence for "placer" type deposits.

III.3.2.1 Strontium

Sr concentration data show significant down-core trends for borehole sediments from Magura and Raipur. Figure III.5 shows a histogram of Sr concentration data from Magura and Raipur III.5(a) and from all available studies within the Bengal Basin III.5(b). Strontium concentration values fall between 65 and 180 ppm, and data cluster within three major groupings defined as "Low [Sr]" from 65 to 105 ppm, "Intermediate [Sr]" from 115 to 145 ppm, and "High [Sr]" from 155 to 185 ppm (Table III.5).

A strong overall correlation exists between Sr and Ca concentration values (Figures III.6 and III.7). Sediment samples with "Low" Sr concentration values

Table III.5: Sr Concentration Grouping Classifications

[Sr] range (ppm)	Classification
65 - 105	Low [Sr]
115 - 145	Intermediate [Sr]
155 - 185	High [Sr]

typically have low Ca concentrations. Direct sampling from the Tista river, an Eastern Himalayan tributary, establishes a probable sediment source for samples with low Sr and Ca concentrations. This relationship between Sr and Ca was documented by Turekian and Kulp (1956), and found to be more robust in granitic rocks and deep sea sediments, which dominate Ganges and Brahmaputra source lithologies. Additional relationships between Sr and Ca are assumed to exist for individual source lithologies, but additional data is required to further develop trends beyond broad elemental relationships discussed in this study.

The ratio of Al to Si is used as a proxy for grain size because quartz Si is the primary constituent in sand and Al is common within finer grained clays and feldspars. Figure III.8 shows Al/Si versus Sr concentration for Magura and Raipur and Figure III.9 shows Al/Si versus Sr concentration for all available Bengal Basin data, including Magura and Raipur. These data show an apparent lack of correlation between Sr concentration and grain size within the sand grain-size fraction and suggest Sr concentration is a robust provenance indicator for sand-sized sediment and is not dependent on grain size.

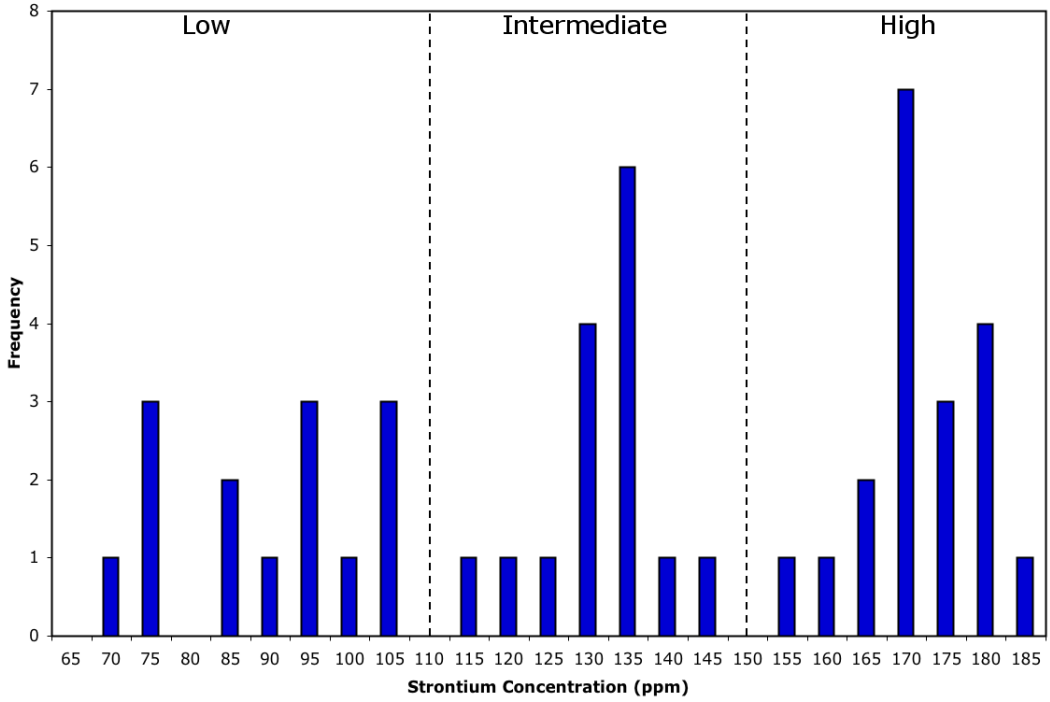

(a) Histogram for Sr concentration data from Magura and Raipur boreholes.

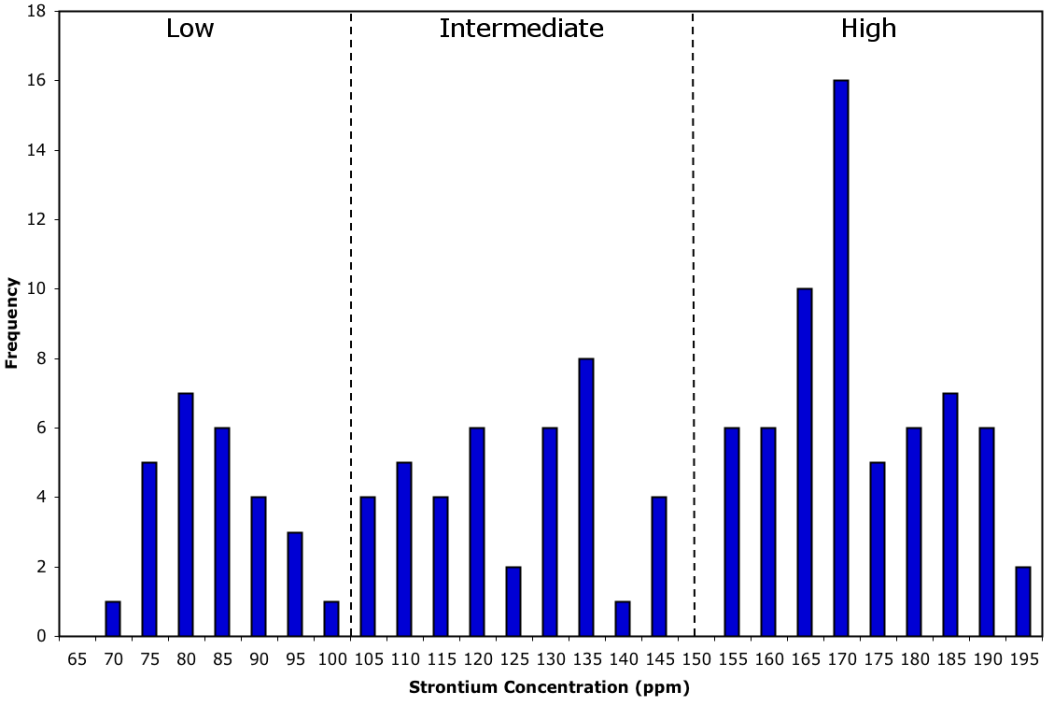

(b) Histogram for all available Bengal Basin Sr concentration data.

Figure III.5: Sr concentration histograms for Magura and Raipur and all available Bengal Basin data. Data are grouped into "Low", "Intermediate", and "High" Sr categories (Table III.5). Data from Youngs et al. (unpublished) and Van Geen et al. (2008).

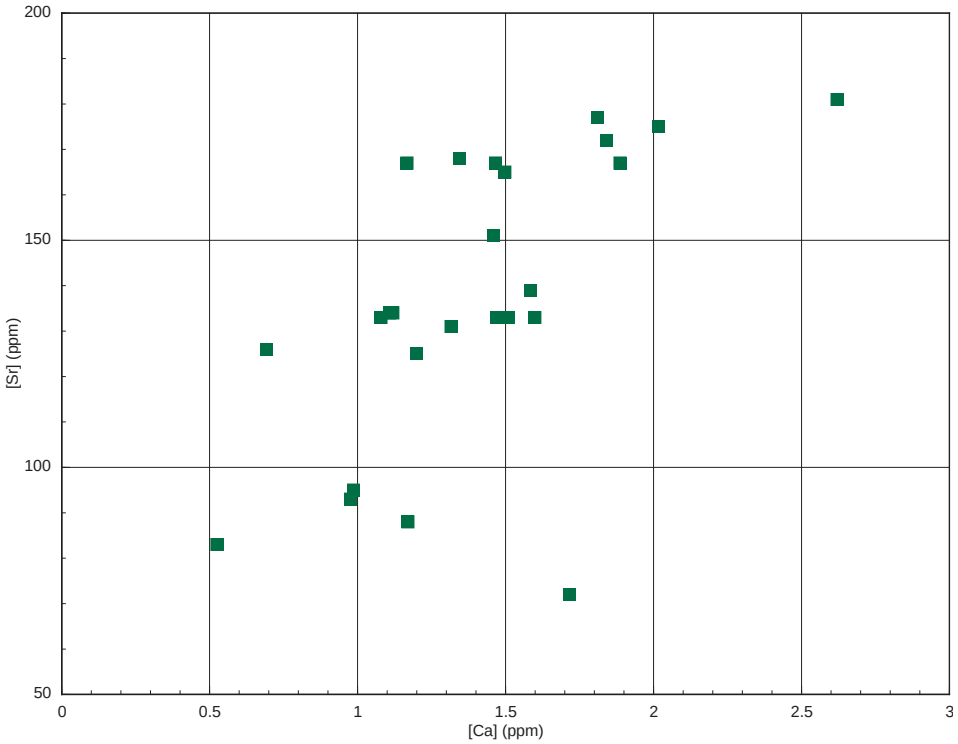

(a) Sr versus Ca concentrations for Magura.

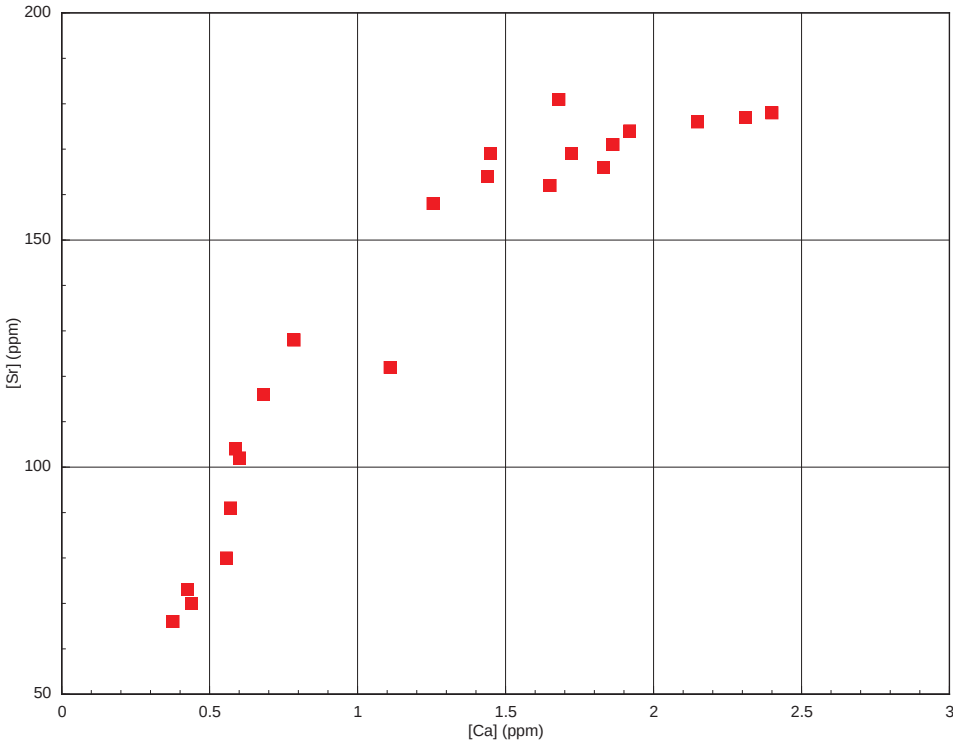

(b) Sr versus Ca concentrations for Raipur.

Figure III.6: Plot of Sr versus Ca concentrations for Magura and Raipur boreholes. Data show a distinct overall correlation between Sr and Ca concentration, probably related to source lithologies.

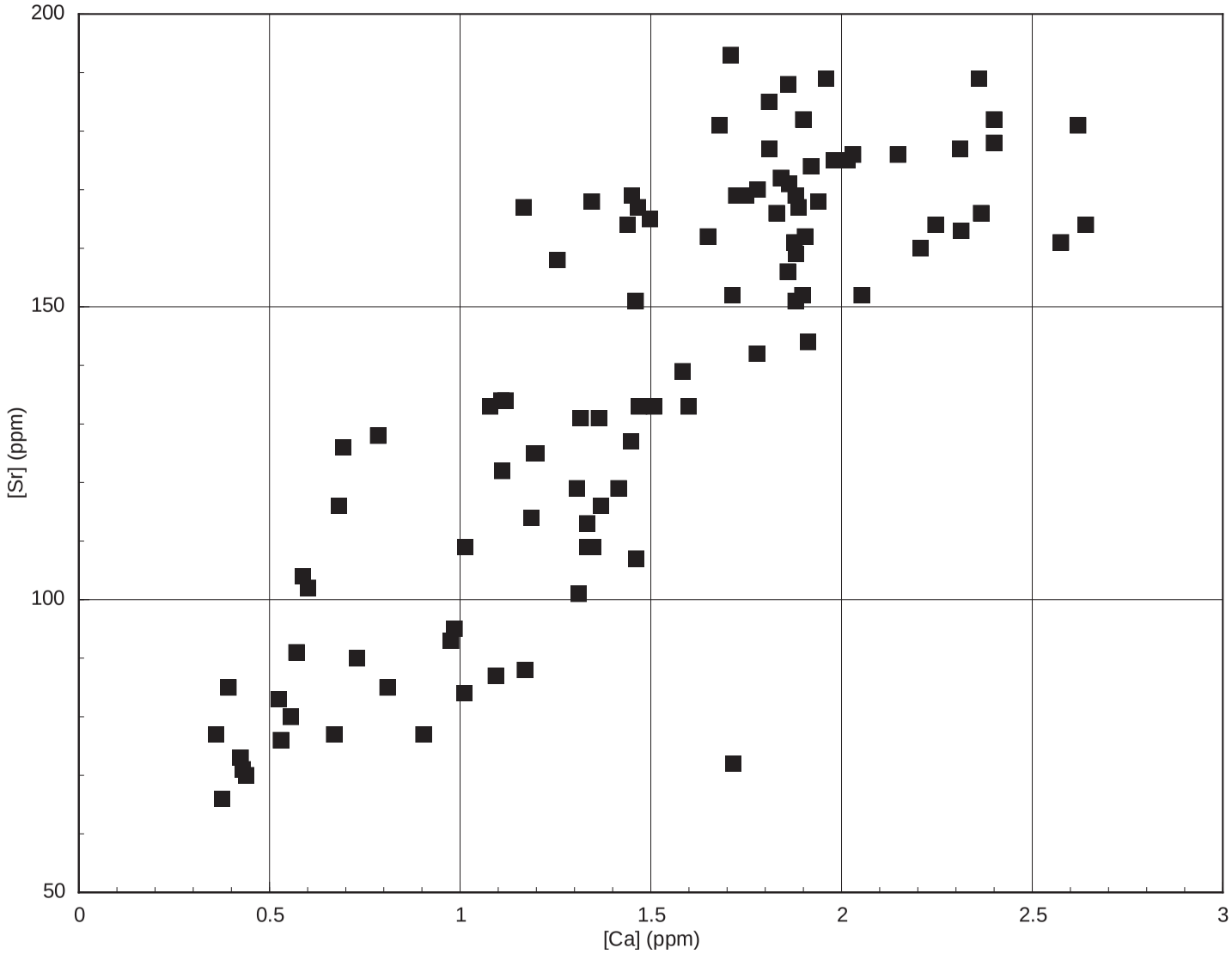

Figure III.7: Plot of Sr versus Ca concentrations for all available Bengal Basin data. Data show a distinct overall correlation between Sr and Ca concentration, probably related to source lithologies. Data from this study, Van Geen et al., 2008, and Goodbred et al., unpublished.

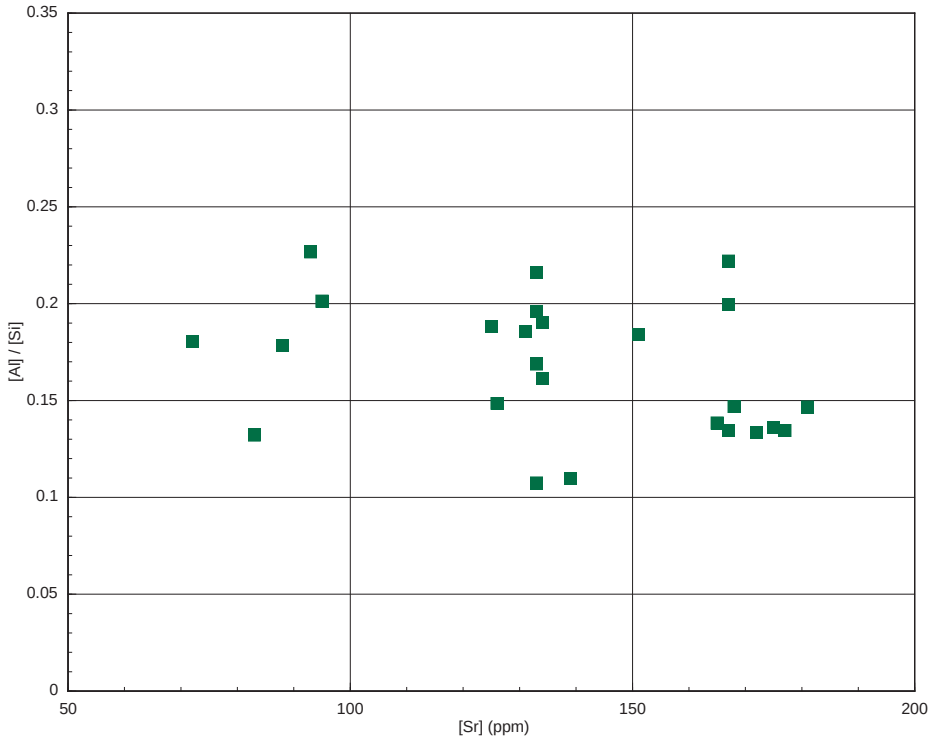

(a) Al/Si versus Sr concentrations for Magura.

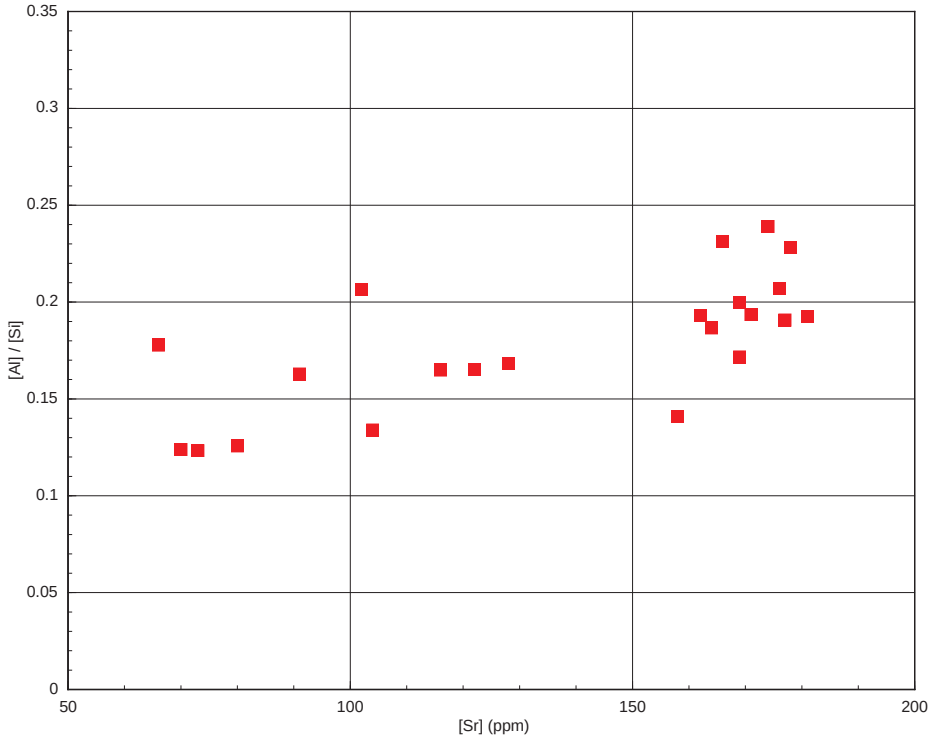

(b) Al/Si versus Sr concentrations for Raipur.

Figure III.8: Al/Si versus Sr concentrations for Magura and Raipur boreholes. Al/Si is used as a proxy for grain size. Note the apparent lack of correlation between grain size and Sr concentration.

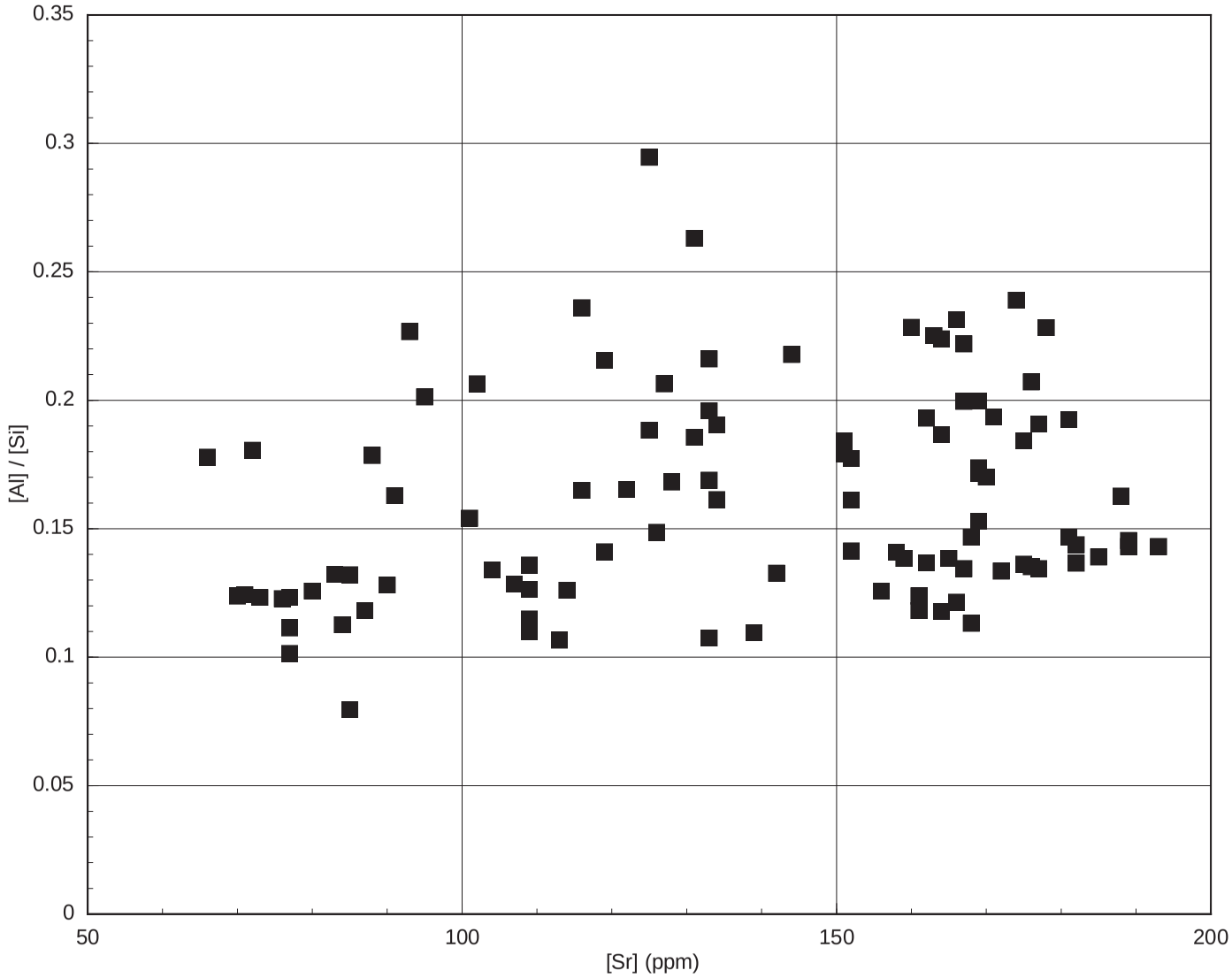

Figure III.9: Plot of Al/Si versus Sr concentrations for all available Bengal Basin data. Al/Si is used as a proxy for grain size. Note the apparent lack of correlation between grain size and Sr concentration. Data from this study, Van Geen et al., 2008, and Goodbred et al., unpublished.

III.4 ^{14}C Data, Accretion Rates, and Sea-level

III.4.1 Magura

Two radiocarbon dates were obtained from organic material collected from the Magura borehole (Table III.6). A white shell, 2 cm across, was sampled from a depth of 25 m and produced a calibrated date of 2,580 yr B.P. A 2 cm plant fragment embedded in unoxidized sand surrounded by oxidized clay was sampled from a depth of 28 m and produced a calibrated date of 12,964 yr B.P. The gastropod shell fragment has a δ^{13}C value of -5.88, which is consistent with measured terrestrial gastropod values (Stuiver and Polach, 1977). The plant fragment had a δ^{13}C of -14.67, which is consistent with terrestrial C4 grasses adapted to an arid environment (Stuiver and Polach, 1977).

Despite the close proximity of radiocarbon samples within the borehole, an accurate accretion rate could not be obtained for Magura. The two dates were obtained only 3 m apart, but produced dates with a difference of more than 10,000 years. The shell fragment was sampled from Holocene facies E2. The small root sampled at 28 m was removed from highly oxidized silt-dominated sediment (facies B2) from the Pleistocene lowstand exposure surface and likely represents a vegetated surface at Magura prior to active Holocene sedimentation. These data suggest Magura may have (1): undergone a long period of non-deposition, or (2): the main river channel regularly occupied the region and actively eroded Holocene sediments deposited before 2,580 yr B.P. Based on where the young age at 25 m plots against sea-level (Figure III.10), the most likely scenario is active erosion before 2,580 yr

B.P. Also, while 25 m is deep, it is not an uncommon depth for the Ganges and Brahmaputra rivers.

III.4.2 Raipur

Three radiocarbon dates were obtained from organic material removed from the Raipur borehole (Table III.6). Black disseminated plant material was sampled at a depth of 40 m from facies A and produced a calibrated date of 9.374 yr B.P. A large reddish-colored root, likely from mangrove species, approximately 5 cm in length with a vertical orientation, was sampled at a depth of 50.5 m from facies C and produced a calibrated date of 10,467 yr B.P. An organic rich, black, stiff clay was sampled at a depth of 53 m from facies A and produced a calibrated date of 10,663 yr B.P. δ^{13}C values range from -26.19 and -28.52, and are consistent with C3 plant material (Stuiver and Polach, 1977).

Three radiocarbon dates from Raipur give an approximate accretion rate of 1 cm/yr over nearly 1,300 yr. Raipur data correspond with the global eustatic sea-level curve (Figure III.10). These data combined with the stratigraphic location of radiocarbon samples support the idea that delta initiation began soon after the Younger Dryas, around 11,000 yr B.P., and delta sedimentation kept pace with rapidly rising sea-level with limited net vertical movement since at least the early Holocene (Goodbred and Kuehl, 2000b; Goodbred, 2003).

Table III.6: Summary of radiocarbon dates.

Lab Sample No.	Borehole	Depth (m)	Material	δ^{13}C	Radiocarbon age (yr BP ± error)	Calibrated age (cal yr BP)	2σ age range (cal yr BP)
OS-65541	Magura	25	gastropod	-5.88	2,490 ± 60	2,580	2,457-2,725
OS-66122	Magura	28	plant	-14.67	11,000 ± 300	12,964	12,778-13,218
OS-64444	Raipur	40	plant	-28.51	8,350 ± 40	9,374	9,275-9,472
OS-64445	Raipur	50.5	root	-28.52	9,280 ± 40	10,467	10,369-10,577
OS-66476	Raipur	53	bulk clay	-26.19	9,430 ± 100	10,663	10,515-10,785

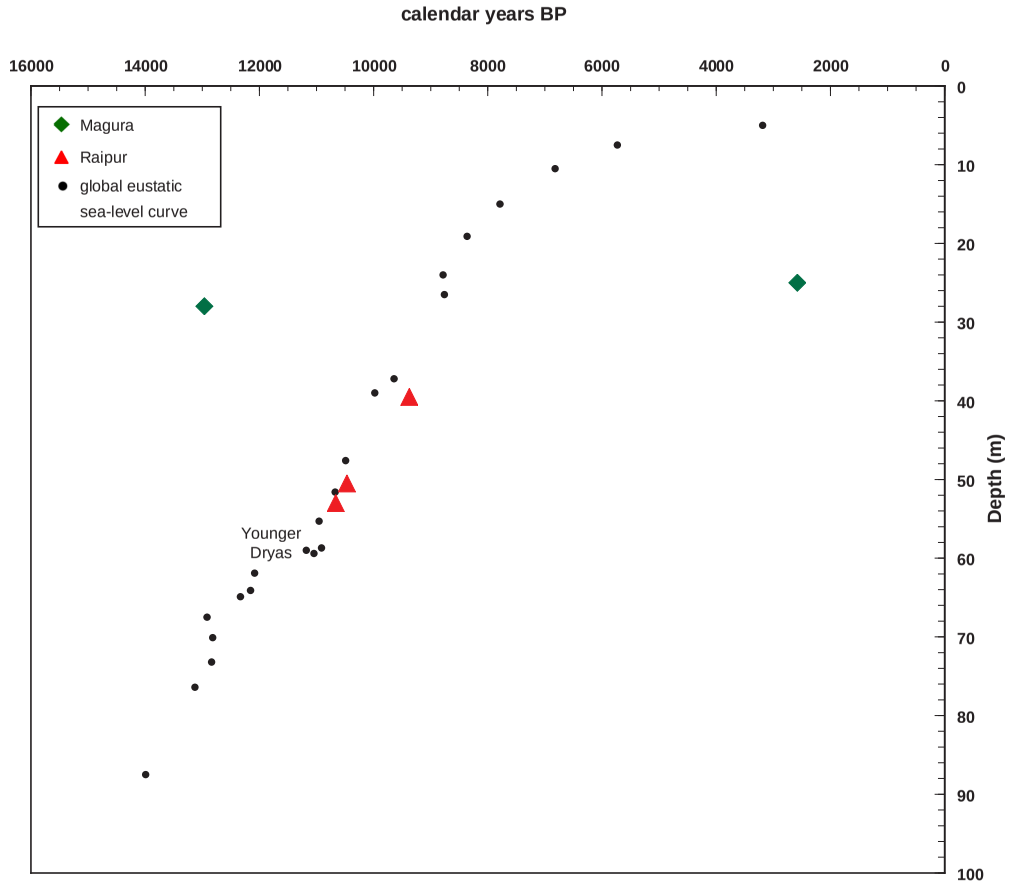

Figure III.10: Plot of calibrated radiocarbon ages against elevation compared with global eustatic sea-level. Raipur data plot along the global eustatic sea-level curve and suggest that delta sedimentation kept pace with rapidly rising sea-level with limited net vertical movement during the early Holocene following delta initiation after 11 ky B.P. Two data points from Magura represent the Pleistocene low-stand surface and late Holocene highstand, and do not plot along the eustatic sea-level curve. Large gaps in the global eustatic sea-level curve are interpreted as periods of immense freshwater discharge to the global ocean (after Fairbanks, 1989; Edwards et al., 1993).

III.5 Stratigraphy

Detailed down-core stratigraphic analysis is presented for Magura and Raipur based on facies, grain size, MS trends, and geochemical trends. Stiff, orange to brown sediments found in both boreholes are interpreted as weathered paleosols of the Late Pleistocene lowstand. Weathered paleosols found throughout the Bengal Basin divide the stratigraphy into Holocene and Pleistocene sequences. Relative paleoshoreline and river position contribute significantly to the very different stratigraphy and environmental interpretations between the two boreholes. Magura is dominated by sequences of fluvial sands with silty floodplain caps while Raipur shows considerable coastal marine influence combined with fluvial processes during the late Pleistocene and Holocene.

III.5.1 Magura

Borehole sediments from Magura reveal a relatively simple sand and mud stratigraphy containing stacked sequences of facies E and B. A general stratigraphic profile for Magura is summarized in Table III.7(a), and a detailed stratigraphic column is presented in Figure III.11.

The Holocene sequence preserved at Magura is approximately 26 m thick and contains silt-dominated deposits (facies B1 and B2), bedded fine sands (facies E1), and unbedded sands (facies E2). Directly overlying the Pleistocene lowstand exposure surface is the fine fluvial sand facies E2. Deposition of facies E1, finely interbedded fine sands with well-developed cross-bedding, from 14-23 m indicates the main river channel avulsed away from Magura during this period. The flow regime necessary

to deposit very fine to fine sand as mm-scale laminae suggests Magura was occupied by a secondary, lower flow channel at this period. A thin floodplain cap, facies B2, directly overlies facies E1 and represents further abandonment and associated low energy conditions. The river returned to Magura over the interval from 9-12 m before avulsing a final time, leaving an abandoned silty floodplain cap.

The Pleistocene lowstand exposure surface occurs at 26 m depth. Pleistocene sediments from 26 to 123 m depth consist of two major sand units (facies E) separated by a thin floodplain mud (facies B) at 94-95 m depth. The upper (26-94 m) and lower (95-123 m) Pleistocene sand units are dominated by sub-facies E2, E3, and E4. Sub-facies E4 occurs five times within the lower Pleistocene sand unit while only occurring three times within the upper Pleistocene sand unit. The upper Pleistocene sand unit can be further broken down into three sub-units divided by two subtle weathering horizons at 50 and 71 m depth. These weathering horizons are not visible to the naked eye and were initially recognized by peaks in MS (Figure III.11) and supported by elemental analysis. Additionally, the weathered Pleistocene lowstand exposure surface has similar trends in sediment geochemistry and MS as the two proposed exposure surfaces (Figure III.4).

III.5.2 Raipur

Stratagraphic analysis at Raipur shows two remarkably similar coarsening upward, stacked, sequences separated by the Pleistocene lowstand exposure surface at 56 m depth. A general stratigraphic profile for Raipur is summarized in Table III.7(b), and a detailed stratigraphic column is presented in Figure III.12.

The Holocene sequence preserved at Raipur is approximately 56 m thick.

Holocene sediments are stacked in a coarsening upward sequence comprised of muddy coastal plain deposits (facies A), followed by tidal rhythmites (facies C), estuarine and distributary-mouth channel muddy sands (facies D), and fine fluvial sands (facies E) capped by abandoned floodplain and overbank deposits (facies B). Holocene deposition at Raipur is dominated by coastal and marine-influenced environments.

The Pleistocene sequence contains a coarsening upward sequence remarkably similar to the overlying Holocene sequence. A distinguishing difference is the addition of coarse sand and gravel (facies F) inter-bedded within tidal rhythmite deposits (facies C). The coarse sands of facies F are the coarsest sands from either borehole, and the occurrence of discrete, pulsed inputs of coarse sand and gravel within tidal rhythmite deposits (facies C) is surprising and unusual. This facies has not been previously identified at the G-B margin, as previous studies typically stopped investigation at the Pleistocene lowstand exposure surface (known locally as the "Dupi Tila"). Interestingly, the gravels in Magura occur at similar depths as the coarse sands and gravels at Raipur.

Pleistocene coastal sediments preserved at Raipur likely represent deposition during stage 3 or 5e sea-level highstand. The stage 3 highstand occurred approximately 60 ky B.P. and the stage 5e highstand occurred approximately 125 ky B.P. Deposition during stage 3 assumes little to no subsidence while deposition during stage 5e assumes a slow subsidence rate of 0.5 mm/yr.

Table III.7: Generalized stratigraphy for Magura (a) and Raipur (b).

(a) **Magura**

Depth (m)	Facies	Description
1 - 9	B1	bedded silty floodplain
9 - 12	E2	fine fluvial sands
12 - 14	B2	silty floodplain
14 - 23	E1	bedded, fine fluvial sands
23 - 26	E2	fine fluvial sands
26 - 28	B2	silty floodplain (highly oxidized)
28 - 31	E2	fine fluvial sands (oxidized)
31 - 94	E2, E3, E4	fine to coarse fluvial sands and gravel
94 - 95	B2	floodplain mud
95 - 123	E2, E3, E4	fine to coarse fluvial sands and gravel

(b) **Raipur**

Depth (m)	Facies	Description
1.5 - 6	B1	bedded silty floodplain
6 - 26	E	clean fluvial fine sands
26 - 40	D	estuarine and distributary-mouth channel
40 - 53	C	tidal rhythmites
53 - 56	A	muddy coastal plain
56 - 57	B	highly oxidized silty floodplain
57 - 67	E	highly oxidized fluvial sands
67 - 78	D	estuarine and distributary-mouth channel
78 - 98	C	tidal rhythmites
98 - 103	F	coarse sand
103 - 115	C	tidal rhythmites
115 - 116	F	coarse sand
119 - 122	A	muddy coastal plain

Magura

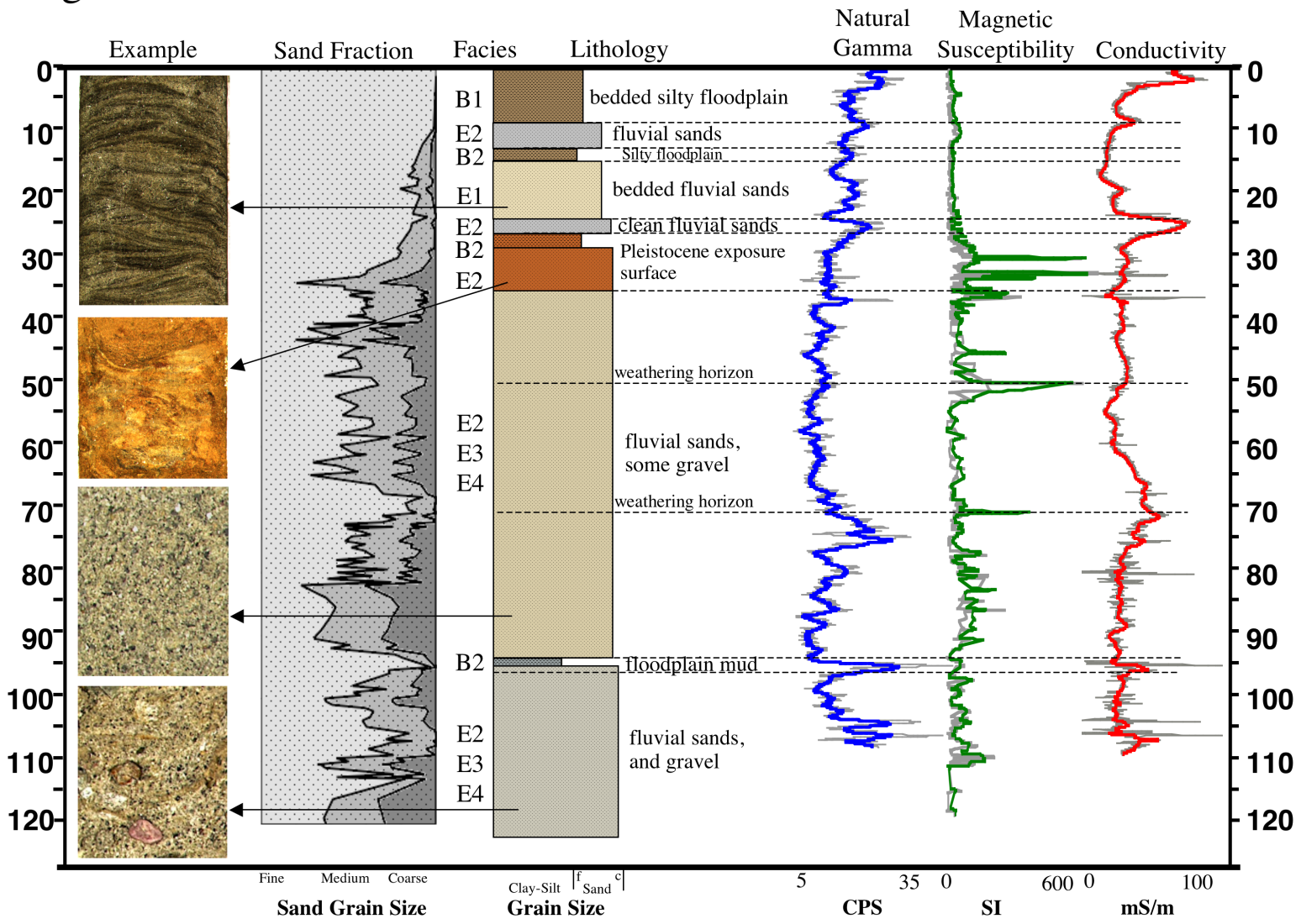

Figure III.11: Compiled stratigraphy, grain size, facies, and electric logs for Magura.

Raipur

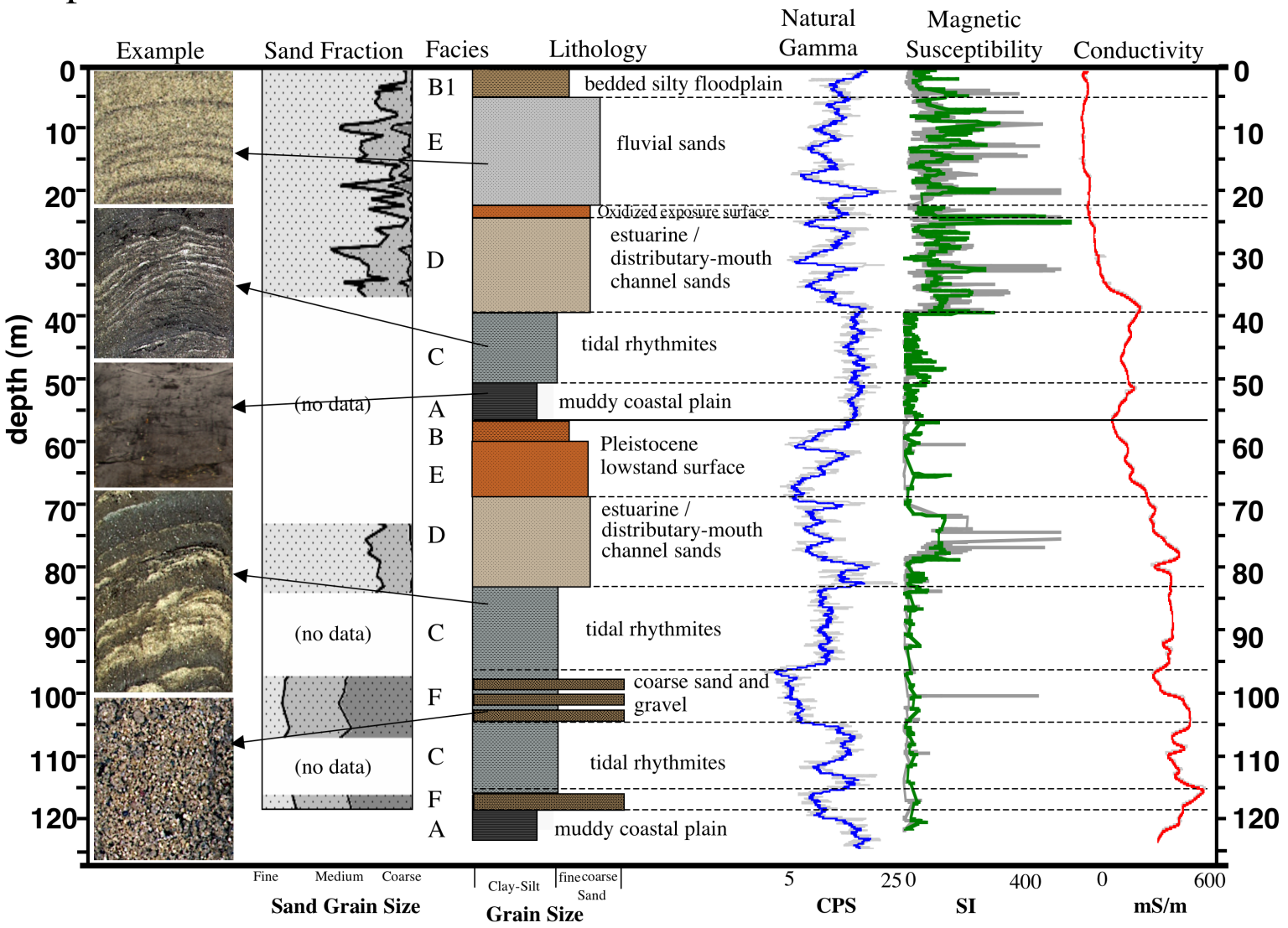

Figure III.12: Compiled stratigraphy, grain size, facies, and electric logs for Raipur.

CHAPTER IV

DISCUSSION

IV.1 Sediment Provenance

Borehole evidence from Magura and Raipur, Bangladesh provide new insight into the processes and mechanisms responsible for the depositional history of the G-B margin. A multiple-proxy sedimentological approach to delta evolution provides stratigraphic, paleoenvironmental, and provenance data which yield evidence for large event deposition, river abandonment and avulsion, and shifting dominant river input to the G-B delta system. Results from this study are consistent with previous findings of early delta initiation around 11,000 ky B.P. and an immense sediment load keeping pace with rapid sea-level rise during the Holocene (Goodbred and Kuehl, 1999, 2000a; Goodbred, 2003).

Data from this study indicate that the G-B delta is not simply an amalgam of delta sediments, but, rather, is made up of stacked units with distinct lithologies deposited from at least three provenance sources. For the first time, phases of river abandonment and avulsion with the G-B delta are identified with the aid of MS and elemental data used to identify weathering horizons for sequences of continuous sand deposition. Two such weathering horizons were identified at Magura that would have otherwise gone unrecognized. Geochemical data suggest the Ganges and Brahmaputra were separate rivers throughout the Late Pleistocene and early Holocene, and not conjoined as in the modern example. Geochemical data also

suggest the Tista river, and potentially other Eastern Himalayan tributaries, have been important sediment sources to the G-B margin during Late Quaternary delta development.

Evidence for the importance of Eastern Himalayan tributaries, particularly the Tista river, to delta development is a new idea proposed by this study. Geochemical data from specific sand facies within Magura (E4) and Raipur (F) closely match geochemical data generated from direct sampling of Tista river fan sediments by Van Geen et al. (2008). Additionally, sediments matching the Tista geochemical fingerprint are significantly coarser grained than typical Ganges and Brahmaputra sediment. At Raipur, Facies F appears as discrete, pulsed inputs of coarse sand with lithic gravel interbedded within sediments deposited in a tidally influenced coastal environment (Facies C). Historically, the Tista river is known to have avulsed between the main trunks of the Ganges and Brahmaputra, and our data record several potential avulsions during the Late Pleistocene and early Holocene.

Facies F from Raipur and, with less supporting evidence, facies E4 from Magura, are interpreted as the product of event deposition originating from the Himalaya. Facies F and E4 occur at similar depths, although facies E4 has less supporting evidence to support the event deposition hypothesis, and may be simply the result of reworking and deposition of local alluvial fan material during the lowstand. Facies F occurs as discrete, pulsed inputs within a tidally-dominated coastal environment with no reasonable local source for input of coarse material. It is difficult to explain the presence of very coarse sands and gravels seen within facies F at a coastal environment

without invoking a depositional event with a significantly higher capacity for coarse bedload transport than seen today.

Geochemical provenance signatures discussed in this section are summarized in Tables IV.2 and IV.3. Strontium concentrations plotted with depth are illustrated in Figure IV.1. For complete geochemical data from Magura, Raipur, and all available data from Bengal Basin boreholes see Tables A.2 through A.7 in Appendix A. Borehole locations discussed in this section are presented in Figure II.1.

Down-core sediment provenance for Magura and Raipur is determined using trends in Sr concentration. Based on these data and data discussed in Figures I.6 and III.5, three major sediment sources to the G-B margin are defined by "Low", "Intermediate", and "High" Sr concentrations (Table IV.1).

- **Brahmaputra:** Brahmaputra sediments (dominated by Tibetan lithologies) are characterized by "High" Sr concentrations (>155 ppm),
- **Ganges:** Ganges sediments are characterized by "Intermediate" Sr concentrations (115-145 ppm),
- **Eastern Himalayan:** Eastern Himalayan (ie: Tista) sediments are characterized by "Low" Sr concentrations (<105 ppm).

Table IV.1: Sr Concentration Grouping Classifications

[Sr] range (ppm)	Classification	Provenance
65 - 105	Low [Sr]	Eastern Himalayan (ie: Tista)
115 - 145	Intermediate [Sr]	Ganges
155 - 185	High [Sr]	Brahmaputra

The Brahmaputra Sr fingerprint is the most clearly defined provenance relationship, with numerous borehole data and direct sampling of modern Brahmaputra

river sediment. The dominant sediment source of the modern Brahmaputra is from its upper reaches in the Himalaya above Assam. The geochemical signature of these sediments is dominated by Tibetan lithologies with high Sr concentrations and lower $^{87}Sr/^{86}Sr$ values compared to Himalayan lithologies.

The range of Sr concentration for the Ganges is less well constrained because of possible heterogeneity within tributaries and less supporting elemental data from borehole sediments believed to be Ganges-dominated. Direct sampling of Ganges river sediments show a potentially greater range of Sr concentration than proposed in this study, with a greater abundance of low values that may reflect the finer-grained suspended sediments that were measured as compared to the sand of this study (France-Lanord, personal communication).

Direct sampling of Tista river fan sediments indicates Eastern Himalayan tributaries are characterized by "Low" Sr concentrations. However, the Tista river is not well studied and there is limited published data, therefore sediment provenance defined by "Low" Sr concentration relies more heavily on additional supporting evidence rather than direct borehole evidence. In this case, these Eastern Himalayan tributary sediments are also distinguished by high SiO_2 concentrations (>80 wt%) and low Ca and Mg concentrations (<0.75 ppm) when compared to Brahmaputra and Ganges sediments. Furthermore, sediments with an Eastern Himalayan geochemical signature often occur as coarse grained, discrete, pulsed inputs within Ganges and Tibetan sediments.

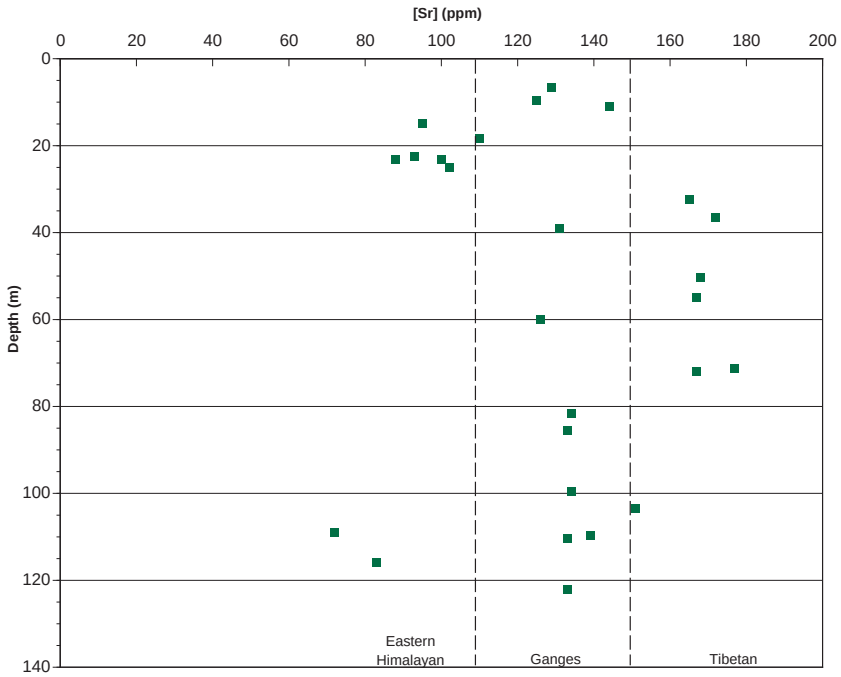

(a) Magura

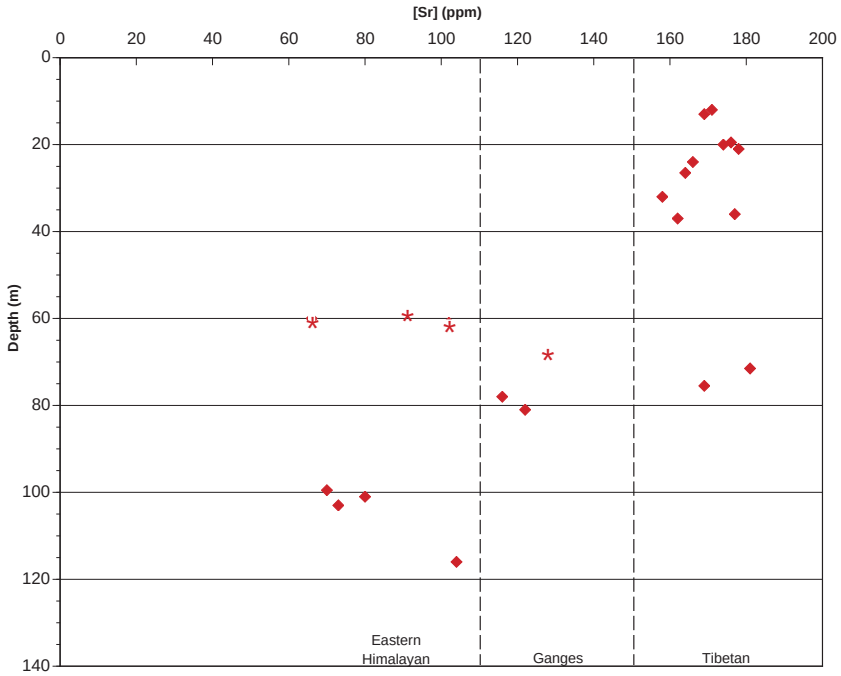

(b) Raipur

Figure IV.1: Down-core Sr concentrations for Magura and Raipur. Dashed lines distinguish Sr provenance groups outlined in Table III.5. The four starred samples from Raipur near 60 m were sampled from the highly weathered Pleistocene exposure surface and likely have low Sr concentrations due to weathering effects and probably do not reflect sediment provenance.

IV.1.1 Magura

Within the stratigraphy at Magura, three major provenance signals are revealed by down-core variation in Sr concentration data. Figure IV.1(a) illustrates these data grouped into "High", "Intermediate", and "Low" Sr concentrations as a function of depth. "High" Sr values occur between 30 and 80 m, "Intermediate" Sr values dominate above 30 m and below 80 m, and scattered "Low" Sr values occur just below 20 m and again near 115 m. These data suggest that Magura has received sediment input from three distinct sources since the Late Pleistocene.

IV.1.1.1 0-30 m

Between 0 and 30 m, Holocene sediments are dominated by "Intermediate" Sr concentration values, although several samples plot within the range of "Low" Sr concentration. Within this interval, eight sediment samples from facies E have a Sr concentration range from 88 to 144 ppm with an average of 111 ppm. Geochemical data, combined with detectable concentrations of carbonate material (unique to Ganges sediments), indicate sediments from 0 to 30 m were deposited under the influence of the Ganges river. Data suggest that the entire Holocene sequence that is preserved is one continuous channel sequence. Unlike the Pleistocene record, there is little indication that the Brahmaputra has influenced this site during the Holocene.

The Tista river has historically avulsed between the Ganges and Brahmaputra rivers through the uplifted Barind Tract (Figure II.1). A general decrease in down-core Sr concentrations from "Intermediate" to "Low" values below 15 m suggests either a waning influence of the Tista moving towards the modern, or a shift in

Table IV.2: Down-core Sr concentration provenance trends for Magura. Data provide evidence for three distinct sediment sources (Ganges, Brahmaputra, and Eastern Himalayan Tributaries) through the Late Plestocene and Holocene.

Depth (m)	Facies Sampled	Sr Average (ppm)	Sr Range (ppm)	# of samples	Provenance
0-30	E	111	88-144	8	Ganges-dominated; with Eastern Himalayan influence below 15 m
30-80	E	159	126-177	8	Brahmaputra-dominated; two samples with Ganges geochemical signature
80-125	E	137	133-151	7	Ganges-dominated; two samples with Eastern Himalayan signature

provenance within the Ganges catchment itself. Supporting sedimentological (ie: grain size, facies) and geochemical data (ie: Ca, Mg) for these samples is not suggestive of Eastern Himalayan influence. This gradual shift in Sr concentration may simply reflect a shifting source from heterogeneous Ganges tributaries.

IV.1.1.2 30-80 m

Below the Pleistocene lowstand exposure surface, from approximately 30 to 80 m, Pleistocene sediments exhibit a strong Brahmaputra geochemical signature with "High" Sr concentrations. Strontium concentration ranges from 126 to 177 ppm with an average value of 159 ppm. Not including the two lowest Sr concentration samples, six samples over the interval from 30 to 72 m have a range of Sr concentrations from 165 to 177 ppm and an average of 169 ppm. These high Sr concentration values are unique to Tibetan lithologies and strongly suggest deposition by the Brahmaputra.

Despite being dominated by Ganges input in the Holocene, the Brahmaputra river was the dominant influence during the Late Pleistocene, depositing several channel sequences. It is perhaps unexpected to find major Brahmaputra influence at this location, west of its modern course and the structurally elevated Barind tract (Figure I.2). This may suggest that during the Pleistocene lowstand, the course of the Brahmaputra was controlled by the position of the Swatch of No Ground canyon, which aligns well with the modern course and the Magura drill site (Figure II.1).

Within the interval of 30-80 m, two out of eight samples have Sr concentrations less than 165 ppm. One sample at 60 m has a Sr concentration of 126 ppm, a high SiO_2 concentration (80 wt%), low Ca and Mg concentrations, and has >20% coarse sand fraction and gravel. Geochemical data and grain size data closely match results from

direct sampling of Tista river sediments, and suggest possible influence from Eastern Himalayan tributaries. Although it is known that the Tista river can avulse between the Ganges and Brahmaputra rivers, it is difficult to identify a provenance shift based on one sample. A second sample at 39 m has a similarly low Sr concentration, but other sediment characteristics trend towards typical Ganges and Brahmaputra sediments and do not suggest Eastern Himalayan influence. These results suggest that despite dominance by a particular fluvial system, other rivers deliver episodic inputs, perhaps via distributary channels during major flood years.

IV.1.1.3 80-125 m

Within the interval from 80 to 125 m, samples fall within the "Intermediate" category of Sr concentration values with the exception of two samples. Sr concentrations range from 133 to 151 ppm with an average of 137 ppm, and sediments are interpreted to be deposited under Ganges influence. These data suggest the Ganges has been the primary influence at Magura through the Late Pleistocene and Holocene except for the latest Pleistocene deposits from 30-80 m, which indicate temporary abandonment by the Ganges and avulsion and occupation by the Brahmaputra. Two samples with "Low" Sr concentrations stand out from Ganges sediments.

Within the interval from 80 to 125 m two samples have significantly lower Sr concentration values of 72 ppm at 109 m and 83 ppm at 116 m. The elemental composition and facies associations (E3 and E4) of these samples suggests periodic influence from Eastern Himalayan tributaries similar to what is seen in the Holocene sequence. Based on their physiographic locations, the Tista and other Eastern

Himalayan tributaries have the capability to transport coarse sands and gravel to the Bengal Basin. The Tista river is highly proximal to the Bengal Basin with an actively building alluvial fan that intersects the northern portion of the delta. During low sea-level of the Pleistocene, the Tista was sufficiently close to the margin and canyon that its gradient was likely steepened significantly, allowing it to deliver coarser material further into the Bengal Basin. However, there is no published data which suggests this is the case, and similar coarse deposits are not typically interbedded with other lowstand deposits.

IV.1.2 Raipur

Within the stratigraphy at Raipur, three major provenance signals are revealed by down-core variation in Sr concentration. Figure IV.1(b) shows down-core Sr concentration data grouped as "High", "Intermediate", and "Low". The highest Sr values occur in the top 40 m and the lowest Sr values occur between 90 and 120 m depth. Like at Magura, Raipur sediments contain the entire range of Sr concentrations. For Holocene and Late Pleistocene sediments, Raipur is generally dominated by Brahmaputra influence, which is expected given its geographic location. However, even here, there is strong evidence for discrete, pulsed inputs of Eastern Himalayan sediments during the Late Pleistocene. From 60-80 m, six samples with "Low" and "Intermediate" Sr concentration values are not likely to be the result of Ganges or Eastern Himalayan influence. Four samples from the highly weathered Pleistocene lowstand exposure surface are depleted in Sr, probably due to weathering effects. Other samples with "Intermediate" Sr values were measured from fine sands

within tidal rhythmites (facies C), and likely represent a mixed geochemical signal from tidal reworking of shelf sediments.

IV.1.2.1 0-40 m

Holocene sediments display strictly Brahmaputra influence with a range of Sr concentrations from 158 to 178 ppm and an average of 170 ppm for 10 samples over a 25 m interval. All of the Holocene Sr concentration values were from fine sands of facies E and D. These data are consistent with Raipur's geographic location in the eastern region of the G-B delta. There is no evidence that the Ganges has migrated farther east than its present location, and clay mineralogy and radiocarbon data from the lower delta plain suggest it has been migrating towards its present location from the west since the Pleistocene (Allison et al., 2003). During the Holocene Raipur was dominated by Brahmaputra influence with little evidence for input from any other provenance source.

IV.1.2.2 40-90 m

The entire 0-90 m interval is likely to have received Brahmaputra sediment flux, but the Sr signal is apparently obscured by weathering effects and tidal reworking of shelf sediments between 40-90 m. Despite a large range of Sr concentrations, I suggest Brahmaputra influence for Holocene and Late Pleistocene sediments within the interval from 40-90 m. Weathered samples and fine sands within tidal facies C are biased towards lower Sr concentrations and do not represent overall river behavior for this site. Future provenance investigations using Sr concentration should be focused

Table IV.3: Down-core Sr concentration provenance trends for Raipur. Raipur is dominated by Brahmaputra influence with dicrete, pulsed inputs of Eastern Himalayan sediments. Samples from fine sand within tidal facies C have "Intermediate" Sr concentrations probably due to sediment mixing and reworking by tidal processes.

Depth (m)	Facies Sampled	Sr Average (ppm)	Sr Range (ppm)	# of samples	Provenance
0-56	E, D	170	158-178	10	Brahmaputra-dominated
58-67	E	97	66-128	4	Inconclusive; highly weathered samples
70-76	D	175	169-181	2	Brahmaputra-dominated
78-81	C	125	123-126	2	Mixed signal; sampled from tidal rhythmites
99-120	F	82	70-104	4	distinct Eastern Himalayan signature

on unweathered sands with background MS values to reduce any possible geochemical bias.

Two samples from 70 and 76 m indicate Brahmaputra influence identical to the provenance signature seen between 0-40 m. Sr concentration data from the Pleistocene lowstand exposure surface produced inconclusive provenance results. Weathered samples were depleted in major elements typically associated with weathering (Ca, Na, and K), and low Sr concentration values are probably the direct result of weathering effects. These samples trended towards a Eastern Himalayan provenance signature, but are more likely to have been deposited under Brahmaputra influence and altered by post-depositional processes. Fine sands from tidal facies C yielded an average Sr concentration of 119 ppm, and probably indicate a mixed provenance signal because of syndepositional reworking of shelf sediments by tidal influence and is probably not a true provenance signal.

IV.1.2.3 90-120 m

All of the Sr concentration data generated between 90-120 m is from facies F, and have "Low" Sr concentration values. Facies F is comprised of coarse grained, poorly sorted sand and gravel that occurs as discrete, pulsed inputs within Ganges and Brahmaputra sediments. Four samples have a Sr concentration range from 70 to 104 ppm and an average of 82 ppm. Elemental analysis from facies F closely resembles that of sediment sampled directly from Tista river fan sediments (Van Geen et al., 2008). These sediments are characterized by "Low" Sr concentrations, typically between 70 and 90 ppm, SiO_2 concentrations >80 wt%, and depleted concentrations Ca and Mg compared to typical Ganges and Brahmaputra sediments.

We suggest Facies F is the result of increased Eastern Himalayan tributary influence. In contrast, the Tibetan source area dominates the geochemical signature of Brahmaputra river sediment flux within the Bengal Basin (Singh et al., 2006). Two main mechanisms by which a distinct Eastern Himalayan signature could be recorded within G-B delta sediments are:

1. Significantly increase Eastern Himalayan (ie: the Tista) sediment flux. This is unlikely to produce a discernible Eastern Himalayan tributary signature because of overwhelming Brahmaputra sediment flux.
2. Significantly reduce Brahmaputra sediment flux to the margin, thus removing the dominant geochemical fingerprint from Tibetan lithologies.

Periods of significantly reduced flow from the Brahmaputra river have been documented based on geomorphological evidence in the Himalaya. Montgomery et al. (2004) describe field evidence of potential Holocene glacially dammed lakes at the eastern syntaxis of the Himalaya which would have significantly, if not completely, reduced flow and sediment flux from the Brahmaputra river. The potential stream power for flood events that occur as a result of rupture is orders of magnitude greater than the Late Pleistocene Missoula and Bonneville floods because of extreme elevation and slope at the eastern syntaxis of the Himalaya. An outburst flood event from the Himalaya has the potential to be one of the most erosive events of the Late Quaternary (Montgomery et al., 2004). Glacial lakes formed within relatively flat, high elevation Tibetan lithologies near the eastern syntaxis, and erosive potential would likely be focused within Greater and Lesser Himalayan lithologies where elevation change is most extreme, thus fingerprinting potential lake outburst sediments with non-Tibetan

geochemical signatures seen within facies F. A study by Sundriyal et al. (2007) documents observations of landslide-dammed lake deposits in the western Himalaya which would have similar impacts on sediment dispersal.

Borehole evidence of anomalous, discrete, coarse grained sediment pulses containing Eastern Himalayan elemental signatures interbedded within Ganges and Brahmaputra sediments suggests numerous depositional events from the Himalaya. Facies F is coarser grained than other borehole sediments from this study, and is the only occurrence of coarse sand and gravel within the stratigraphy at Raipur. Furthermore, deposition of facies F is within fine-grained coastal tidal deposits of facies C. A large event, such as an outburst flood from a glacial or landslide-dammed lake is the most likely mechanism for depositing this coarse grained material at the coast. There is no published evidence anywhere within the Bengal Basin for similar coarse-grained deposits at a proximal location to the coastal environment. We propose these anomalous sediments are the result of repeated outburst floods from glacially dammed lakes similar to those described by Montgomery et al. (2004).

IV.2 Detrital zircon geochronology

The coarse sand and gravel at Raipur are not the only evidence for possible dammed river lakes and outburst floods. Preliminary evidence by Youngs et al., (unpublished) of an abrupt source change at another borehole location prompted a study of detrital zircon provenance. Detrital zircon geochronology data were generated for two sediment samples from borehole BH8, near Ajmiriganj, Bangladesh, within the tectonically subsiding Sylhet Basin (Goodbred and Kuehl, 2000b). The

Sylhet Basin has been actively subsiding since the Miocene due to overthrusting of the Shillong Massif. The basin has a Plio-Pleistocene subsidence rate of 1 mm/yr and radiocarbon data from Goodbred and Kuehl (2000b) indicate more rapid subsidence rates of 2-4 mm/yr during the Late Quaternary. The Sylhet Basin is believed to have received primarily Brahmaputra sediment flux since the Late Quaternary based on its physiographic location, therefore, shifts in geochemical signatures directly reflect changes within the Brahmaputra drainage basin (Goodbred and Kuehl, 2000b).

Down-core strontium isotope data for BH8 generated by Youngs et al. (unpublished) show a significant increase in $^{87}Sr/^{86}Sr$ values from 0.73 at 92 m to 0.79 at 99 m (Figure IV.2). Associated with increased $^{87}Sr/^{86}Sr$ values is a significant decrease in Sr concentration from 168 to 77 ppm and an overall coarsening of the sand grain-size fraction with deposition of coarse sand below 92 m. $^{87}Sr/^{86}Sr$ values indicate a shift in sediment provenance from less radiogenic (ie: Tibetan) to more radiogenic (ie: Himalayan) lithologies. During typical conditions, the Brahmaputra river receives sediment from both Lesser and Greater Himalayan lithologies (Figure IV.4). Under conditions of significantly reduced Tibetan influence, Eastern Himalayan tributaries such as the Tista supply the majority of sediment to the eastern G-B delta. These smaller tributaries originate within the Lesser Himalaya, and therefore recieve limited input from Greater Himalayan lithologies. Detrital zircon geochronology data are used to further investigate the major source area change in sediment provenance seen reflected in down-core Sr data from borehole BH8.

Figure IV.3, modified from Clift et al. (2008), is a probability density plot showing the range of detrital zircon ages from samples AZ300 and AZ325 from

borehole BH8. Detrital zircon geochronology age populations generated from this study are compared with zircon age distributions generated from various tectono-sedimentary studies within the Himalaya (Clift et al., 2008; DeCelles et al., 2000; Amidon et al., 2005; Gehrels et al., 2003; Campbell et al., 2005; Najman, 2006). These data indicate a provenance shift between 92 and 99 m. Greater Himalaya lithologies contribute overall younger zircon grain populations, predominantly less than 1,000 Ma. The largest age population of zircon grains from Greater Himalaya lithologies date between 500 and 1,000 Ma. The Lesser Himalaya contribute significantly older zircon populations. The dominant population of zircon grains from Lesser Himalaya lithologies date between 1,500 and 2,000 Ma, and smaller populations exist younger than 1,500 Ma and greater than 2,000 Ma. Sample AZ300, collected from a depth of 92 m, contains detrital zircon age populations dominated by populations seen within Greater Himalayan lithologies. Sample AZ325, from a depth of 99 m, contains detrital zircon age populations dominated by populations found within Lesser Himalayan lithologies. Peaks in detrital zircon age population distributions for samples AZ300 and AZ325 correspond closely, which suggests both samples likely received continuous sediment input from the Lesser and Greater Himalaya. An overall shift in detrital zircon age populations away from the Lesser Himalaya, at 99 m, towards the Greater Himalaya, at 92 m, indicates a major shift in sediment provenance within the Brahmaputra watershed.

Results from detrital zircon geochronology, $^{87}Sr/^{86}Sr$ values, and Sr concentration values create a compelling argument for a major provenance shift to the Sylhet

Basin. Below 99 m in borehole BH8, $^{87}Sr/^{86}Sr$ values indicate a Lesser Himalaya-dominated source, detrital zircon geochronology suggests a shift away from Greater Himalaya-dominated sediment input towards a Lesser Himalaya-dominated sediment source, and Sr concentration data are suggestive of Eastern Himalayan tributary (ie: Tista) sediment flux. Montgomery et al. (2004) describe field evidence for Holocene glacially dammed lakes at the eastern syntaxis of the Himalaya which would have significantly, if not completely, reduced flow and sediment flux from the Brahmaptra river. Detrital zircon age population distributions generated from this study combined with $^{87}Sr/^{86}Sr$ values and Sr concentration values from Youngs et al. (unpublished) provide direct borehole evidence for the apparent shut-off of Brahmaputra sediment flux to the G-B delta.

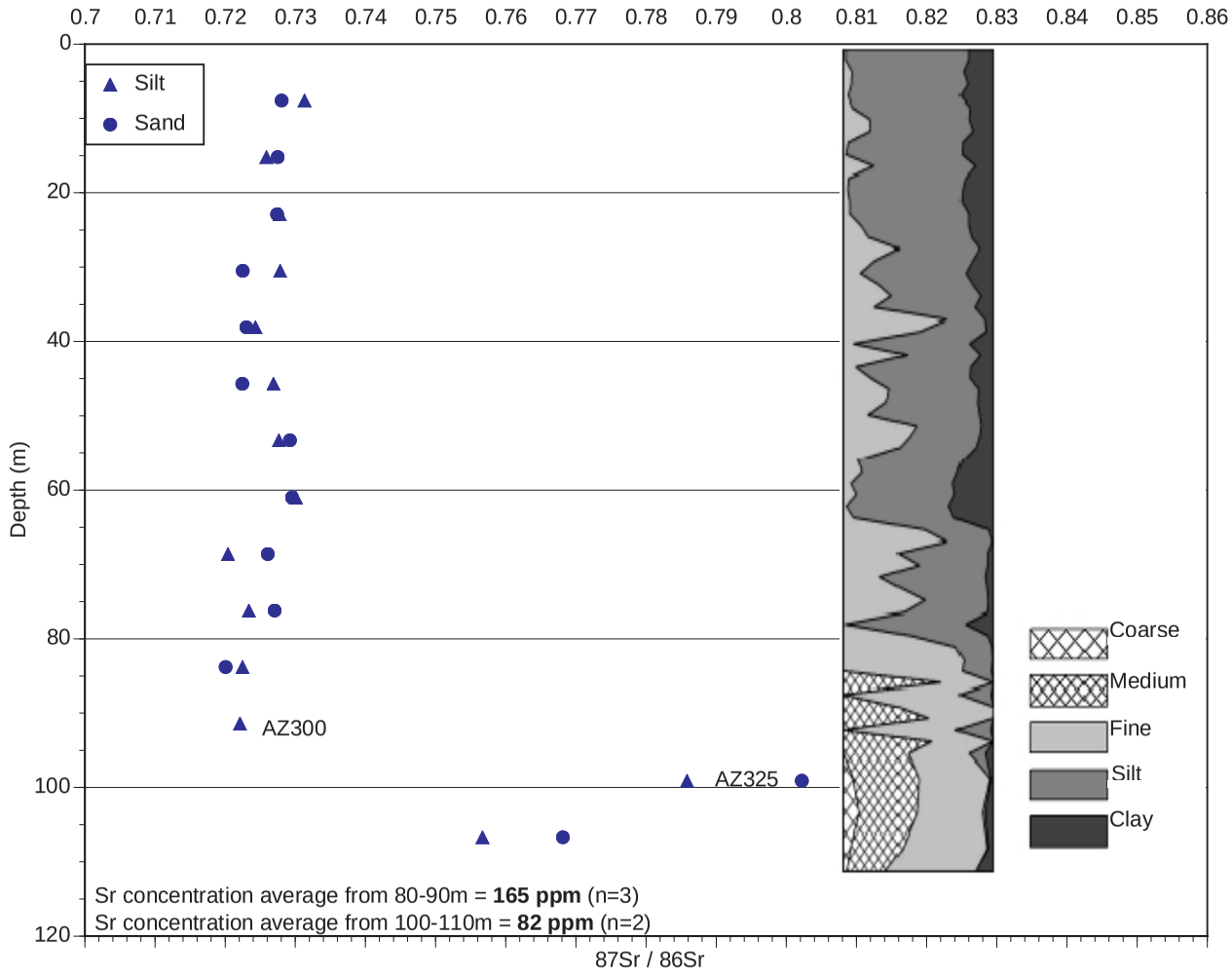

Figure IV.2: Down-core $^{87}Sr/^{86}Sr$ values for BH8. Note the $^{87}Sr/^{86}Sr$ excursion between samples AZ300 and AZ325 associated with a decrease in Sr concentration and appearance of coarse sand (data from Youngs et al., unpublished).

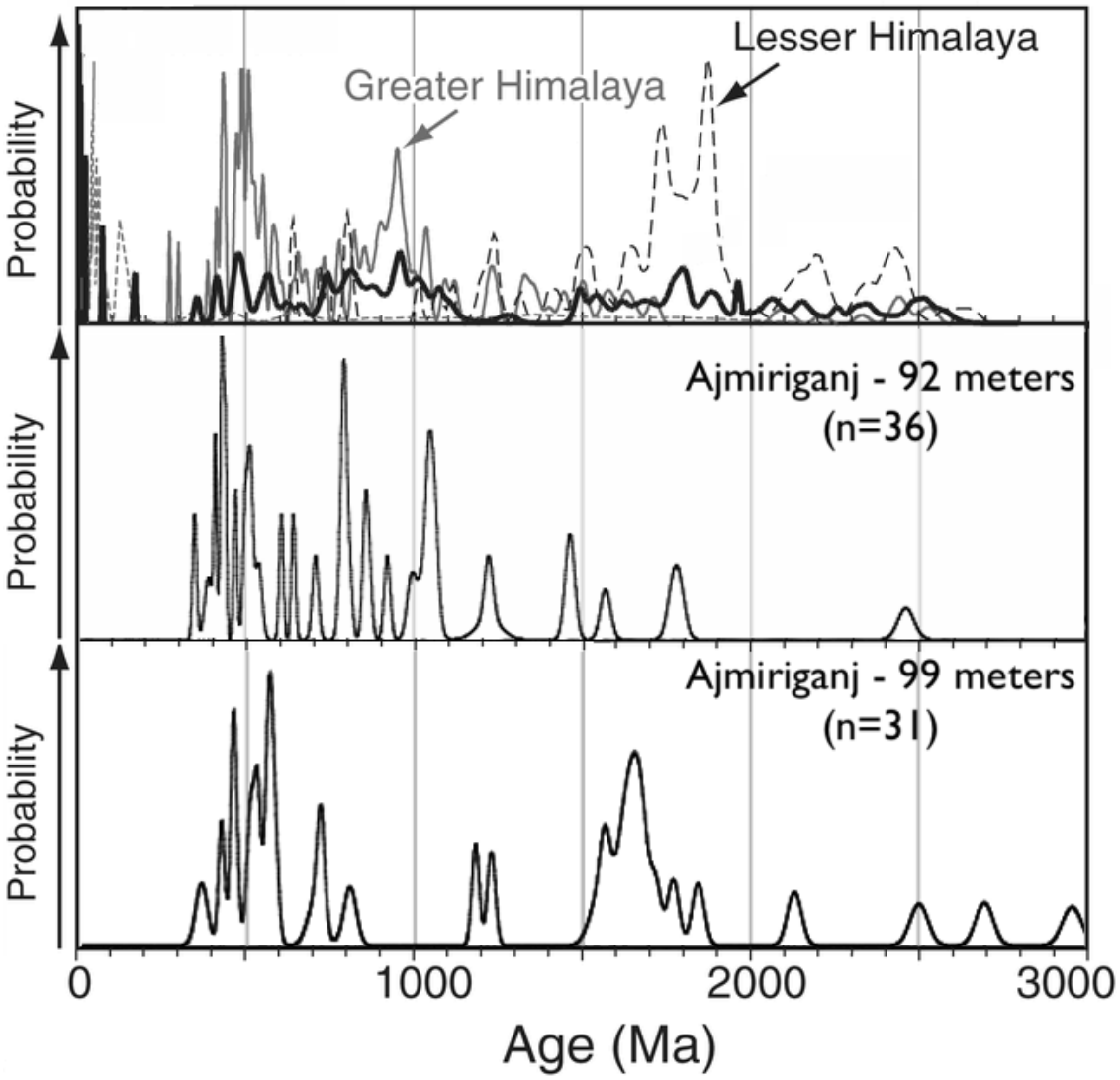

Figure IV.3: Probability density plots showing U-Pb ages in detrital zircons from BH8 samples AZ300 (92 m) and AZ325 (99 m) compared with source terrain values. Note the down-core shift in detrital zircon age population distribution from Greater Himalaya dominated towards a more significant Lesser Himalaya distribution. See Appendix A for complete data (modified from Clift et al., 2008).

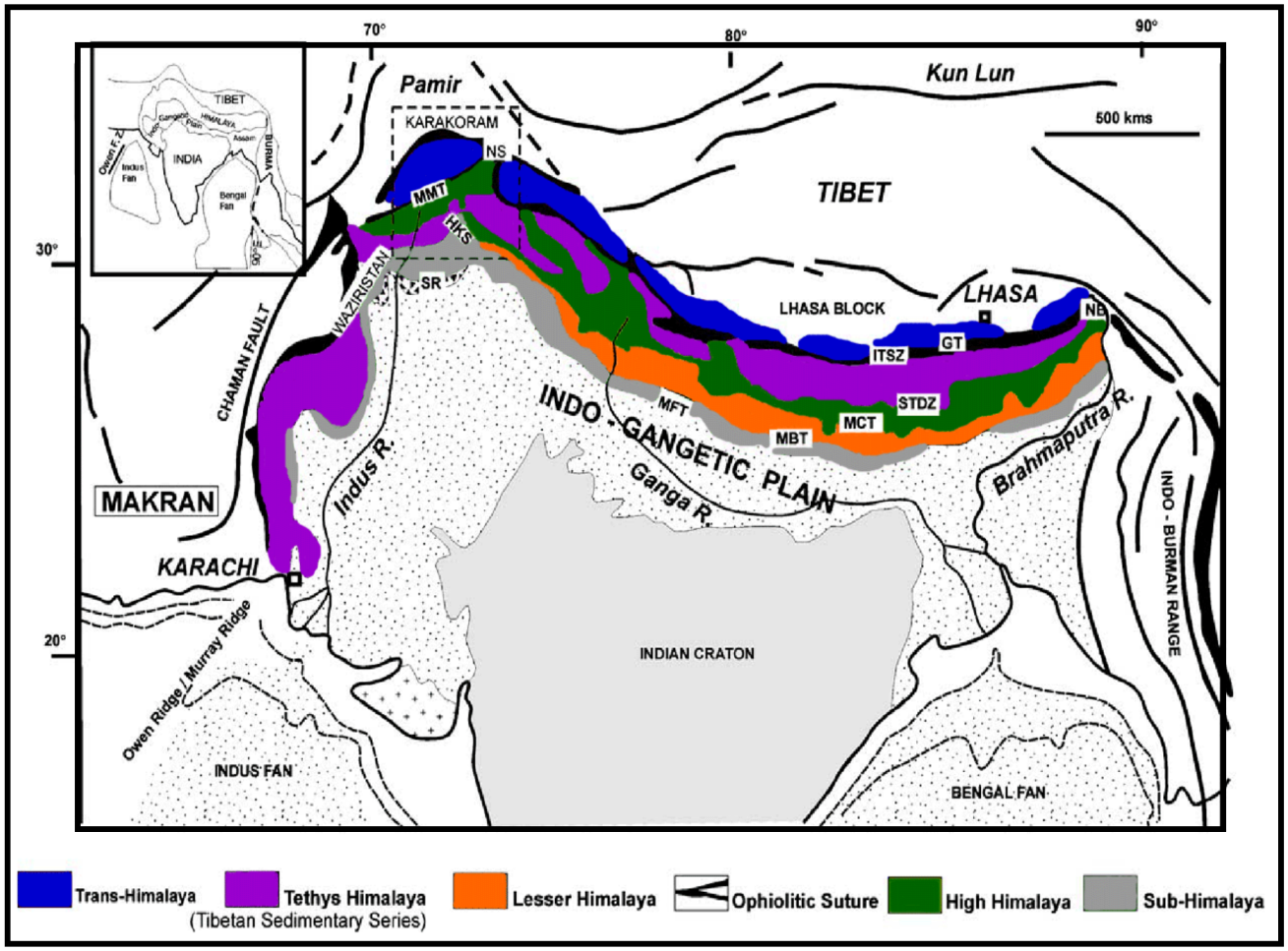

Figure IV.4: Geologic map of major lithologic units within the Ganges and Brahmaputra watersheds. The Brahmaputra river receives sediment input from Tibetan, High (Greater) Himalaya, and Lesser Himalaya lithologies. Eastern Himalayan tributaries such as the Tista (not shown here) originate within Lesser Himalaya lithologies and do not receive significant input from Greater Himalaya lithologies (modified from Najman, 2006).

CHAPTER V

CONCLUSIONS

A multiple-proxy study for borehole sediments from the Bengal Basin reveals stratigraphic, paleoenvironmental, and provenance data which suggest repeated event deposition, river avulsion and abandonment, and shifting provenance sources to the G-B margin during Late Quaternary delta evolution. Results indicate that the G-B delta system is not simply an amalgam of homogenous sediments, but, rather, is comprised of stacked units with distinct lithologies deposited from at least three major provenance sources. Important provenance sources recognized for Late Quaternary G-B delta sediments are the Ganges, Brahmaputra, and previously unrecognized Eastern Himalayan tributaries (ie: Tista).

Major controls on delta development are reflected within the general stratigraphy at Magura and Raipur. Magura is dominated by fluvial processes and is comprised of stacked fluvial sand sequences sometimes capped by silty floodplain and overbank deposits. Raipur exhibits considerable coastal marine influence combined with fluvial processes and is comprised of two coarsening upward, stacked sequences of muddy coastal plain deposits, tidal rythmites, estuarine and distributary mouth channel muddy sands, and fine fluvial sands capped by silty abandoned floodplain and overbank deposits. Relative paleoshoreline and river position contribute significantly to the different stratigraphy and environmental interpretations.

Strontium (Sr) concentration data is presented as a method for determining

G-B delta sediment provenance. Traditionally, $^{87}Sr/^{86}Sr$ values have been used to determine delta sediment provenance within the Bengal Basin, but Sr concentration data can be produced more rapidly and inexpensively. Based on data gathered from this study, previous borehole investigations (Van Geen et al., 2008 and Youngs et al., unpublished) and direct sampling of river sediments throughout the Bengal Basin (Singh et al., 2006 and France-Lanord, personal communication), we propose Brahmaputra (ie: Tibetan) sediments are characterized by "High" Sr concentrations (>155 ppm), Ganges sediments by "Intermediate" Sr concentrations (115-145 ppm), and Eastern Himalayan (ie: Tista) sediments by "Low" Sr concentrations (<105 ppm).

The importance of Eastern Himalayan tributary sediment input during the Late Quaternary is a new concept proposed by this study. Currently, the Tista river and other Eastern Himalayan tributaries provide sediment flux to the G-B delta system, but are overwhelmed by the immense sediment load of the Brahmaputra river. Two mechanisms by which a distinct Eastern Himalayan signature can be recorded within delta sediments are: 1) Significantly increase Eastern Himalayan sediment flux (unlikely to overpower Brahmaputra signal) and 2) Significantly reduce Brahmaputra sediment flux to the margin (thus reducing the dominant geochemical fingerprint from Tibetan lithologies). Montgomery et al. (2004) describe field evidence for Holocene glacially dammed lakes at the eastern syntaxis of the Himalaya which would have significantly, if not completely, reduced flow and sediment flux from the Brahmaptra river. Sundriyal et al. (2007) describe landslide-dammed lakes from the western Himalaya which would have similar impacts on the catchment. Detrital zircon

geochronology data generated from this study combined with $^{87}Sr/^{86}Sr$ values and Sr concentration data from Youngs et al. (unpublished) provide direct borehole evidence for the apparent shut-off of Tibetan sediment flux to the G-B delta. Borehole evidence of discrete, coarse grained sediment pulses containing Eastern Himalayan elemental signatures interbedded within Ganges and Brahmaputra sediments suggests numerous depositional events from the Himalaya. We propose these anomalous sediments are the result of repeated outburst floods from glacially dammed lakes similar to those described by Montgomery et al. (2004).

In addition to these new findings, results, particularly from the Holocene sequence at Raipur, support previous findings of early delta initiation around 11,000 yr B.P. following the Younger Dryas, a stable delta plain environment during rapid Holocene sea-level rise, and an immense sediment load delivered to the G-B margin with a significant portion trapped within inland tectonic basins.

APPENDIX A

DATA TABLES

Table A.1: Selected borehole locations from this study, Goodbred and Kuehl (2000b), and Van Geen et al. (2008).

Location	Reference	Latitude (°N)	Longitude (°E)
Magura	this study	23°35.97'	89°25.25'
Raipur	this study	23°02.18'	90°45.85'
BH1	Goodbred et al., 2000	22°38.78'	89°47.35'
BH2	Goodbred et al., 2000	22°45.33'	90°8.57'
BH3	Goodbred et al., 2000	21°52.12'	90°07.93'
BH4	Goodbred et al., 2000	24°03.18'	89°29.82'
BH5	Goodbred et al., 2000	23°32.02'	89°45.30'
BH6	Goodbred et al., 2000	24°50.78'	90°37.65'
BH7	Goodbred et al., 2000	24°27.52'	90°58.01'
BH8	Goodbred et al., 2000	24°32.89'	91°13.49'
BH9	Goodbred et al., 2000	24°56.45'	91°24.20'
Araihazar	Van Geen et al., 2008	23°46.48'	90°37.12'
Lak	Van Geen et al., 2008	23°04.34'	90°49.48'
Tista	Van Geen et al., 2008	26°00.00'	88°34.12'

Table A.2: Major element XRF data (wt%) for Magura.

Sample ID	Depth (m)	SiO_2	Al_2O_3	TiO_2	FeO	MnO	CaO	MgO	K_2O	Na_2O	P_2O_5	Al_2O_3/SiO_2
Magura S11	6.7	70.34	12.31	0.68	4.33	0.07	5.59	2.25	2.88	1.42	0.13	0.18
Magura S15	9.5	70.57	13.29	0.60	2.70	0.03	1.20	1.58	2.53	1.87	0.23	0.19
Magura S18	11	74.72	10.36	0.61	3.83	0.08	4.78	1.72	2.27	1.50	0.14	0.14
Magura S24	15	69.76	14.04	0.55	3.03	0.03	0.99	2.14	2.76	1.70	0.18	0.20
Magura S30	18.3	76.29	10.27	0.56	3.54	0.05	3.58	1.69	2.42	1.47	0.12	0.13
Magura S37	22.5	66.65	15.11	0.63	4.03	0.03	0.98	2.64	2.92	1.53	0.16	0.23
Magura S38	23.1	72.29	12.91	0.46	2.00	0.03	1.17	1.39	2.54	1.83	0.20	0.18
Magura S38	23.1	81.02	8.51	0.46	2.48	0.05	2.76	1.18	1.97	1.45	0.13	0.10
Magura S41	25.0	80.80	8.69	0.51	2.44	0.06	2.76	1.14	1.99	1.47	0.14	0.11
Magura S50	30.5	69.47	11.62	1.58	7.25	0.16	4.51	1.78	1.53	1.61	0.49	0.17
Magura S53	32.3	78.98	10.93	0.37	2.70	0.05	1.50	0.81	2.60	1.99	0.07	0.14
Magura S54	32.9	77.18	10.38	0.63	4.87	0.09	1.89	0.85	2.18	1.83	0.09	0.13
Magura S60A	36.6	77.89	10.61	0.57	3.70	0.07	2.02	0.93	2.18	1.93	0.10	0.14
Magura S60B	36.6	78.96	10.54	0.43	2.99	0.06	1.84	0.85	2.29	1.96	0.08	0.13
Magura S63	39.0	73.00	13.54	0.30	2.02	0.03	1.32	1.15	3.02	2.35	0.09	0.19
Magura S73A	50.3	70.01	11.49	1.24	8.10	0.25	3.56	1.74	1.70	1.75	0.17	0.16
Magura S73B	50.3	78.02	11.45	0.32	2.84	0.04	1.35	0.92	2.92	2.09	0.06	0.15
Magura S76	55.0	68.59	15.22	0.44	3.52	0.03	1.17	2.05	3.33	2.01	0.08	0.22
Magura S79	60.0	79.27	11.78	0.19	1.61	0.03	0.69	0.72	3.12	1.81	0.07	0.15
Magura S84	67.0	65.54	14.16	0.88	9.72	0.11	1.60	3.04	3.26	1.57	0.12	0.22
Magura S91A	71.3	75.18	11.02	0.76	5.01	0.12	2.62	1.31	1.92	1.90	0.15	0.15
Magura S91B	71.3	79.16	10.65	0.34	2.68	0.04	1.81	0.98	2.20	2.07	0.07	0.13
Magura S92	72.0	70.77	14.12	0.35	2.47	0.03	1.47	1.52	2.81	2.23	0.09	0.20
Magura S107	81.5	71.25	13.56	0.37	2.40	0.03	1.12	1.52	2.86	1.89	0.14	0.19
Magura S110	85.5	71.81	14.06	0.34	2.45	0.03	1.47	1.54	2.96	2.38	0.09	0.20
Magura S122	99.5	77.38	12.48	0.27	1.64	0.03	1.11	1.11	2.84	2.14	0.07	0.16
Magura S128	103.5	72.60	13.37	0.35	2.38	0.03	1.46	1.38	2.60	2.06	0.10	0.18
Magura S137	109.0	73.70	13.30	0.43	2.54	0.03	1.72	1.58	2.59	2.25	0.14	0.18
Magura S139	109.7	82.22	9.01	0.33	2.36	0.08	1.58	0.82	2.00	1.55	0.06	0.11
Magura S140	110.3	82.23	8.83	0.39	2.61	0.08	1.51	0.76	1.98	1.54	0.06	0.11
Magura S144	116.0	82.75	10.94	0.19	1.85	0.05	0.53	0.71	2.36	1.28	0.08	0.13
Magura S146	122.0	75.67	12.78	0.29	1.93	0.04	1.08	1.18	2.87	2.04	0.08	0.17

Table A.3: Trace element XRF data (ppm) for Magura.

Sample ID	Depth (m)	Ni	Cr	Sc	V	Ba	Rb	Sr	Zr	Y	Nb	Ga	Cu	Zn	Pb	La	Ce	Th	Nd	U	Cs
Magura S11	6.7	19	54	11	69	431	144	129	272	30	12	14	20	57	21	35	78	17	34	2	8
Magura S15	9.5	100	42	-	-	1841	115	125	355	28	12	-	18	30	24	-	-	15	31	3	-
Magura S18	11.0	15	48	10	59	941	107	144	334	32	11	12	19	48	20	43	80	17	36	4	8
Magura S24	15.0	98	63	-	-	351	132	95	255	24	11	-	10	37	25	-	-	15	39	3	-
Magura S30	18.3	14	44	8	55	380	123	110	286	28	10	13	10	46	21	36	70	15	30	4	6
Magura S37	22.5	56	68	-	-	406	139	93	213	25	10	-	14	50	26	-	-	16	51	3	-
Magura S38	23.1	125	51	-	-	281	118	88	237	24	10	-	8	25	23	-	-	14	41	3	-
Magura S41	25.0	6	31	7	42	310	92	102	363	36	10	10	2	29	32	49	98	22	42	4	4
Magura S50	30.5	32	155	22	139	261	61	209	874	89	26	15	7	66	18	131	270	53	110	9	2
Magura S53	32.3	16	48	7	45	403	110	165	134	19	7	12	5	33	23	26	53	12	21	3	5
Magura S54	32.9	15	103	10	80	333	85	167	629	39	12	12	4	38	19	80	159	50	63	6	0
Magura S60A	36.6	16	76	10	64	337	88	175	307	33	8	12	4	37	18	50	95	21	37	3	3
Magura S60B	36.6	16	54	10	52	371	91	172	180	24	8	12	5	32	22	37	78	15	31	3	1
Magura S63	39.0	169	66	-	-	379	36	131	112	59	52	-	1	20	25	-	-	13	10	3	-
Magura S73A	50.3	19	180	20	135	261	69	190	715	80	21	14	6	65	17	151	295	60	108	6	0
Magura S73B	50.3	19	35	6	45	450	141	168	102	14	6	13	7	36	22	18	31	8	14	2	5
Magura S76	55.0	82	62	-	-	421	158	167	124	24	8	-	9	46	27	-	-	15	42	4	-
Magura S79	60.0	139	56	-	-	355	133	126	118	20	6	-	3	17	25	-	-	14	-	3	-
Magura S84	67.0	65	84	12	100	441	225	133	156	20	14	18	27	111	26	25	48	8	22	3	18
Magura S91A	71.3	15	84	14	84	313	82	181	381	47	12	14	4	45	18	68	134	28	52	4	3
Magura S91B	71.3	15	36	7	45	351	97	177	112	17	6	13	4	33	19	21	39	8	17	2	3
Magura S92	72.0	125	61	-	-	396	132	167	132	22	8	-	7	30	24	-	-	14	-	3	-
Magura S107	81.5	112	45	-	-	1687	125	134	149	23	8	-	5	27	25	-	-	13	-	3	-
Magura S110	85.5	167	66	-	-	409	35	133	109	58	50	-	7	21	24	-	-	13	-	3	-
Magura S122	99.5	137	56	-	-	329	127	134	128	20	6	-	2	19	23	-	-	14	38	3	-
Magura S128	103.5	123	51	-	-	479	119	151	149	22	8	-	6	26	24	-	-	14	43	3	-
Magura S137	109.0	197	51	-	-	341	-	72	127	131	137	-	3	11	21	-	-	14	61	2	-
Magura S139	109.7	8	40	7	42	346	76	139	130	21	5	10	3	25	19	29	57	13	23	2	2
Magura S140	110.3	7	49	8	45	316	73	133	167	27	6	10	1	24	19	44	86	19	33	4	3
Magura S144	116	120	40	-	-	587	114	83	120	21	6	-	5	16	23	-	-	12	96	3	-
Magura S146	122.0	139	51	-	-	332	131	133	137	22	7	-	4	23	24	-	-	14	43	3	-

Table A.4: Major element XRF data (wt%) for Raipur.

Sample ID	Depth (m)	SiO_2	Al_2O_3	TiO_2	FeO	MnO	CaO	MgO	K_2O	Na_2O	P_2O_5	Al_2O_3/SiO_2
Raipur S14	12.0	71.42	13.82	0.52	1.65	0.03	1.86	1.78	2.69	2.31	0.18	0.19
Raipur S15	13.0	71.15	14.20	0.40	1.90	0.03	1.72	1.63	2.98	2.55	0.12	0.20
Raipur S26	19.5	69.02	14.30	0.63	1.01	0.02	2.15	2.32	2.53	2.21	0.23	0.21
Raipur S27a	20.0	65.35	15.62	0.77	1.59	0.01	1.92	2.58	2.75	1.95	0.20	0.24
Raipur S28a	21.0	66.08	15.08	0.80	1.14	0.10	2.40	2.52	2.51	2.01	0.26	0.23
Raipur S33a	24.0	66.55	15.39	0.69	1.63	0.02	1.83	2.54	2.71	1.98	0.16	0.23
Raipur S37	26.5	72.99	13.63	0.33	2.89	0.03	1.44	1.40	2.96	2.44	0.10	0.19
Raipur S46a	32.0	81.38	11.47	0.34	2.52	0.03	1.26	0.93	2.54	2.04	0.10	0.14
Raipur S53a	36.0	71.56	13.65	0.65	3.64	0.01	2.31	1.99	2.36	2.16	0.20	0.19
Raipur S54	37.0	71.04	13.72	0.40	4.81	0.03	1.65	1.62	2.79	2.23	0.18	0.19
Raipur S86	58.5	75.58	12.31	0.36	4.29	0.03	0.57	0.59	2.58	1.03	0.07	0.16
Raipur S88	60.0	72.17	12.84	0.44	4.42	0.04	0.38	0.79	2.37	0.69	0.08	0.18
Raipur S90	61.0	69.13	14.27	0.65	2.05	0.03	0.60	1.58	2.39	1.38	0.09	0.21
Raipur S95	67.0	76.05	12.79	0.32	2.02	0.03	0.79	1.06	3.03	1.74	0.06	0.17
Raipur S97	71.5	71.18	13.70	0.47	3.35	0.03	1.68	1.61	2.64	2.11	0.16	0.19
Raipur S99	75.5	75.04	12.88	0.38	2.69	0.03	1.45	1.44	2.60	2.07	0.13	0.17
Raipur S103	78.0	75.83	12.51	0.25	1.74	0.04	0.68	0.83	2.99	1.59	0.06	0.16
Raipur S108	81.0	75.93	12.55	0.41	2.64	0.03	1.11	1.17	2.66	1.74	0.11	0.17
Raipur S119	99.5	85.40	10.58	0.19	2.96	0.04	0.44	0.42	2.40	1.17	0.05	0.12
Raipur S120	101.0	84.66	10.65	0.23	1.71	0.05	0.56	0.56	2.21	1.05	0.07	0.13
Raipur S121	103.0	85.60	10.55	0.17	2.90	0.05	0.42	0.45	2.39	1.06	0.05	0.12
Raipur S130	116.0	82.37	11.03	0.24	2.44	0.04	0.59	0.70	2.38	1.14	0.07	0.13

Table A.5: Trace element XRF data (ppm) for Raipur.

Sample ID	Depth (m)	Ni	Cr	Ba	Rb	Sr	Zr	Y	Nb	Cu	Zn	Pb	Th	Nd	U
Raipur S14	12.0	70	63	333	115	171	225	25	12	13	36	24	15	37	3
Raipur S15	13.0	106	64	368	120	169	204	25	10	6	27	24	15	0	3
Raipur S26	19.5	46	63	316	109	176	296	27	12	13	47	24	13	18	3
Raipur S27a	20.0	46	70	402	116	174	273	27	13	19	64	25	14	0	3
Raipur S28a	21.0	42	66	337	106	178	284	28	13	14	53	23	13	29	3
Raipur S33a	24.0	42	73	389	120	166	201	25	11	19	53	25	14	0	3
Raipur S37	26.5	125	55	373	131	164	134	23	8	3	25	24	14	19	3
Raipur S46a	32.0	132	55	282	115	158	158	22	9	2	27	23	14	21	3
Raipur S53a	36.0	85	65	298	107	177	266	26	12	11	40	23	16	44	3
Raipur S54	37.0	100	66	329	117	162	168	24	9	15	47	24	14	0	3
Raipur S86	58.5	135	65	282	126	91	173	20	7	4	23	23	14	11	3
Raipur S88	60.0	107	57	294	119	66	147	20	6	6	35	26	15	42	3
Raipur S90	61.0	129	75	307	124	102	229	22	8	9	50	24	14	33	3
Raipur S95	67.0	148	58	405	137	128	124	22	6	5	32	25	13	0	3
Raipur S97	71.5	91	53	1314	117	181	197	23	10	9	63	24	14	37	3
Raipur S99	75.5	98	55	1117	117	169	188	24	11	12	36	24	14	50	3
Raipur S103	78.0	141	53	358	132	116	106	20	5	2	21	25	14	0	3
Raipur S108	81.0	132	57	299	121	122	146	21	8	4	25	23	13	37	3
Raipur S119	99.5	160	47	373	113	70	114	20	6	0	19	23	14	90	2
Raipur S120	101.0	133	37	630	107	80	122	21	6	2	32	22	13	118	2
Raipur S121	103.0	144	43	645	111	73	106	19	6	0	22	23	12	88	2
Raipur S130	116.0	139	35	1749	112	104	125	21	7	8	48	24	14	114	3

Table A.6: Major element XRF data (wt%) for all available Bengal Basin data. Geochemical data for samples labeled BH# from Youngs et al. (unpublished) and named samples from Van Geen et al. (2008).

Sample ID	Depth (m)	SiO_2	Al_2O_3	TiO_2	FeO	MnO	CaO	MgO	K2O	Na_2O	P_2O_5	Al_2O_3/SiO_2
BH8-050C	15.2	72.00	12.77	0.68	5.47	0.09	2.05	2.34	2.66	1.80	0.14	0.18
BH8-050FA	15.2	68.50	15.34	0.98	5.83	0.11	2.25	2.42	2.69	1.71	0.18	0.22
BH8-050FB	15.2	68.19	15.57	0.99	5.88	0.12	2.21	2.43	2.72	1.71	0.18	0.23
BH8-100C	30.5	75.03	12.10	0.54	4.05	0.09	1.90	1.83	2.50	1.86	0.11	0.16
BH8-100F	30.5	69.49	15.14	0.99	5.93	0.11	1.91	2.17	2.53	1.55	0.18	0.22
BH8-150C	45.7	71.98	12.89	0.62	5.46	0.08	1.88	2.36	2.74	1.88	0.11	0.18
BH8-150F	45.7	68.23	15.36	1.00	5.88	0.13	2.31	2.48	2.68	1.74	0.19	0.23
BH8-200C	61.0	87.44	6.96	0.25	1.22	0.13	0.39	0.31	2.22	1.05	0.03	0.08
BH8-250F	76.2	79.32	10.78	0.81	3.57	0.05	1.01	1.00	1.95	1.38	0.12	0.14
BH8-265F	80.8	78.89	9.32	0.90	3.53	0.07	2.58	1.13	1.71	1.67	0.20	0.12
BH8-275C	83.8	79.43	9.36	0.75	3.11	0.07	2.64	1.13	1.67	1.64	0.19	0.12
BH8-275F	83.8	71.20	10.76	2.77	7.52	0.16	3.07	1.30	1.51	1.33	0.38	0.15
BH8-300C	91.5	81.21	9.19	0.42	2.40	0.05	1.94	0.82	2.08	1.80	0.08	0.11
BH8-325C	99.1	82.99	9.25	0.28	1.89	0.03	0.90	0.67	2.34	1.58	0.07	0.11
BH8-350CA	106.7	82.35	9.73	0.29	1.79	0.04	1.09	0.67	2.26	1.71	0.08	0.12
BH8-350CB	106.7	83.21	9.37	0.25	1.56	0.03	1.01	0.59	2.22	1.67	0.07	0.11
BH1-030	9.1	79.03	10.15	0.60	3.42	0.06	1.46	1.25	2.26	1.61	0.15	0.13
BH1-060	18.3	79.54	10.05	0.54	3.28	0.05	1.35	1.13	2.28	1.65	0.13	0.13
BH1-080	24.4	80.23	10.12	0.38	2.80	0.04	1.19	1.03	2.42	1.71	0.08	0.13
BH1-120	36.6	75.75	11.67	0.63	4.56	0.08	1.31	1.67	2.65	1.53	0.14	0.15
BH1-170	51.8	68.03	16.05	0.82	6.04	0.09	1.37	2.44	3.45	1.56	0.14	0.24
BH1-210	64.0	82.11	9.03	0.45	2.35	0.05	1.33	0.83	2.07	1.65	0.13	0.11
BH1-250	76.2	81.42	9.35	0.46	2.55	0.05	1.34	0.90	2.14	1.66	0.13	0.11
BH2-030	9.1	64.47	18.99	0.92	6.56	0.13	1.19	2.83	3.43	1.34	0.13	0.29
BH2-045	13.7	66.00	17.35	0.95	6.66	0.11	1.36	2.61	3.26	1.56	0.14	0.26
BH2-070	21.3	80.34	9.95	0.40	2.33	0.05	1.88	0.92	2.08	1.96	0.10	0.12
BH2-130	39.6	77.86	11.01	0.46	3.23	0.06	1.71	1.22	2.46	1.87	0.11	0.14
BH2-225	68.6	78.37	10.85	0.50	2.90	0.06	1.88	1.16	2.27	1.90	0.12	0.14
BH2-275	83.8	78.50	10.74	0.49	2.89	0.06	1.90	1.14	2.24	1.91	0.12	0.14
BH5-065	19.8	82.64	8.82	0.38	2.24	0.04	1.33	0.75	2.03	1.67	0.10	0.11
BH5-130	39.6	78.98	9.59	0.59	3.43	0.09	2.37	1.09	1.90	1.82	0.15	0.12
BH5-260	79.3	79.88	10.04	0.43	2.64	0.05	1.86	0.96	2.18	1.86	0.10	0.13
Araihazar36-25	7.6	78.30	11.20	0.37	2.99	0.06	1.71	1.16	2.38	2.13	0.09	0.14
Araihazar36-45	13.7	78.40	10.90	0.47	3.60	0.08	1.81	1.21	2.20	1.83	0.11	0.14
Araihazar36-52	15.9	76.90	10.40	0.51	5.83	0.12	2.03	1.09	2.04	1.74	0.15	0.14
Araihazar37-35	10.7	77.70	11.30	0.43	3.25	0.07	1.96	1.33	2.28	2.11	0.14	0.15
Araihazar37-45	13.7	75.60	12.30	0.49	3.99	0.09	1.86	1.65	2.47	2.06	0.20	0.16
Araihazar37-65	19.8	72.20	13.30	0.67	5.45	0.10	1.98	2.39	2.61	1.95	0.18	0.18
BH3-035	10.7	67.87	14.01	0.82	8.21	0.13	1.45	2.49	2.93	1.95	0.14	0.21
BH3-100	30.5	77.69	10.95	0.56	3.57	0.06	1.42	1.35	2.44	1.82	0.13	0.14
BH3-150	45.7	69.30	14.94	0.82	6.10	0.09	1.31	2.45	3.03	1.83	0.13	0.22
BH3-260	79.3	78.28	10.39	0.58	3.39	0.06	1.78	1.23	2.26	1.89	0.15	0.13
LAK21-32	9.8	74.70	12.70	0.60	4.59	0.09	1.78	1.81	2.44	1.88	0.34	0.17
LAK21-37	11.3	73.70	12.80	0.65	5.11	0.09	1.75	2.06	2.56	1.86	0.18	0.17
LAK21-72	22.0	76.90	11.00	0.64	3.95	0.09	2.36	1.56	1.96	2.00	0.21	0.14
LAK23-27	8.2	76.50	11.70	0.57	3.88	0.08	1.88	1.50	2.44	1.92	0.18	0.15
LAK23-44	13.4	77.60	10.60	0.58	3.78	0.08	2.40	1.49	1.95	1.95	0.20	0.14
LAK23-57	17.4	77.20	11.10	0.48	4.00	0.08	1.90	1.41	2.34	1.90	0.14	0.14
Tista19-60	18.3	83.70	10.40	0.18	1.96	0.03	0.43	0.57	2.45	1.27	0.07	0.12
Tista19-70	21.3	83.10	10.20	0.18	1.78	0.03	0.53	0.59	2.40	1.57	<0.05	0.12
Tista19-80	24.4	85.30	8.65	0.17	1.87	0.03	0.36	0.63	1.92	1.45	<0.05	0.10
Tista20-20	6.1	83.50	10.30	0.19	1.75	0.04	0.67	0.60	2.31	1.63	<0.05	0.12
Tista20-50	15.2	81.80	10.80	0.22	1.87	0.05	0.81	0.67	2.52	1.76	0.06	0.13
Tista20-60	18.3	82.80	10.60	0.19	1.53	0.03	0.73	0.61	2.69	1.84	<0.05	0.13

Table A.7: Trace element XRF data (ppm) for all available Bengal Basin data. Geochemical data for samples labeled BH# from Youngs et al. (unpublished) and named samples from Van Geen et al. (2008).

Sample ID	Depth (m)	Ni	Cr	Sc	V	Ba	Rb	Sr	Zr	Y	Nb	Ga	Cu	Zn	Pb	La	Ce	Th	Nd	U	Cs
BH8-050C	15.2	43	79	20	78	423	140	152	206	26	13	17	20	71	18	22	54	11	-	-	-
BH8-050FA	15.2	50	106	21	120	450	136	164	359	46	18	18	30	81	22	60	118	24	-	-	-
BH8-050FB	15.2	57	110	18	116	459	139	160	345	44	17	19	32	82	25	53	132	26	-	-	-
BH8-100C	30.5	32	59	14	80	413	121	152	116	21	10	14	8	60	16	27	51	7	-	-	-
BH8-100F	30.5	55	113	19	118	420	127	144	361	44	17	18	23	76	23	52	108	22	-	-	-
BH8-150C	45.7	43	69	14	88	436	145	151	135	22	12	17	19	76	17	29	44	9	-	-	-
BH8-150F	45.7	54	106	20	119	461	136	163	374	45	18	20	31	82	30	62	119	26	-	-	-
BH8-200C	61.0	16	24	4	24	377	80	85	52	9	4	8	4	18	17	6	26	5	8	0	3
BH8-250F	76.2	38	100	16	71	315	86	109	490	38	14	13	10	48	16	39	87	19	-	-	-
BH8-265F	80.8	16	110	12	74	279	63	161	865	54	15	10	3	34	16	73	146	34	61	4	1
BH8-275C	83.8	20	80	9	68	274	65	164	323	43	14	11	2	31	12	57	112	23	-	-	-
BH8-275F	83.8	33	432	20	141	250	61	163	6216	201	52	10	11	65	26	295	602	156	242	30	1
BH8-300C	91.5	9	46	8	46	327	78	168	178	25	7	11	1	25	17	32	68	15	27	3	2
BH8-325C	99.1	4	24	5	28	331	109	77	141	23	6	11	2	24	23	28	51	13	23	2	4
BH8-350CA	106.7	10	17	5	26	348	108	87	187	28	7	12	1	21	20	37	77	15	-	-	-
BH8-350CB	106.7	7	12	4	20	318	106	84	158	25	6	7	1	22	20	35	84	17	-	-	-
BH1-030	9.1	16	44	9	54	355	118	107	350	34	12	12	8	42	18	48	98	20	39	4	7
BH1-060	18.3	16	42	9	52	357	111	109	332	31	10	12	11	51	19	46	87	19	36	3	5
BH1-080	24.4	14	34	7	46	370	118	114	150	20	7	12	5	38	20	25	50	10	22	2	8
BH1-120	36.6	23	53	10	69	406	148	101	286	30	13	15	15	64	22	43	83	17	36	4	9
BH1-170	51.8	39	83	14	104	538	180	116	215	33	15	20	33	86	25	42	90	18	36	4	14
BH1-210	64.0	8	35	7	39	324	95	109	316	30	8	10	3	38	18	40	82	18	36	5	5
BH1-250	76.2	10	34	7	46	340	101	109	307	30	9	11	5	42	19	43	83	19	38	3	6
BH2-030	9.1	63	116	16	136	505	194	125	173	34	17	23	44	101	31	52	94	18	-	-	-
BH2-045	13.7	54	108	16	118	476	175	131	224	36	16	22	38	92	28	47	98	21	41	4	12
BH2-070	21.3	17	37	8	35	339	84	161	227	26	8	14	3	27	16	32	61	13	-	-	-
BH2-130	39.6	23	42	10	49	385	121	152	205	23	9	14	5	46	20	32	57	13	-	-	-
BH2-225	68.6	21	49	8	52	375	100	159	250	28	10	13	5	35	15	37	83	16	-	-	-
BH2-275	83.8	20	44	15	52	362	98	162	276	31	9	10	7	39	18	45	87	16	-	-	-
BH5-065	19.8	8	33	6	39	310	89	113	227	25	8	10	3	42	18	34	65	16	29	2	4
BH5-130	39.6	10	60	9	62	303	72	166	372	39	10	11	2	45	20	58	117	25	47	2	1
BH5-260	79.3	10	45	8	51	345	88	156	212	24	7	11	5	33	19	33	70	15	28	3	3
Araihazar36-25	7.6	18	45	-	58	-	107	193	170	28	-	-	-	35	21	-	-	40	12	25	-
Araihazar36-45	13.7	19	70	-	69	-	101	185	220	38	-	-	12	47	20	-	-	34	17	29	-
Araihazar36-52	15.9	22	85	-	78	-	88	176	292	51	-	-	11	41	25	-	-	42	16	35	-
Araihazar37-35	10.7	18	51	-	63	-	113	189	195	30	-	-	-	43	19	-	-	42	13	21	-
Araihazar37-45	13.7	25	58	-	70	-	132	188	184	29	-	-	14	61	20	-	-	29	13	33	-
Araihazar37-65	19.8	35	72	-	89	-	147	175	248	36	-	-	21	84	18	-	-	35	16	34	-
BH3-035	10.7	51	84	13	99	432	166	127	217	30	14	17	55	88	25	39	78	14	33	4	14
BH3-100	30.5	17	47	9	59	363	119	119	327	31	10	12	9	49	21	40	85	19	34	4	6
BH3-150	45.7	44	82	13	99	423	163	119	256	32	14	18	25	81	27	42	87	17	35	4	11
BH3-260	79.3	16	51	9	57	354	100	142	343	33	10	12	5	70	21	43	91	20	39	4	4
LAK21-32	9.8	28	68	-	77	-	131	170	266	41	-	-	16	53	21	-	-	43	16	32	-
LAK21-37	11.3	34	74	-	81	-	147	169	296	38	-	-	14	63	21	-	-	43	19	40	-
LAK21-72	22.0	17	78	-	80	-	95	189	453	58	-	-	-	41	19	-	-	59	20	40	-
LAK23-27	8.2	20	63	-	67	-	118	169	337	37	-	-	13	43	19	-	-	36	16	26	-
LAK23-44	13.4	18	63	-	75	-	90	182	308	39	-	-	-	39	16	-	-	41	16	30	-
LAK23-57	17.4	21	58	-	68	-	121	182	185	38	-	-	-	45	20	-	-	40	15	28	-
Tista19-60	18.3	¡10	19	-	28	-	122	71	77	25	-	-	-	18	20	-	-	28	11	20	-
Tista19-70	21.3	¡10	19	-	27	-	130	76	86	19	-	-	-	20	25	-	-	39	12	32	-
Tista19-80	24.4	¡10	16	-	24	-	91	77	77	18	-	-	-	19	21	-	-	33	10	26	-
Tista20-20	6.1	¡10	16	-	25	-	109	77	83	23	-	-	-	15	19	-	-	32	10	29	-
Tista20-50	15.2	¡10	18	-	28	-	124	85	91	29	-	-	-	20	23	-	-	36	11	29	-
Tista20-60	18.3	¡10	17	-	27	-	127	90	86	20	-	-	-	19	27	-	-	27	12	18	-

Table A.8: River sediment Sr data for the Bengal Basin (from Singh et al. (2006)).

Brahmaputra Main Channel			
Bank Sediments			
		$^{87/86}$**Sr**	**[Sr] ppm**
BR	**19**	0.718655	243
	19 clay	0.72054	109
	29	0.728481	160
	66	0.725211	157
	9	0.717726	208
	9 clay	0.717293	91
	56	0.718249	244
	74	0.721507	196
BGP	**14**	0.734572	148
	82	0.721019	183
Suspended Sediments			
		$^{87/86}$**Sr**	**[Sr] ppm**
BR	**65 SL**	0.719199	195
	2	0.72105	187
	3	0.722013	175
	4	0.729567	184
	6	0.720553	170
	7	0.719331	211
	8	0.719791	198
	52 SL	0.719656	232
	53 SL	0.720589	167
	54 SL	0.721623	194
	55 SL	0.721859	160
	73 SL	0.734388	148
BGP	**18**	0.748838	89
Himalayan Tributaries			
Bank Sediments			
		$^{87/86}$**Sr**	**[Sr] ppm**
BR	**21**	0.735633	75
	62	0.741897	71
	25	0.730654	89
	58	0.738124	70
	27	0.777051	69
	64	0.777346	53
	35	0.758673	61
	70	0.764176	39
	76	0.784524	38
BGP	**11**	0.809621	92
	76	0.824959	89
Suspended Sediments			
		$^{87/86}$**Sr**	**[Sr] ppm**
BR	**61 SL**	0.730133	117
	63 SL	0.776816	56
	69 SL	0.7703	69
Southern Tributaries			
Bank Sediments			
		$^{87/86}$**Sr**	**[Sr] ppm**
BR	**31**	0.733421	58
	68	0.736137	32
	11	0.718137	80
	13	0.727418	129
	78	0.750154	47
Suspended Sediments			
		$^{87/86}$**Sr**	**[Sr] ppm**
BR	**67 SL**	0.732516	85

Table A.9: **Bengal Basin borehole Sr data. Borehole samples from Goodbred and Kuehl (2000b) and geochemical data from Youngs et al., (unpublished).**

Borehole	Depth (m)	$^{87/86}$ Sr	[Sr] (ppm)
BH1	9.1	0.751493	107
	18.3	0.739862	109
	24.4	0.743244	114
	30.5	0.749842	-
	36.6	0.754034	101
	41.1	0.751839	-
	51.8	0.750244	116
	54.9	0.747315	-
	64.0	0.746215	109
	76.2	0.751341	109
	83.8	0.751384	-
	91.4	0.747329	-
BH2	3.0	0.735123	-
	6.1	0.734697	-
	7.6	0.734212	-
	9.1	0.727453	125
	12.2	0.733176	-
	13.7	0.733769	131
	16.8	0.733082	-
	21.3	0.725197	161
	22.9	0.727773	-
	30.5	0.724920	-
	32.0	0.730842	-
	33.5	0.728703	-
	35.1	0.723821	-
	39.6	0.731332	152
	42.7	0.731477	-
	50.3	0.731534	-
	62.5	0.729093	-
	64.0	0.724848	-
	65.5	0.729442	-
	68.6	0.729524	159
	70.1	0.731374	-
	74.7	0.724664	-
	83.8	0.725585	162
	86.9	0.729541	-
	91.4	0.724692	-
BH5	19.8	0.748458	113
	39.6	0.724606	166
	59.4	0.725364	-
	79.2	0.728485	156
BH-7	3.0	0.728371	-
	19.8	0.723040	-
	42.7	0.729738	-
	51.8	0.722831	-
	82.3	0.723071	-
BH8	7.6	0.728048	-
(<63um)	15.2	0.727490	162
	22.9	0.727402	-
	30.5	0.722505	144
	38.1	0.723023	-
	45.7	0.722443	163
	53.3	0.729232	-
	61.0	0.729529	-
	68.6	0.726077	-
	76.2	0.727052	109
	83.8	0.720069	163
	99.1	0.802209	-
	106.7	0.768142	-
BH8	7.6	0.731319	-
(>63um)	15.2	0.725887	152
	22.9	0.727778	-
	30.5	0.727841	152
	38.1	0.724326	-
	45.7	0.726891	151
	53.3	0.727662	-
	61.0	0.730081	85
	68.6	0.720404	-
	76.2	0.723390	-
	83.8	0.722483	164
	91.4	0.722112	168
	99.1	0.785840	77
	106.7	0.756679	86
BH9	15.2	0.726620	-
	30.5	0.730164	-
	45.7	0.729015	-
	61.0	0.730272	-
	82.3	0.728118	-

Table A.10: **Magura grain size data. Data for each sample are the average of three consecutive analyses with a Malvern Mastersizer 2000 laser-diffraction grain size analyzer. Sand fraction data normalized to 100% are provided in the final three columns.**

Sample Name	Depth (m)	Mean	Std Dev	Skew	Silt & Clay	Fine Sand	Medium Sand	Coarse Sand	Normalized Fine	Normalized Medium	Normalized Coarse
Magura S1	1	19.26	17.38	1.30	78.94	2.96	0.00	0.00	100.00	0.00	0.00
Magura S2	1.5	33.34	30.15	1.46	73.57	15.02	0.00	0.00	100.00	0.00	0.00
Magura S15	9.5	88.09	51.09	0.97	33.01	64.63	0.82	0.00	98.75	1.25	0.00
Magura S19	12	118.23	115.49	4.18	25.09	67.91	3.72	2.00	92.24	5.05	2.71
Magura S24	15	109.65	116.76	3.28	35.44	54.32	5.67	1.86	87.82	9.17	3.00
Magura S25	15.5	112.04	120.10	3.10	35.83	52.95	6.48	1.94	86.28	10.56	3.16
Magura S26	16	115.94	112.02	3.06	31.15	59.09	6.33	1.70	88.04	9.43	2.53
Magura S27	17	123.41	129.51	2.85	32.42	54.92	7.94	2.54	83.98	12.14	3.88
Magura S28	17.5	101.59	103.99	3.57	36.00	55.45	4.41	1.28	90.69	7.21	2.10
Magura S29	18	118.11	106.89	3.04	27.21	63.36	6.21	1.49	89.17	8.74	2.10
Magura S30	18.5	109.12	109.46	3.32	33.31	57.45	5.37	1.56	89.25	8.33	2.42
Magura S31	19	153.76	152.63	2.49	23.18	59.86	11.22	4.33	79.38	14.88	5.74
Magura S32	20	95.75	104.55	3.81	40.83	51.45	3.67	1.38	91.08	6.49	2.43
Magura S37	23	105.88	93.32	1.57	36.21	52.88	7.87	0.29	86.65	12.88	0.47
Magura S38	23.5	100.47	69.47	0.63	30.10	64.02	3.12	0.00	95.35	4.65	0.00
Magura S40	24.5	137.80	122.00	2.94	20.98	66.69	8.64	1.97	86.28	11.17	2.54
Magura S41	25.5	154.95	100.33	2.13	10.94	75.31	12.08	0.78	85.43	13.69	0.88
Magura S46	28.5	139.12	112.22	1.05	27.08	54.40	14.66	0.80	77.87	20.98	1.15
Magura S47	29	118.72	135.30	2.62	38.26	46.11	8.91	2.54	80.11	15.49	4.40
Magura S49	30	105.87	116.32	1.83	43.51	40.01	9.88	1.34	78.10	19.28	2.62
Magura S52	32	177.11	167.42	1.29	28.13	41.60	21.23	5.71	60.70	30.96	8.34
Magura S53	32.5	185.38	200.23	1.70	30.81	39.58	17.77	8.62	60.04	26.91	13.05
Magura S54	33	212.67	221.70	1.52	27.13	39.38	19.23	11.64	56.05	27.37	16.57
Magura S55	34	382.21	245.10	0.49	11.22	17.68	41.25	28.45	20.23	47.21	32.56
Magura S56	34.5	227.36	175.66	0.73	20.55	37.08	31.97	8.37	47.89	41.30	10.81
Magura S57	35	226.95	171.59	0.68	20.28	37.09	32.90	7.77	47.70	42.30	10.00
Magura S58	35.5	128.05	137.17	1.35	41.10	34.93	16.25	2.13	65.52	30.49	3.99
Magura S58	35.75	190.28	169.52	0.90	28.61	35.32	26.57	6.03	52.00	39.12	8.88
Magura S59	36	197.71	164.39	0.72	26.36	35.56	29.57	5.53	50.32	41.85	7.83
Magura S59	36.5	137.31	141.68	1.27	38.73	36.15	17.70	2.55	64.11	31.37	4.52
Magura S60	36.75	160.54	187.50	1.75	38.25	33.09	16.92	6.74	58.32	29.81	11.87
Magura S60	37	166.75	144.46	0.89	29.51	40.68	23.76	2.78	60.52	35.35	4.13
Magura S61	37.5	161.70	179.17	1.59	36.44	35.30	17.54	6.35	59.70	29.62	10.68
Magura S62	37.75	149.05	168.99	1.79	37.80	37.52	15.30	5.27	64.62	26.33	9.05
Magura S62	38	175.40	154.87	0.90	29.46	38.29	24.77	4.10	57.03	36.87	6.10
Magura S63	39	172.94	161.78	1.19	30.28	40.40	21.47	5.22	60.22	32.00	7.78
Magura S64	39.25	216.18	210.76	1.28	27.53	34.01	24.37	10.69	49.24	35.28	15.48
Magura S64	39.5	159.71	166.64	1.43	34.73	36.98	18.75	5.26	60.68	30.72	8.61
Magura S65	40	127.28	154.42	1.90	44.45	33.18	13.33	3.89	65.83	26.45	7.72
Magura S66	40.25	141.17	176.38	2.10	41.39	34.83	13.08	5.60	65.11	24.43	10.46
Magura S66	40.5	304.60	274.59	0.78	24.99	21.35	26.85	23.52	29.78	37.44	32.77
Magura S67	40.75	148.83	206.85	1.99	43.73	26.41	12.65	8.26	55.89	26.70	17.41
Magura S67	41.25	343.46	289.42	0.61	21.60	19.88	26.67	28.97	26.34	35.32	38.34
Magura S68	42.75	223.83	235.02	1.29	30.43	30.02	21.84	13.56	45.91	33.38	20.71
Magura S68	43	377.35	291.70	0.43	19.74	15.23	29.46	33.11	19.59	37.86	42.55
Magura S69	44.25	156.54	183.91	1.82	38.50	34.29	16.02	6.41	60.45	28.25	11.31
Magura S69	44.5	181.69	205.90	1.56	35.80	31.79	18.74	9.06	53.34	31.45	15.20
Magura S70	45.75	242.82	222.64	1.10	24.88	31.58	27.46	13.37	43.62	37.92	18.46
Magura S70	46	183.20	200.18	1.54	33.72	33.58	19.69	8.52	54.36	31.85	13.78
Magura S71	47.5	140.26	186.58	1.99	45.67	27.47	13.79	6.38	57.67	28.95	13.38
Magura S72	48.75	244.85	187.02	0.48	23.21	26.54	37.17	10.23	35.89	50.27	13.84
Magura S72	49	160.72	148.19	1.11	31.41	41.17	20.89	3.53	62.80	31.83	5.37
Magura S73	50.25	119.33	147.71	2.00	46.51	32.42	12.54	3.22	67.28	26.03	6.68
Magura S73	50.5	172.49	174.20	1.56	31.34	40.86	19.18	5.98	61.89	29.05	9.06
Magura S74	52	242.79	231.32	1.12	26.29	29.63	26.23	14.19	42.35	37.44	20.22
Magura S75	53.5	180.09	202.43	1.64	34.63	33.97	18.35	8.50	55.85	30.17	13.97
Magura S76	55	255.37	224.17	1.15	20.63	36.13	27.52	14.18	46.42	35.36	18.22
Magura S76	55.5	185.51	192.62	1.76	28.54	43.89	17.77	7.94	63.07	25.53	11.40
Magura S77	56.5	149.77	184.34	2.06	40.45	35.87	13.47	6.36	64.40	24.18	11.42
Magura S77	57	168.31	195.88	1.84	35.77	36.78	15.69	7.74	61.08	26.06	12.86
Magura S78	58	225.35	243.18	1.27	33.23	27.56	20.82	14.66	43.72	33.03	23.24
Magura S78	58.5	167.19	153.35	2.11	22.20	56.49	15.59	4.09	74.18	20.46	5.36
Magura S79	59.5	196.46	232.39	1.61	35.12	32.42	16.00	12.00	53.65	26.48	19.87
Magura S79	59.75	231.91	252.92	1.28	32.45	28.74	19.24	15.94	45.03	30.09	24.89
Magura S79	60	244.08	253.55	1.24	27.99	31.68	20.36	16.52	46.22	29.70	24.08
Magura S80	61	180.85	171.24	1.01	31.88	34.07	24.49	6.05	52.73	37.90	9.37
Magura S80	61.25	119.17	152.03	1.73	48.24	26.97	13.88	3.65	60.63	31.18	8.19
Magura S80	61.5	176.97	180.88	1.14	35.11	31.05	22.53	7.10	51.17	37.12	11.71
Magura S81	62.5	304.23	238.21	0.72	19.57	23.01	35.63	19.59	29.43	45.55	25.02
Magura S82	63	217.39	188.99	0.77	27.44	30.22	30.01	9.36	43.43	43.12	13.45
Magura S82	64	171.69	192.41	1.59	36.63	33.01	18.63	7.53	55.80	31.49	12.71
Magura S82	64.5	298.85	241.15	0.71	21.71	21.18	35.06	19.39	28.01	46.35	25.64
Magura S83	66	187.10	175.90	1.68	23.62	48.37	19.61	6.45	64.99	26.34	8.67
Magura S84	67.5	171.88	144.06	1.40	22.59	53.31	19.15	3.85	69.87	25.08	5.05
Magura S85	68	76.32	78.05	2.28	51.72	40.79	3.15	0.20	92.42	7.13	0.46
Magura S86	68.5	121.05	94.19	1.42	28.22	60.55	8.86	0.27	86.90	12.71	0.39
Magura S87	69	150.34	97.67	1.04	16.98	68.22	13.95	0.43	82.60	16.89	0.51
Magura S88	70	127.40	106.21	1.70	27.21	58.99	10.10	0.87	84.31	14.44	1.24
Magura S89	70.5	126.76	82.79	0.73	21.04	68.79	8.33	0.00	89.20	10.80	0.01

Table A.11: **Magura grain size data. Data for each sample are the average of three consecutive analyses with a Malvern Mastersizer 2000 laser-diffraction grain size analyzer. Sand fraction data normalized to 100% are provided in the final three columns.**

Sample Name	Depth (m)	Mean	Std Dev	Skew	Silt & Clay	Fine Sand	Medium Sand	Coarse Sand	Normalized Fine	Normalized Medium	Normalized Coarse
Magura S90	71	171.03	173.99	1.94	26.63	49.00	15.92	5.92	69.20	22.47	8.34
Magura S91	71.5	107.58	109.60	1.39	42.66	40.31	11.35	0.49	77.31	21.75	0.94
Magura S91	72	152.72	124.00	0.82	28.39	47.59	20.39	0.89	69.12	29.60	1.28
Magura S92	72.25	238.59	206.40	1.16	21.42	37.01	28.23	11.41	48.30	36.82	14.88
Magura S92	72.5	254.87	196.50	1.07	16.03	39.38	32.12	11.39	47.52	38.75	13.74
Magura S93	72.75	177.45	149.99	2.12	14.67	63.66	16.13	4.34	75.67	19.17	5.16
Magura S93	73	232.66	206.88	1.20	23.04	36.76	27.13	11.11	49.03	36.18	14.79
Magura S94	73.5	190.30	209.83	1.66	32.31	37.42	17.71	9.61	57.79	27.36	14.85
Magura S95	74	152.88	188.72	2.00	39.74	34.90	13.96	6.70	62.81	25.12	12.07
Magura S95	74.25	209.02	214.37	1.42	29.66	34.82	21.69	10.79	51.80	32.21	15.99
Magura S96	75	234.46	240.79	1.31	28.42	33.06	21.25	14.58	47.99	30.84	21.17
Magura S97	75.5	191.64	203.25	1.69	29.86	40.65	18.16	9.04	59.92	26.76	13.32
Magura S98	76	222.52	207.39	1.31	24.74	37.65	24.88	10.66	51.45	33.99	14.56
Magura S99	76.5	185.57	170.93	1.30	27.74	41.21	22.75	5.99	58.91	32.52	8.57
Magura S101	77.5	174.24	195.22	1.91	31.26	42.62	15.11	7.80	65.06	23.04	11.89
Magura S101	78	267.54	236.22	1.07	21.08	32.92	27.79	16.26	42.79	36.11	21.10
Magura S102	78.25	129.16	187.20	2.26	47.74	26.71	11.05	6.27	60.75	25.06	14.19
Magura S102	78.5	186.55	210.12	1.58	35.44	32.54	18.56	9.61	53.62	30.57	15.81
Magura S103	79	267.91	222.29	1.07	18.92	34.33	30.77	14.56	43.09	38.63	18.28
Magura S104	79.5	134.12	164.85	2.38	39.35	40.66	10.96	4.60	72.34	19.49	8.17
Magura S104	80	264.19	238.49	1.11	22.64	32.80	26.79	16.14	43.33	35.37	21.29
Magura S105	80.5	187.79	206.54	1.82	28.66	43.72	15.55	9.24	63.84	22.69	13.47
Magura S106	80.75	229.33	245.33	1.29	30.74	29.62	20.59	14.83	45.54	31.66	22.80
Magura S106	81	277.26	226.53	0.91	19.78	29.53	32.66	15.95	37.79	41.79	20.42
Magura S107	81.5	208.47	174.94	2.23	6.23	69.56	16.70	7.28	74.37	17.85	7.78
Magura S108	81.75	209.66	241.52	1.45	34.76	29.34	17.68	13.56	48.44	29.19	22.36
Magura S108	82	369.62	291.31	0.49	19.50	17.73	28.38	32.03	22.71	36.32	40.97
Magura S109	84	326.82	247.83	0.87	12.83	32.15	32.24	22.08	37.18	37.29	25.53
Magura S110	85.5	287.93	235.90	1.03	16.40	35.14	29.77	17.58	42.60	36.09	21.32
Magura S111	87	309.62	250.54	0.94	15.53	33.16	29.48	20.85	39.72	35.30	24.97
Magura S112	89	323.52	254.43	0.81	15.62	28.76	31.46	22.69	34.70	37.94	27.36
Magura S113	90	336.22	260.53	0.72	15.91	25.87	31.95	24.76	31.33	38.69	29.98
Magura S113	90.5	358.08	260.14	0.67	12.69	26.34	33.28	27.02	30.41	38.41	31.19
Magura S114	91.5	214.99	245.01	1.45	32.16	32.18	16.98	14.10	50.89	26.84	22.27
Magura S114	92	259.58	268.37	1.08	29.56	26.40	20.91	19.32	39.62	31.38	29.00
Magura S115	93	182.69	165.55	2.33	13.47	65.51	14.32	5.67	76.62	16.75	6.63
Magura S115	93.5	182.57	157.19	2.70	8.10	74.03	12.59	5.11	80.70	13.73	5.57
Magura S116	95	30.67	32.33	2.25	75.99	11.06	0.43	0.00	97.12	2.85	0.03
Magura S117	95.5	176.32	176.91	2.13	21.30	55.71	14.43	6.34	72.85	18.87	8.29
Magura S118	96	185.12	176.61	2.16	17.11	59.90	15.00	6.54	73.55	18.42	8.03
Magura S119	98	218.31	207.70	1.38	26.49	37.41	24.11	10.32	52.08	33.56	14.37
Magura S120	98.5	206.74	178.94	2.05	9.47	64.78	17.61	7.58	72.01	19.57	8.43
Magura S121	99	211.48	184.04	1.15	24.36	38.78	26.90	8.01	52.63	36.50	10.87
Magura S122	99.5	192.08	182.47	1.43	28.13	39.78	22.82	7.00	57.17	32.78	10.05
Magura S122	100	312.18	244.14	0.87	15.52	30.06	32.56	20.45	36.20	39.20	24.60
Magura S123	100.5	288.19	249.66	0.94	21.03	28.57	29.01	19.10	37.27	37.83	24.90
Magura S124	101	280.94	241.59	1.00	19.22	31.95	28.90	17.71	40.68	36.78	22.54
Magura S125	101.5	199.60	151.01	0.85	19.31	46.93	27.47	4.71	59.32	34.73	5.95
Magura S126	102	184.92	141.93	0.95	20.16	50.30	24.39	3.54	64.30	31.18	4.52
Magura S127	103	191.33	154.26	1.09	20.63	48.06	24.57	4.80	62.08	31.73	6.19
Magura S128	103.5	206.35	158.14	0.90	18.56	46.17	27.80	5.80	57.88	34.85	7.27
Magura S130	104.5	203.23	138.60	0.69	16.37	49.77	29.32	3.43	60.31	35.53	4.16
Magura S131	105	131.64	118.59	1.00	34.42	44.63	16.27	0.53	72.66	26.48	0.86
Magura S132	105.5	73.37	88.32	1.92	53.30	32.16	5.57	0.13	84.94	14.71	0.35
Magura S132	106	97.64	103.71	1.34	46.44	36.94	10.33	0.03	78.09	21.85	0.06
Magura S133	106.25	156.32	111.06	0.62	21.97	55.85	19.79	0.05	73.79	26.14	0.07
Magura S133	106.5	174.52	109.00	0.39	15.55	58.67	23.52	0.04	71.35	28.60	0.05
Magura S134	106.75	69.93	91.99	2.82	55.23	30.92	4.13	0.62	86.67	11.59	1.75
Magura S134	107	137.13	114.37	0.87	30.58	48.94	16.78	0.21	74.23	25.46	0.31
Magura S135	107.5	158.65	119.35	0.56	25.07	49.30	22.34	0.11	68.71	31.13	0.16
Magura S136	108	201.67	150.59	0.97	17.16	49.80	26.80	4.77	61.20	32.93	5.87
Magura S137	109	130.61	112.23	0.96	31.74	48.81	15.20	0.20	76.02	23.67	0.31
Magura S138	109.5	249.66	246.89	1.17	27.12	29.86	23.68	16.02	42.95	34.04	23.01
Magura S139	110	223.55	224.04	1.35	26.95	34.91	22.55	12.26	50.12	32.33	17.56
Magura S140	110.5	298.01	270.41	0.84	24.49	22.97	26.53	22.47	32.02	36.87	31.11
Magura S140	110.5	300.03	250.92	0.84	19.79	26.46	30.85	20.31	34.09	39.74	26.17
Magura S141	111	295.23	251.06	0.91	19.78	28.45	29.58	19.79	36.56	38.01	25.43
Magura S142	112	191.01	165.05	2.29	10.01	68.01	15.48	5.97	76.02	17.31	6.67
Magura S143	112.5	235.17	259.49	1.25	32.15	27.00	19.07	16.67	43.07	30.38	26.55
Magura S143	112.75	68.40	117.18	4.12	56.66	24.81	3.41	1.79	82.56	11.36	6.08
Magura S144	116	362.83	285.34	0.73	8.98	37.12	23.14	30.11	41.08	25.61	33.31
Magura S145	119	314.25	270.15	0.83	19.97	28.10	26.60	23.69	35.84	33.93	30.23
Magura S146	122	288.48	259.74	0.98	21.31	30.45	25.75	20.19	39.86	33.71	26.42
Magura S146	122	256.72	245.38	1.19	23.27	34.54	23.43	16.30	46.51	31.54	21.95

Table A.12: **Raipur grain size data. Data for each sample are the average of three consecutive analyses with a Malvern Mastersizer 2000 laser-diffraction grain size analyzer. Sand fraction data normalized to 100% are provided in the final three columns.**

Sample Name	Depth (m)	Mean	Std Dev	Skew	Silt & Clay	Fine Sand	Medium Sand	Coarse Sand	Normalized Fine	Normalized Medium	Normalized Coarse
Raipur Sect 6	5.3	3.69	5.22	6.66	56.30	36.00	2.06	0.64	93.03	5.33	1.64
Raipur Sect 6	5.5	5.17	6.09	7.13	67.44	23.27	1.05	0.15	95.11	4.28	0.61
Raipur Sect 7	7.0	2.58	3.23	4.19	42.15	51.40	2.12	0.80	94.64	3.90	1.46
Raipur Sect 8	7.8	2.24	2.48	2.81	29.38	51.34	14.75	0.69	76.89	22.08	1.03
Raipur Sect 8	8.0	4.04	5.58	7.01	59.10	33.48	1.98	0.64	92.77	5.46	1.76
Raipur Sect 9	8.5	1.15	1.15	1.16	13.13	63.61	21.02	0.77	74.49	24.61	0.90
Raipur Sect 10	9.0	0.73	0.51	0.34	6.88	72.25	19.03	1.33	78.02	20.55	1.44
Raipur Sect 11	10.0	1.84	1.87	2.01	22.75	55.54	18.02	1.06	74.43	24.15	1.42
Raipur Sect 12	11.0	2.11	2.18	2.32	25.10	56.75	15.69	0.00	78.35	21.64	0.01
Raipur Sect 13	11.5	0.89	0.66	0.63	12.02	76.42	10.38	0.00	88.04	11.96	0.00
Raipur Sect 14	12.0	2.33	2.34	2.73	34.07	55.26	5.57	0.77	89.71	9.03	1.26
Raipur Sect 15	13.0	0.80	0.71	0.54	6.74	68.67	23.83	0.02	74.22	25.76	0.03
Raipur Sect 16	13.5	0.99	1.07	1.20	12.83	45.66	29.21	11.53	52.85	33.80	13.34
Raipur Sect 17	14.0	0.92	1.11	1.36	13.46	44.02	29.06	12.94	51.19	33.78	15.04
Raipur Sect 18	14.5	1.31	1.35	1.44	16.01	49.77	26.08	6.94	60.11	31.50	8.38
Raipur Sect 19	15.0	3.04	3.09	3.36	39.23	44.37	9.64	1.22	80.34	17.46	2.21
Raipur Sect 20	16.0	1.68	1.84	2.08	22.34	48.84	23.87	2.46	64.97	31.76	3.27
Raipur Sect 21	16.5	1.84	1.93	2.14	24.05	48.48	23.02	1.86	66.09	31.37	2.54
Raipur Sect 22	17.0	1.73	2.03	2.46	25.05	46.83	20.53	5.53	64.25	28.15	7.59
Raipur Sect 23	17.5	1.87	1.93	2.10	23.17	49.51	20.33	4.41	66.69	27.38	5.93
Raipur Sect 24	18.0	1.29	1.24	1.30	16.41	56.49	24.64	0.45	69.25	30.20	0.55
Raipur Sect 25	18.8	1.41	1.69	2.06	20.48	48.54	22.17	7.96	61.71	28.17	10.12
Raipur Sect 26	19.5	2.40	2.62	3.35	39.57	51.52	3.18	1.88	91.05	5.63	3.32
Raipur Sect 27	20.0	3.29	3.44	4.02	46.78	40.91	4.89	1.85	85.89	10.23	3.88
Raipur Sect 28	21.0	5.54	5.33	5.59	66.36	17.87	1.37	2.04	83.99	6.42	9.59
Raipur Sect 29	21.5	1.68	1.74	2.13	26.31	62.38	8.18	0.38	87.94	11.52	0.54
Raipur Sect 30	22.5	0.86	1.02	1.28	13.46	44.45	26.78	14.70	51.74	31.16	17.10
Raipur Sect 31	23.0	1.72	1.97	2.43	26.03	51.65	14.84	5.71	71.55	20.55	7.90
Raipur Sect 32	23.5	0.63	0.60	1.08	17.53	69.13	9.28	3.17	84.74	11.38	3.88
Raipur Sect 32	23.8	4.39	5.09	6.04	61.13	29.36	1.64	0.39	93.58	5.19	1.23
Raipur Sect 33	24.0	2.06	2.28	2.88	33.51	56.67	5.46	0.99	89.78	8.65	1.57
Raipur Sect 34	24.5	1.44	1.50	1.66	18.82	57.15	19.15	3.22	71.88	24.08	4.04
Raipur Sect 35	25.5	1.24	1.07	1.09	16.01	77.83	4.71	0.00	94.29	5.71	0.00
Raipur Sect 36	26.0	1.39	1.34	1.41	17.63	56.46	21.59	2.42	70.16	26.83	3.01
Raipur Sect 37	26.5	2.06	2.23	2.55	27.84	55.78	13.59	0.08	80.32	19.57	0.11
Raipur Sect 39	27.3	4.79	4.73	5.09	60.06	27.44	1.65	0.43	92.99	5.57	1.44
Raipur Sect 39	27.5	5.57	5.92	6.54	69.26	18.90	0.46	0.19	96.74	2.32	0.93
Raipur Sect 40	28.5	2.40	2.42	2.88	36.05	55.61	3.36	0.93	92.84	5.61	1.55
Raipur Sect 41	29.0	1.50	1.34	1.31	18.36	58.68	18.52	1.63	74.45	23.50	2.05
Raipur Sect 42	30.0	1.36	1.20	1.30	19.94	64.10	12.56	0.42	83.16	16.29	0.55
Raipur Sect 45	31.5	1.42	1.24	1.28	19.86	59.29	16.90	0.85	76.97	21.94	1.09
Raipur Sect 46	32.0	1.48	1.57	1.82	20.65	34.88	34.25	7.88	45.29	44.47	10.23
Raipur Sect 47	33.0	1.57	1.77	2.07	22.38	41.38	31.05	2.19	55.45	41.61	2.94
Raipur Sect 48	33.5	0.95	0.97	1.08	13.72	54.60	27.17	2.67	64.66	32.18	3.16
Raipur Sect 49	34.0	1.55	1.60	1.81	21.65	50.34	24.09	1.41	66.38	31.76	1.86
Raipur Sect 50	34.5	1.45	1.46	1.68	21.47	53.26	20.71	1.79	70.30	27.34	2.37
Raipur Sect 51	35.0	2.26	2.63	3.21	33.46	44.67	16.36	2.57	70.24	25.72	4.03
Raipur Sect 52	36.0	0.90	0.92	1.10	14.69	58.20	22.69	2.79	69.56	27.12	3.33
Raipur Sect 53	36.5	0.73	0.67	0.65	9.09	75.22	15.06	0.00	83.32	16.68	0.00
Raipur Sect 54	37.0	1.04	0.99	1.07	13.82	45.61	30.81	8.34	53.84	36.38	9.78
Raipur Sect 55	37.5	1.26	1.31	1.49	17.73	54.85	22.62	2.95	68.21	28.13	3.66
Raipur Sect 56	38.0	1.46	1.52	1.72	19.99	48.98	25.38	3.44	62.95	32.63	4.42
Raipur Sect 57	39.0	1.46	1.51	1.72	20.27	52.68	21.82	3.04	67.94	28.13	3.92
Raipur Sect 93	63.0	1.95	2.32	2.96	32.81	56.35	6.04	0.00	90.32	9.68	0.00
Raipur Sect 94	65.0	3.57	3.45	3.70	45.96	22.30	19.71	2.47	50.15	44.31	5.54
Raipur Sect 95	67.0	1.78	1.86	2.11	23.55	22.47	32.70	17.69	30.86	44.88	24.26
Raipur Sect 97	71.5	1.91	1.88	2.10	26.49	42.71	23.58	3.70	61.03	33.69	5.28
Raipur Sect 98	73.5	3.37	3.73	4.37	47.86	37.47	6.94	1.09	82.36	15.24	2.40
Raipur Sect 99	75.5	2.01	1.97	2.21	28.64	46.02	19.83	1.62	68.21	29.39	2.40
Raipur Sect 100	76.5	0.85	0.85	0.89	11.33	62.95	23.39	0.87	72.18	26.82	1.00
Raipur Sect 101	77.0	0.79	0.79	0.86	10.85	63.77	23.00	1.32	72.40	26.11	1.50
Raipur Sect 102	77.5	1.84	1.82	1.92	23.20	51.39	21.78	0.53	69.73	29.55	0.71
Raipur Sect 103	78.0	2.35	2.38	2.56	29.58	48.37	17.05	0.45	73.44	25.88	0.69
Raipur Sect 104	78.8	2.05	2.01	2.04	23.89	56.64	15.89	0.00	78.10	21.90	0.00
Raipur Sect 108	81.0	1.46	1.36	1.35	17.42	60.51	19.24	0.02	75.86	24.11	0.02
Raipur Sect 109	81.5	2.88	2.90	3.11	35.70	46.10	11.88	0.79	78.45	20.21	1.34
Raipur Sect 110	82.5	4.45	3.65	3.50	54.05	26.18	5.92	0.58	80.12	18.11	1.77
Raipur Sect 111	83.0	2.99	2.82	2.99	38.13	43.15	12.08	0.69	77.17	21.60	1.23
Raipur Sect 119	99.5	1.05	1.03	1.14	14.17	13.00	33.12	37.31	15.58	39.70	44.71
Raipur Sect 120	101.3	1.94	1.81	1.91	24.49	10.59	28.31	32.63	14.82	39.58	45.59
Raipur Sect 121	103.0	1.90	1.75	1.83	23.56	9.74	26.89	35.78	13.46	37.13	49.40
Raipur Sect 124	106.8	2.59	2.40	2.52	31.95	11.41	25.35	25.54	18.31	40.69	40.99
Raipur Sect 125	108.5	2.85	2.84	3.07	36.07	8.39	20.54	28.75	14.19	35.70	50.10
Raipur Sect 130	116.0	2.55	2.43	2.58	32.07	14.58	23.01	26.03	22.99	36.20	40.81

Table A.13: **MSCL whole-core MS and density data for Magura. Data is an average for each section of core based on a 3-point moving average process.**

Section #	Bottom (m)	Top (m)	Density (gm/cc)	MS (SI)
1	0.6	1.2	2.1	21.3
2	1.2	1.8	2.1	21.8
3	1.8	2.4	2.1	22.9
4	2.4	3.0	2.1	29.8
5	3.0	3.7	2.1	30.3
6	3.7	4.3	2.1	34.6
7	4.3	4.9	2.1	64.4
8	4.9	5.5	2.1	37.8
9	5.5	6.1	2.1	35.1
10	6.1	6.7	2.1	31.9
11	6.7	7.3	2.1	30.9
12	7.3	7.9	2.1	35.1
13	7.9	8.5	2.1	
14	8.5	9.1	2.1	31.4
15	9.1	9.8	2.1	57.4
16	9.8	10.4	2.0	60.6
17	10.4	11.0	2.1	65.4
18	11.0	11.6	2.0	61.2
19	11.6	12.2	2.2	48.9
20	12.2	12.8	2.0	31.4
21	12.8	13.4	2.0	30.3
22	13.4	14.0	2.1	33.5
23	14.0	14.6	2.1	33.0
24	14.6	15.2	2.1	35.1
25	15.2	15.8	2.1	33.0
26	15.8	16.5	2.1	30.9
27	16.5	17.1	2.0	27.7
28	17.1	17.7	2.0	28.7
29	17.7	18.3	2.1	30.3
30	18.3	18.9	2.1	30.3
31	18.9	19.5	2.0	31.9
32	19.5	20.1	2.1	30.3
33	20.1	20.7	2.1	30.3
34	20.7	21.3	2.1	38.3
36	21.9	22.6	2.1	35.1
37	22.6	23.2	2.1	33.0
38	23.2	23.8	2.1	53.7
39	23.8	24.4	2.1	60.6
40	24.4	25.0	2.1	25.0
41	25.0	25.6	2.1	61.7
42	25.6	26.2	2.3	26.6
43	26.2	26.8	2.2	67.0
44	26.8	27.4	2.2	84.6
45	27.4	28.0	2.2	53.7
46	28.0	28.7	2.1	88.8
47	28.7	29.3	2.2	121.8
48	29.3	29.9	2.2	109.6
49	29.9	30.5	2.2	128.7
50	30.5	31.1	2.2	589.4
51	31.1	31.7	2.1	137.2
52	31.7	32.3	2.2	100.5
53	32.3	32.9	2.1	75.5
54	32.9	33.5	2.1	1105.3
55	33.5	34.1	2.1	370.2
56	34.1	34.7	2.2	89.4
57	34.7	35.4	2.2	90.4
58	35.4	36.0	2.2	194.2
59	36.0	36.6	2.1	260.1
60	36.6	37.2	2.2	234.0
61	37.2	37.8	2.3	103.2
62	37.8	38.4	2.2	120.2
63	38.4	39.0	2.2	71.8
64	39.0	39.6	2.2	96.3
65	39.6	40.2	2.3	54.3
66	40.2	40.8	2.2	70.2
67	40.8	41.5	2.2	67.6
68	42.7	43.3	2.1	63.3
69	44.2	44.8	2.2	61.2
70	45.7	46.3	2.2	250.5
71	47.2	47.9	2.2	42.0
72	48.8	49.4	2.2	121.3

Table A.14: **MSCL whole-core MS and density data for Magura. Data is an average for each section of core based on a 3-point moving average process.**

Section #	Bottom (m)	Top (m)	Density (gm/cc)	MS (SI)
73	50.3	50.9	2.2	524.5
74	51.8	52.4	2.2	359.0
75	53.3	53.9	2.2	118.1
76	54.9	55.5	2.2	23.4
77	56.4	57.0	2.1	48.4
78	57.9	58.5	2.2	26.1
79	59.4	60.0	2.2	76.6
80	61.0	61.6	2.1	33.5
81	62.5	63.1	2.2	69.1
82	64.0	64.6	2.2	63.8
83	65.5	66.1	2.1	78.7
84	67.1	67.7	2.2	27.7
85	67.7	68.3	2.2	38.3
86	68.3	68.9	2.1	41.5
87	68.9	69.5	2.1	31.4
88	69.5	70.1	2.1	79.8
89	70.1	70.7	2.1	87.2
90	70.7	71.3	2.1	64.9
91	71.3	71.9	2.2	348.9
92	71.9	72.5	2.1	48.9
93	72.5	73.2	2.1	43.1
94	73.2	73.8	2.2	71.3
95	73.8	74.4	2.2	66.0
96	74.4	75.0	2.2	75.5
97	75.0	75.6	2.2	51.1
98	75.6	76.2	2.1	35.1
99	76.2	76.8	2.0	42.6
101	77.4	78.0	2.1	148.4
102	78.0	78.6	2.2	142.6
103	78.6	79.2	2.1	67.6
104	79.2	79.9	2.1	51.1
105	79.9	80.5	2.2	85.1
106	80.5	81.1	2.1	137.2
107	81.1	81.7	2.1	59.6
108	81.7	82.3	2.2	131.3
109	83.8	84.4	2.1	208.5
110	85.3	86.0	2.1	134.0
111	86.9	87.5	2.2	164.9
112	88.4	89.0	2.2	122.3
113	89.9	90.5	2.2	124.5
114	91.4	92.0	2.2	156.9
115	93.0	93.6	2.1	62.8
116	94.5	95.1	2.1	19.1
117	95.1	95.7	2.1	64.9
118	95.7	96.3	2.1	62.2
119	97.5	98.1	2.1	17.6
120	98.1	98.8	2.2	109.6
121	98.8	99.4	2.1	
122	99.4	100.0	2.1	47.9
123	100.0	100.6	2.2	59.0
124	100.6	101.2	2.2	64.4
125	101.2	101.8	2.1	23.9
126	101.8	102.4	2.1	26.1
127	102.4	103.0	2.0	66.5
128	103.0	103.6	2.1	88.3
130	104.2	104.9	2.2	70.7
131	104.9	105.5	2.1	104.8
132	105.5	106.1	2.3	75.0
133	106.1	106.7	2.2	41.0
134	106.7	107.3	2.1	34.0
135	107.3	107.9	2.1	40.4
136	107.9	108.5	2.1	69.7
137	108.5	109.1	2.1	99.5
138	109.1	109.7	2.1	90.4
139	109.7	110.3	2.2	66.5
140	110.3	110.9	2.2	158.0
141	110.9	111.6	2.2	167.0
142	111.6	112.2	2.1	103.2
143	112.2	112.8	2.1	16.5
144	115.8	116.4	2.0	42.6
145	118.9	119.5	2.2	42.6
146	121.9	122.5	2.1	60.6

Table A.15: **MSCL whole-core MS and density data for Raipur. Data is an average for each section of core based on a 3-point moving average process.**

Section #	Bottom (m)	Top (m)	Density (gm/cc)	MS (SI)
1	1.98	2.59	1.98	50.53
2	3.05	3.66	1.95	127.66
3	4.11	4.72	1.89	87.77
4	6.40	7.01	1.89	62.23
5	7.62	8.23	1.93	193.62
6	8.23	8.84	1.93	107.45
7	8.84	9.45	1.79	86.17
8	9.45	10.06	1.92	223.94
9	10.67	11.28	1.87	190.43
10	11.28	11.89	1.90	161.17
11	11.89	12.50	1.90	86.17
12	12.50	13.11	1.92	164.89
13	13.11	13.72	1.90	197.34
14	13.72	14.33	1.80	23.40
15	14.33	14.94	1.80	90.96
16	14.94	15.54	1.77	163.83
17	15.54	16.15	1.88	93.62
18	16.15	16.76	1.85	47.34
19	16.76	17.37	1.95	64.36
20	17.37	17.98	1.83	94.68
21	17.98	18.59	1.79	61.17
22	18.59	19.20	1.93	57.98
23	19.20	19.81	1.81	88.30
24	19.81	20.42	1.86	217.02
25	20.42	21.03	1.92	201.13
26	22.86	23.47	1.93	93.62
27	23.93	24.54	1.96	332.45
28	24.99	25.60	1.95	1362.24
29	26.06	26.67	1.87	36.17
30	27.13	27.74	1.92	92.55
31	28.19	28.80	1.91	81.92
32	28.80	29.41	1.88	136.17
33	29.41	30.02	1.89	101.06
34	30.02	30.63	1.93	73.40
35	30.63	31.24	1.94	32.45
36	31.24	31.85	1.94	86.70
37	31.85	32.46	1.95	125.00
38	32.46	33.07	2.02	196.28
39	33.07	33.68	1.93	63.30
40	33.68	34.29	1.98	90.43
41	34.29	34.90	1.97	78.72
42	34.90	35.51	1.94	110.64
43	35.51	36.12	1.84	148.94
44	36.12	36.73	1.89	163.30
45	36.73	37.34	1.88	86.17
46	37.34	37.95	1.97	102.66
47	37.95	38.56	1.93	93.09
48	38.56	39.17	1.90	91.49
49	39.62	40.23	1.99	10.11
50	40.69	41.30	1.83	15.43
51	41.76	42.37	1.94	15.96
52	42.37	42.98	1.92	15.96
53	43.59	44.20	1.79	35.11
54	44.81	45.42	1.94	18.09
55	46.02	46.63	1.90	19.15
56	47.24	47.85	1.88	17.55
57	48.46	49.07	1.90	20.74
58	50.90	51.51	1.91	15.96
59	52.12	52.73	1.98	20.21
60	53.34	53.95	2.06	17.55
61	54.56	55.17	2.03	15.43
62	58.22	58.83	1.97	42.02
63	58.83	59.13	2.00	9.57
64	60.81	61.26	1.84	10.11
65	61.26	61.57	1.80	18.62

Table A.16: **Detrital zircon isotope ratio data for samples AZ300 and AZ325 from a borehole near BH8. AZ300 is from 92 m and AZ325 is from 99 m depth.**

	Isotope Ratios	1σ						
Sample	$^{207}Pb/^{206}Pb$		$^{207}Pb/^{206}Pb$	$^{207}Pb/^{235}U$	$^{207}Pb/^{235}U$	$^{206}Pb/^{238}U$	$^{206}Pb/^{238}U$	$^{208}Pb/^{232}Th$	$^{208}Pb/^{232}Th$
AZ300-1	0.0999	0.0012	3.5016	0.0420	0.2543	0.0026	0.0751	0.0008
AZ300-2	0.0991	0.0016	3.7656	0.0583	0.2755	0.0030	0.0895	0.0010
AZ300-3	0.0652	0.0010	1.2747	0.0191	0.1419	0.0015	0.0400	0.0005
AZ300-4	0.0645	0.0022	0.6156	0.0204	0.0692	0.0009	0.0243	0.0005
AZ300-5	0.0602	0.0011	0.8200	0.0150	0.0988	0.0011	0.0282	0.0004
AZ300-6	0.0637	0.0009	0.0288	0.0003	0.2529	0.0038	0.0107	0.0001
AZ300-7	0.0552	0.0014	0.5394	0.0133	0.0708	0.0008	0.0208	0.0003
AZ300-8	0.0713	0.0010	1.2908	0.0179	0.1313	0.0014	0.0418	0.0004
AZ300-9	0.0577	0.0008	0.0743	0.0008	0.5909	0.0084	0.0246	0.0003
AZ300-10	0.0603	0.0012	0.0766	0.0009	0.6366	0.0123	0.0258	0.0004
AZ300-11	0.0554	0.0015	0.1320	0.0034	0.0173	0.0002	0.0060	0.0001
AZ300-12	0.0650	0.0083	0.0695	0.0087	0.0078	0.0003	0.0028	0.0002
AZ300-13	0.1124	0.0018	0.0868	0.0010	1.3448	0.0221	0.0474	0.0009
AZ300-14	0.0595	0.0008	0.0610	0.0007	0.4997	0.0073	0.0185	0.0002
AZ300-15	0.0534	0.0009	0.0344	0.0004	0.2533	0.0045	0.0099	0.0001
AZ300-16	0.0354	0.0014	0.1211	0.0018	0.4725	0.0186	0.0067	0.0002
AZ300-17	0.0371	0.0010	0.1721	0.0021	0.7035	0.0177	0.0089	0.0002
AZ300-18	0.0304	0.0016	0.0216	0.0003	0.0725	0.0038	0.0020	0.0002
AZ300-19	0.0913	0.0012	0.1835	0.0020	1.8479	0.0217	0.0094	0.0002
AZ300-20	0.0292	0.0032	0.0067	0.0002	0.0217	0.0023	0.0021	0.0004
AZ300-21	0.0923	0.0007	0.4734	0.0047	4.8193	0.0328	0.0242	0.0003
AZ300-22	0.0441	0.0008	0.2402	0.0026	1.1689	0.0201	0.0126	0.0004
AZ300-23	0.0352	0.0008	0.1063	0.0012	0.4123	0.0094	0.0058	0.0002
AZ300-24	0.0410	0.0006	0.1957	0.0020	0.8842	0.0126	0.0106	0.0003
AZ300-25	0.0693	0.0008	0.1747	0.0018	1.8075	0.0213	0.0308	0.0003
AZ300-26	0.1634	0.0020	0.1930	0.0021	4.7069	0.0588	0.0521	0.0007
AZ300-27	0.1568	0.0015	0.4386	0.0045	10.2659	0.1085	0.0742	0.0006
AZ300-28	0.0736	0.0016	0.1510	0.0018	1.6583	0.0362	0.0265	0.0003
AZ300-29	0.0526	0.0009	0.0675	0.0007	0.5293	0.0088	0.0110	0.0001
AZ300-30	0.0958	0.0050	0.1632	0.0034	2.3342	0.1182	0.0351	0.0019
AZ300-31	0.0729	0.0011	0.1084	0.0012	1.1799	0.0180	0.0230	0.0003
AZ300-32	0.0689	0.0008	0.1738	0.0018	1.7881	0.0219	0.0333	0.0004
AZ300-33	0.0802	0.0010	0.1949	0.0020	2.3326	0.0295	0.0369	0.0004
AZ300-34	0.0611	0.0010	0.1332	0.0014	1.2148	0.0198	0.0242	0.0003
AZ300-35	0.0350	0.0030	0.0349	0.0008	0.2041	0.0172	0.0026	0.0001
AZ300-36	0.0624	0.0012	0.0613	0.0007	0.6632	0.0131	0.0103	0.0001
AZ300-37	0.0602	0.0009	0.1418	0.0015	1.4784	0.0239	0.0204	0.0003
AZ300-38	0.0356	0.0018	0.0661	0.0011	0.3942	0.0198	0.0057	0.0002
AZ300-39	0.0509	0.0013	0.2159	0.0028	1.8388	0.0464	0.0162	0.0003
AZ300-40	0.0402	0.0008	0.1500	0.0016	1.0090	0.0194	0.0133	0.0004
AZ300-41	0.1442	0.0041	0.0263	0.0004	0.6571	0.0176	0.0066	0.0001
AZ300-42	0.0641	0.0015	0.1562	0.0019	1.7343	0.0416	0.0243	0.0004
AZ300-43	0.0818	0.0014	0.2287	0.0026	3.2392	0.0588	0.0306	0.0005
AZ325-1	0.1014	0.0010	0.1427	0.0015	2.3514	0.0260	0.0096	0.0001
AZ325-2	0.1038	0.0012	0.2512	0.0027	4.2366	0.0533	0.0465	0.0007
AZ325-3	0.0602	0.0009	0.2437	0.0028	2.2012	0.0332	0.0197	0.0006
AZ325-4	0.2759	0.0020	0.3204	0.0034	13.2533	0.0945	0.1008	0.0005
AZ325-5	0.0638	0.0013	0.0720	0.0008	0.7463	0.0157	0.0176	0.0003
AZ325-6	0.0379	0.0011	0.1019	0.0013	0.5788	0.0161	0.0083	0.0002
AZ325-7	0.0764	0.0019	0.3339	0.0051	3.8221	0.0956	0.0225	0.0006
AZ325-8	0.0295	0.0005	0.0584	0.0006	0.2582	0.0040	0.0044	0.0001
AZ325-9	0.1002	0.0013	0.2896	0.0032	4.7171	0.0660	0.0404	0.0008
AZ325-10	0.0287	0.0014	0.0024	0.0000	0.0103	0.0005	0.0003	0.0000
AZ325-11	0.0681	0.0043	0.0460	0.0009	0.4339	0.0268	0.0242	0.0021
AZ325-12	0.1131	0.0018	0.3289	0.0044	5.1496	0.0904	0.0877	0.0017
AZ325-13	0.0667	0.0023	0.0809	0.0012	0.7477	0.0254	0.0270	0.0007
AZ325-14	0.0594	0.0015	0.0795	0.0011	0.6540	0.0165	0.0234	0.0005
AZ325-15	0.0653	0.0017	0.0854	0.0012	0.7728	0.0197	0.0277	0.0008
AZ325-16	0.1553	0.0020	0.2055	0.0026	4.4227	0.0631	0.0945	0.0014
AZ325-17	0.0736	0.0017	0.0675	0.0009	0.6882	0.0160	0.0519	0.0011
AZ325-18	0.2148	0.0024	0.5850	0.0072	17.4164	0.2221	0.1457	0.0019
AZ325-19	0.1525	0.0020	0.3390	0.0043	7.1567	0.1040	0.0696	0.0012
AZ325-20	0.1142	0.0019	0.2639	0.0035	4.1706	0.0735	0.1444	0.0053
AZ325-21	0.0903	0.0015	0.2808	0.0033	4.0955	0.0686	0.0672	0.0013
AZ325-22	0.0481	0.0014	0.0668	0.0008	0.5193	0.0145	0.0242	0.0005
AZ325-23	0.0561	0.0013	0.1140	0.0014	1.0327	0.0235	0.0285	0.0006
AZ325-24	0.0549	0.0027	0.1132	0.0019	1.0040	0.0476	0.0318	0.0019
AZ325-25	0.1550	0.0046	0.4299	0.0081	10.7617	0.3227	0.1108	0.0050
AZ325-26	0.0929	0.0014	0.2629	0.0030	3.9445	0.0605	0.0759	0.0021
AZ325-27	0.0547	0.0045	0.0783	0.0019	0.6924	0.0560	0.0201	0.0011
AZ325-28	0.0908	0.0014	0.2507	0.0029	3.6768	0.0596	0.0711	0.0018
AZ325-29	0.0932	0.0023	0.0380	0.0005	0.5722	0.0140	0.0101	0.0005
AZ325-30	0.0598	0.0022	0.1257	0.0018	1.2148	0.0435	0.0414	0.0011
AZ325-31	0.0908	0.0011	0.2750	0.0030	4.0322	0.0537	0.0710	0.0009
AZ325-32	0.1009	0.0035	0.2192	0.0037	3.5722	0.1203	0.0823	0.0044

Table A.17: **Detrital zircon age estimates for samples AZ300 and AZ325 from a borehole near BH8. AZ300 is from 92 m and AZ325 is from 99 m depth.**

Age Estimate (ma) 1σ (ma)

Sample	$^{207}Pb/^{206}Pb$	$^{207}Pb/^{206}Pb$	$^{207}Pb/^{235}U$	$^{207}Pb/^{235}U$	$^{206}Pb/^{238}U$	$^{206}Pb/^{238}U$	$^{208}Pb/^{232}Th$	$^{208}Pb/^{232}Th$
AZ300-1	1621.3	22.46	1527.6	9.46	1460.5	13.37	1462.7	14.5
AZ300-2	1607.2	29.22	1585.4	12.42	1568.8	15.03	1731.9	18.86
AZ300-3	779.2	31.78	834.5	8.54	855.3	8.34	792.9	9.33
AZ300-4	757	70.05	487.1	12.81	431.6	5.34	484.8	10.72
AZ300-5	610.2	39.91	608.1	8.39	607.3	6.19	562.8	8.18
AZ300-6	731.5	30.24	183	2.04	228.9	3.06	215.5	2.46
AZ300-7	420.5	54.8	438	8.78	441.2	4.84	416.5	5.8
AZ300-8	965.2	28.5	841.6	7.92	795.4	7.72	828.4	8.1
AZ300-9	518.1	29.78	461.9	5	471.4	5.34	490.8	5.84
AZ300-10	614.1	40.85	475.7	5.37	500.2	7.64	514.6	8.21
AZ300-11	428.2	57.3	125.9	3.05	110.4	1.25	120.5	1.95
AZ300-12	773.6	248.95	68.2	8.22	49.8	1.6	56.4	3.93
AZ300-13	1838.9	29.2	536.5	6.07	865.3	9.58	935.2	16.41
AZ300-14	584.6	30.42	381.4	4.17	411.5	4.97	371	4.06
AZ300-15	345.7	38.89	218.1	2.46	229.3	3.64	199.2	2.54
AZ300-16	0.1	0	737.1	10.07	392.9	12.82	134	4.16
AZ300-17	0.1	0	1023.6	11.31	540.9	10.54	179.9	3.67
AZ300-18	0.1	0	137.7	2.15	71.1	3.57	39.7	3.02
AZ300-19	1452.1	24.36	1086.2	10.75	1062.7	7.75	189.7	4.33
AZ300-20	0.1	0	43.2	1.15	21.7	2.26	41.3	7.84
AZ300-21	1472.8	14.68	2498.6	20.48	1788.3	5.72	483.3	5.64
AZ300-22	0.1	0	1387.7	13.67	786.1	9.4	253.9	8.09
AZ300-23	0.1	0	651.1	7.03	350.5	6.76	117.2	3.12
AZ300-24	0.1	0	1152	10.96	643.2	6.78	213.9	5.96
AZ300-25	908	22.88	1038.1	9.82	1048.2	7.68	612.7	5.09
AZ300-26	2491.5	20.3	1137.5	11.16	1768.5	10.47	1025.7	14.24
AZ300-27	2421.7	16.62	2344.4	20.14	2459	9.78	1446	10.41
AZ300-28	1030	43.74	906.6	10	992.7	13.81	529.5	6.62
AZ300-29	310.4	36.76	420.8	4.32	431.3	5.81	220.7	2.71
AZ300-30	1544.3	94.97	974.6	18.84	1222.8	36	696.9	36.65
AZ300-31	1011.5	30.25	663.6	6.73	791.3	8.4	460.3	5.43
AZ300-32	896.9	23.97	1033	9.83	1041.1	7.96	662.3	7.68
AZ300-33	1201.6	23.8	1147.9	10.94	1222.3	8.98	732.3	7.11
AZ300-34	643.2	34.27	806.1	8.13	807.4	9.09	483	6.37
AZ300-35	0.1	0	220.8	5.11	188.6	14.49	52.6	2.74
AZ300-36	688.2	40.86	383.8	4.06	516.5	7.97	206.8	2.05
AZ300-37	610.5	33.07	854.8	8.37	921.6	9.8	408.3	5.14
AZ300-38	0.1	0	412.5	6.48	337.4	14.45	113.8	4.42
AZ300-39	234.3	58.12	1260	14.57	1059.4	16.6	324.6	6.69
AZ300-40	0.1	0	900.7	9.05	708.4	9.79	266	7.14
AZ300-41	2278.7	47.69	167.3	2.39	512.8	10.8	132.6	2.76
AZ300-42	744.4	49.61	935.8	10.39	1021.3	15.44	484.4	8.41
AZ300-43	1239.8	34.16	1327.7	13.53	1466.6	14.09	609.3	8.88
AZ325-1	1649.7	17.52	859.9	8.36	1228	7.87	193.8	2.13
AZ325-2	1692.6	20.72	1444.7	13.85	1681.1	10.33	918.6	12.58
AZ325-3	612.2	32.82	1406.1	14.42	1181.4	10.53	393.8	11.62
AZ325-4	3340.1	11.1	1791.5	16.52	2697.9	6.73	1940.4	9.09
AZ325-5	734	43.25	448.3	5.01	566.1	9.11	351.9	6.62
AZ325-6	0.1	0	625.4	7.61	463.7	10.34	167.5	4.08
AZ325-7	1104.2	50.1	1857.4	24.79	1597.4	20.13	450.2	11.9
AZ325-8	0.1	0	365.7	3.73	233.2	3.2	88.8	1.49
AZ325-9	1628.5	23.82	1639.3	15.93	1770.3	11.72	799.5	15.88
AZ325-10	0.1	0	15.4	0.23	10.4	0.5	5.3	0.5
AZ325-11	871	125.6	290.1	5.8	365.9	18.95	482.3	40.36
AZ325-12	1849.6	29.19	1833.2	21.18	1844.3	14.92	1699.4	31.77
AZ325-13	829.4	69.62	501.7	7.25	566.9	14.78	537.8	14.48
AZ325-14	581.7	52.86	493.4	6.42	511	10.14	467.8	10.44
AZ325-15	783.7	52.1	528.3	6.85	581.3	11.28	551.2	14.89
AZ325-16	2404.8	21.78	1205	13.76	1716.6	11.81	1825.8	26.01
AZ325-17	1030.4	45.17	421.3	5.49	531.7	9.61	1022.1	21.9
AZ325-18	2942.4	17.58	2969	29.36	2958.1	12.25	2749.9	33.42
AZ325-19	2374	21.72	1882	20.87	2131.1	12.94	1359.8	22.4
AZ325-20	1866.8	29.4	1509.7	17.82	1668.3	14.44	2726.8	92.95
AZ325-21	1431.3	30.66	1595.5	16.48	1653.4	13.68	1314.2	23.97
AZ325-22	104.3	65.1	417.1	4.97	424.7	9.69	482.5	10.02
AZ325-23	454.6	49.4	696.1	7.82	720.3	11.72	567.3	12.15
AZ325-24	408.8	104.28	691.1	11.06	705.8	24.1	632.6	37.53
AZ325-25	2401.5	49.97	2305.2	36.55	2502.8	27.86	2123.7	90.45
AZ325-26	1485.3	27.75	1504.7	15.22	1622.9	12.41	1478.5	38.6
AZ325-27	401.3	175.81	486	11.52	534.2	33.59	402.1	22
AZ325-28	1442.4	29.59	1441.8	14.86	1566.3	12.94	1388.2	33.39
AZ325-29	1491.9	46.53	240.5	3.06	459.4	9.01	202.8	8.96
AZ325-30	596.6	76.9	763.5	10.5	807.4	19.95	819.9	22.16
AZ325-31	1441.3	23.54	1566.3	15.15	1640.7	10.83	1385.8	16.35
AZ325-32	1640.4	62.46	1277.6	19.58	1543.4	26.72	1597.7	82.6

APPENDIX B

FIGURES

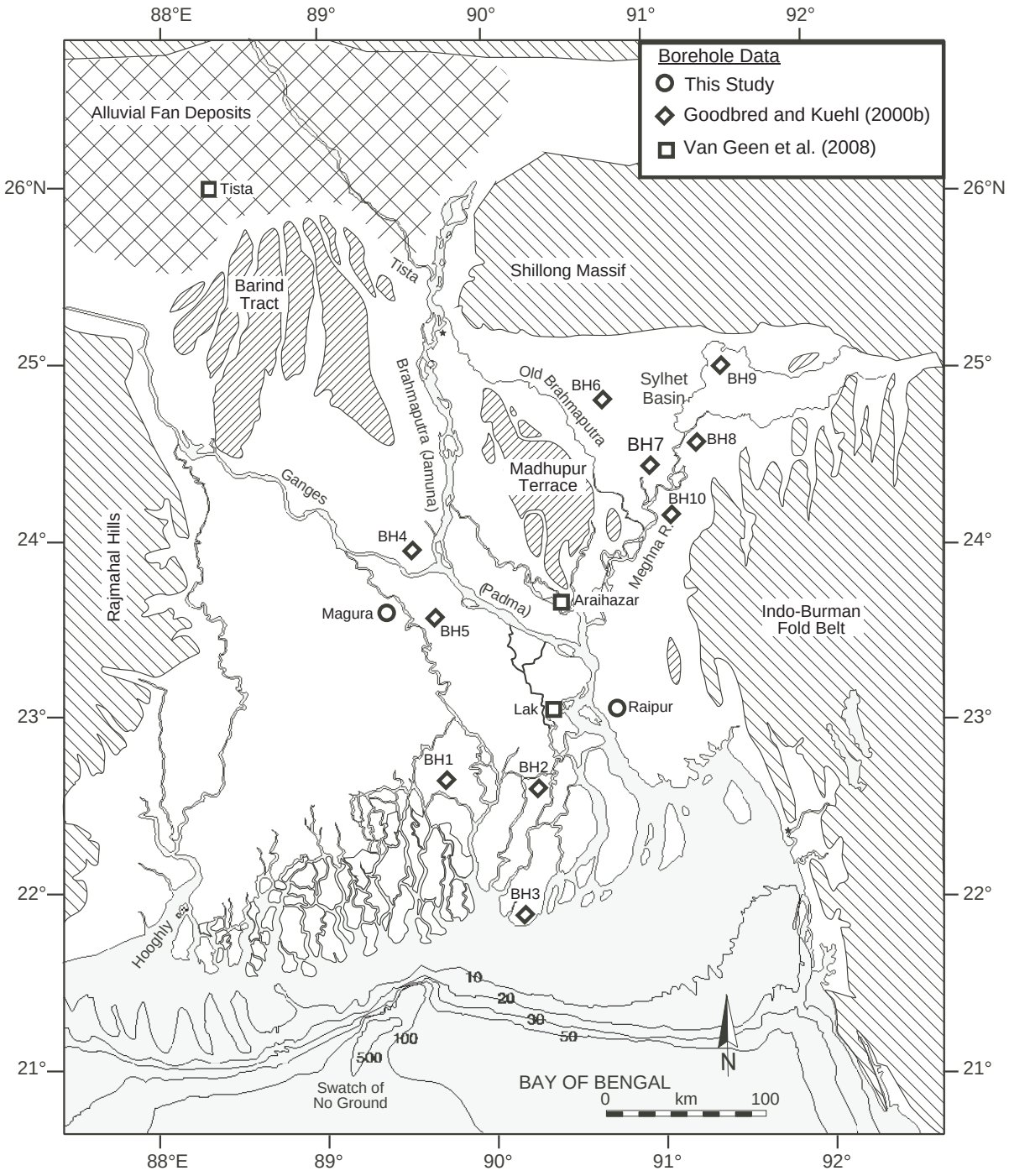

Figure B.1: Borehole locations from this study, Goodbred and Kuehl, 2000b, and Van Geen et al., 2008.

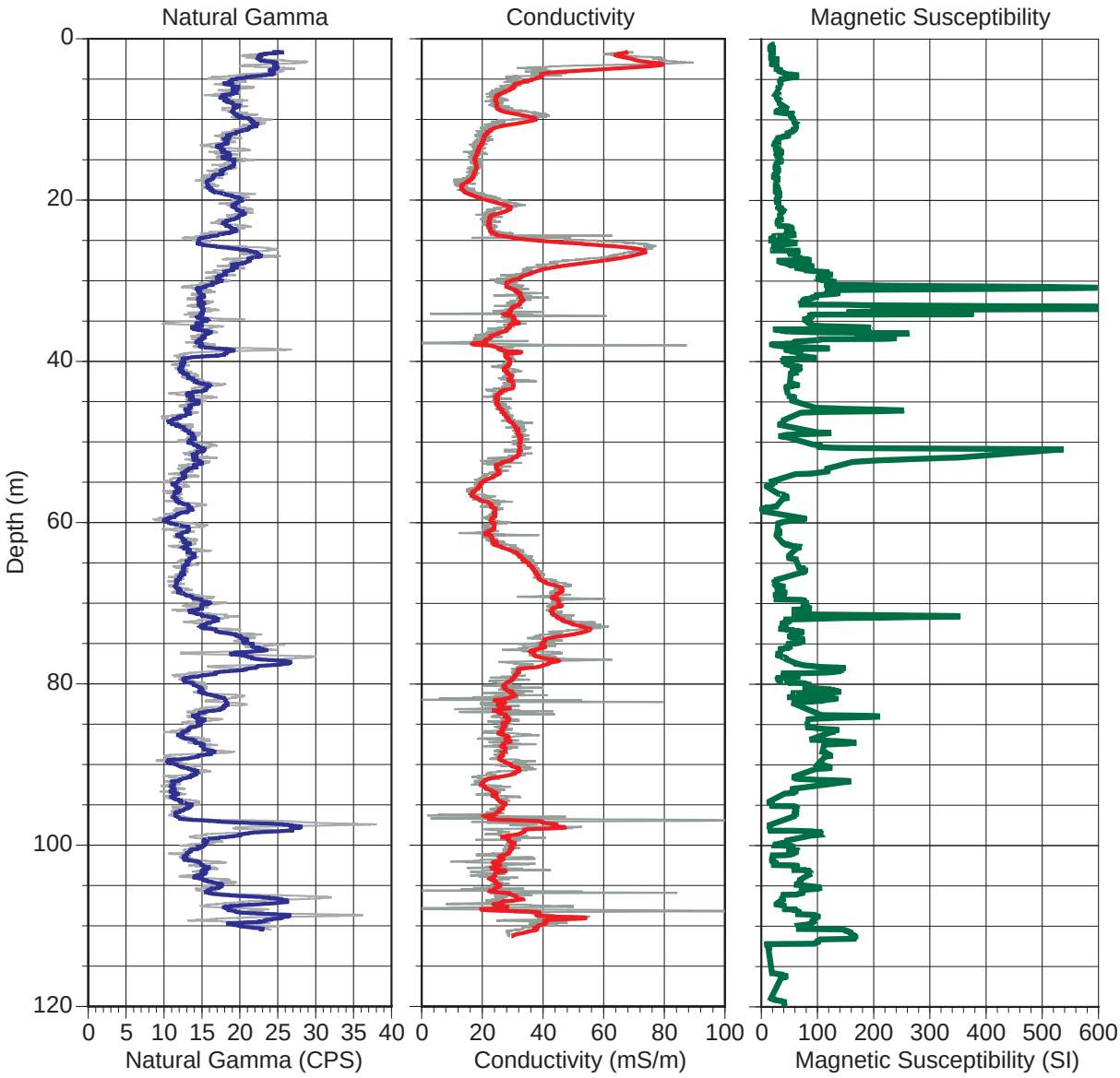

Figure B.2: Natural gamma, conductivity, and magnetic susceptibility down-core plots for Magura.

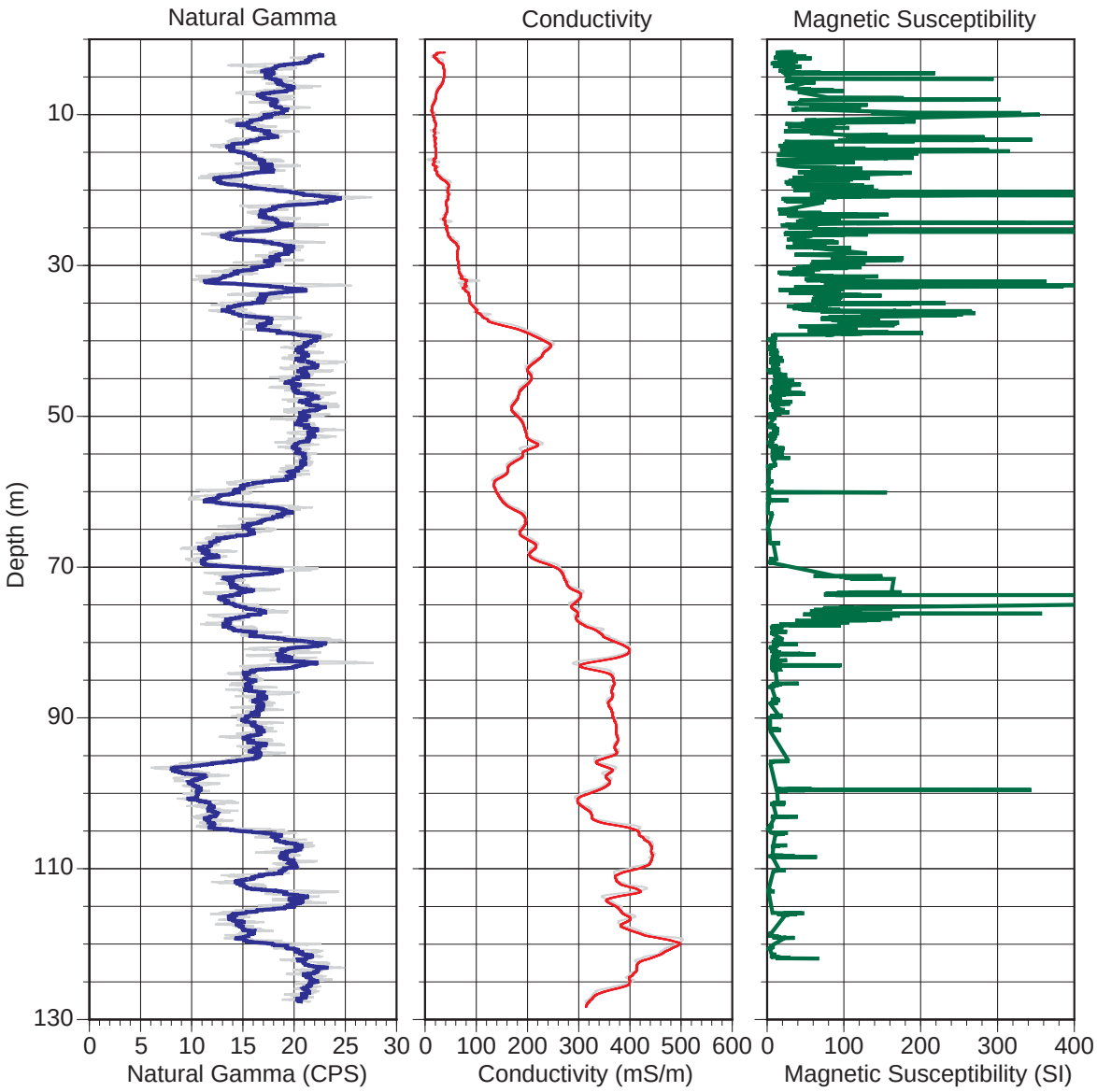

Figure B.3: Natural gamma, conductivity, and magnetic susceptibility down-core plots for Raipur.

REFERENCES CITED

Allison, M. A., Khan, S. R., Goodbred, S. L., and Kuehl, S. A. (2003). Stratigraphic evolution of the late Holocene Ganges-Brahmaputra lower delta plain. *Sedimentary Geology*, 155:317–342.

Amidon, W. H., Burbank, D. W., and Gehrels, G. E. (2005). UPb zircon ages as a sediment mixing tracer in the Nepal Himalaya. *Earth and Planetary Science Letters*, 235:244–260.

Bard, E., Hamelin, B., Arnold, M., Montaggioni, L., Cabioch, G., Faure, G., and Rougerie, F. (1996). Deglacial sea-level record from Tahiti corals and the timing of global meltwater discharge. *Nature*, 382:241–244.

Bickle, M. J., Bunbury, J., Chapman, H. J., Harris, N. B. W., Fairchild, I. J., and Ahmad, T. (2003). Fluxes of Sr into the headwaters of the Ganges. *Geochimica et Cosmochimica Acta*, 67:2567–2584.

Bickle, M. J., Chapman, H. J., Bunbury, J., Harris, N. B. W., Fairchild, I. J., Ahmad, T., and Pomies, C. (2005). Relative contributions of silicate and carbonate rocks to riverine Sr fluxes in the headwaters of the Ganges. *Geochimica et Cosmochimica Acta*, 69:2221–2240.

Bickle, M. J., Harris, N. B. W., Bunbury, J., Chapman, H. J., Fairchild, I. J., and Ahmad, T. (2001). Controls on the $^{87}Sr/^{86}Sr$ of carbonates in the Garwal Himalaya, headwaters of the Ganges. *Journal of Geology*, 109:737–753.

Bloemendal, J., Tauxe, L., and Valet, J. P. (1988). High-resolution, whole-core magnetic susceptibility logs from Leg 108. *Proceedings of Ocean Drilling Program Initial Report, Part A*, pages 1005–1013.

Burke, W. H., Denison, R. E., Hetherington, E. A., Keopnick, R. B., Nelson, H. F., and Otto, J. B. (1982). Variation of seawater $^{87}Sr/^{86}Sr$ throughout Phanerozoic time. *Geology*, 10:516–519.

Campbell, I. H., Reiners, P. W., Allen, C. M., Nicolescu, S., and Upadhyay, R. (2005). HePb double dating of detrital zircons from the Ganges and Indus Rivers: Implication for quantifying sediment recycling and provenance studies. *Earth and Planetary Science Letters*, 237:402–432.

Chauhan, O. S., Borole, D. V., Gujar, A. R., Mascarenhas, A., Mislanker, P. G., and Rao, C. M. (1993). Evidences of climatic variations during late Pleistocene-Holocene in the eastern Bay of Bengal. *Current Science*, 65:558–562.

Clift, P. D., Giosan, L., Blusztajn, J., Campbell, I. H., Allen, C., Pringle, M., Tabrez, A. R., Danish, M., Rabbani, M. M., Alizai, A., Carter, A., and Luckge, A. (2008).

Holocene erosion of the Lesser Himalaya triggered by intensified summer monsoon. *Geology*, pages 79–82.

COHMAP (1988). Climatic changes of the last 18,000 years: observations and model simulations. *Science*, 241:1043–1052.

Colin, C., Turpin, L., Bertaux, J., Desprairies, A., and Kissel, C. (1999). Erosional history of the Himalayan and Burman ranges during the last two glacial-interglacial cycles. *Earth and Planetary Science Letters*, 171:647–660.

Cullen, J. L. (1981). Microfossil evidence for changing salinity patterns in the Bay of Bengal over the last 20,000 years. *Palaeoceanography, Palaeoclimatology, Palaeoecology*, 35:315–356.

Dalai, T. K., Krishnaswami, S., and Kumar, A. (2003). Sr and $^{87}Sr/^{86}Sr$ in the Yamuna River System in the Himalaya: Sources, fluxes, and controls on Sr isotope composition. *Geochimica et Cosmochimica Acta*, 67:2931–2948.

DeCelles, P. G., Gehrels, G. E., Quade, J., and Spurlin, L. M. (2000). Tectonic implications of U-Pb zircon ages of the Himalayan orogenic belt in Nepal. *Science*, 288:497–499.

Derry, L. A. and France-Lanord, C. (1997). Himalayan weathering and erosion fluxes: Climate and tectonic controls. *Global Tectonics and Climate Change*, pages 289–312.

Dill, H. G. (2003). Infilling of the younger Kathmandu-Banepa intermontane lake basin during the Late Quaternary (Lesser Himalaya, Nepal): a sedimentological study. *Journal of Quaternary Science*, 18:41–60.

Edwards, R. L., Beck, J. W., Burr, G. S., Donahue, D. J., Chappell, J. M. A., Bloom, A. L., Druffel, E. R. M., and Taylor, F. W. (1993). A large drop in atmospheric $^{14}C/^{12}C$ and reduced melting in the Younger Dryas, documented with ^{230}Th ages of corals. *Science*, 260:962–968.

Fairbanks, R. (1989). A 17,000-year glacio-eustatic sea level record: influence of glacial melting rates on the Younger Dryas event and deep-ocean circulation. *Nature*, 342:637–642.

Fang, X., Ono, Y., Fulusawa, H., Bao-Tian, P., Li, J., Dong-Hong, G., Oi, K., Tsukamoto, S., Torii, M., and Mishima, T. (1999). Asian summer monsoon instability during the past 60,000 years: magnetic susceptibility and pedogenic evidence from the western Chinese loess plateau. *Earth and Planetary Science Letters*, 168:219–232.

Fergusson, J. (1863). On recent changes in the delta of the Ganges: Geological Society of London. *Quaternary Journal*, 19:321–354.

Galy, A. and France-Lanord, C. (1999). The strontium isotope budget of Himalayan rivers in Nepal and Bangladesh. *Geochimica et Cosmochimica Acta*, 63:1905–1925.

Galy, A. and France-Lanord, C. (2001). Higher erosion rates in the Himalaya: geochemical constraints on riverine fluxes. *Geology*, 29:23–26.

Gasse, F., Arnold, M., Fontes, J. C., Fort, M., Gilbert, E., Huc, A., Bingyan, L., Yuanfang, L., Qing, L., Melieres, F., Van Campo, E., Fubao, W., and Quingsong, Z. (1991). A 13,000 year climate record from western Tibet. *Nature*, 353:742–745.

Gehrels, G. E., Yin, A., and Wang, X. (2003). Detrital-zircon geochronology of the northeastern Tibetan plateau. *GSA Bulletin*, 115:881–896.

Goodbred, S. L. (2003). Response of the ganges dispersal system to climate change: a source-to-sink view since the last interstade. *Sedimentary Geology*, 162:83–104.

Goodbred, S. L. and Kuehl, S. A. (1999). Holocene and modern sediment budgets for the Ganges-Brahmaputra river system: Evidence for highstand dispersal to floodplain, shelf, and deep-sea depocenters. *Geology*, 27:559–562.

Goodbred, S. L. and Kuehl, S. A. (2000a). Enormous Ganges-Brahmaputra sediment discharge during strengthened early Holocene monsoon. *Geology*, 28:1083–1086.

Goodbred, S. L. and Kuehl, S. A. (2000b). The significance of large sediment supply, active tectonism, and eustasy on margin sequence development: Late Quaternary stratigraphy and evolution of the Ganges-Brahmaputra delta. *Sedimentary Geology*, 133:227–248.

Goodbred, S. L., Kuehl, S. A., Steckler, M. S., and Sarker, M. H. (2003). Controls on facies distribution and stratigraphic preservation in the Ganges-Brahmaputra delta sequence. *Sedimentary Geology*, 155:301–316.

Heroy, D. C., Kuehl, S. A., and Goodbred, S. L. (2003). Mineralogy of the ganges and brahmaputra rivers: implications for river switching and late quaternary climate change. *Sedimentary Geology*, 155:343–359.

Jones, R. L. and Beavers, A. H. (1964). Magnetic susceptibility as an aid in characterization and differentiation of loess. *Journal of Sedimentary Petrology*, 34:881–883.

Krishnaswami, S., Trivedi, J. R., Sarin, M. M., Ramesh, R., and Sharma, K. K. (1992). Strontium isotopes and rubidium in the Ganga-Brahmaputra river system: Weathering in the Himalaya, fluxes to the Bay of Bengal and contributions to the evolution of oceanic $^{87}Sr/^{86}Sr$. *Earth and Planetary Science Letters*, 109:11–26.

Kuehl, S. A., Allison, M. A., Goodbred, S. L., and Kudrass, H. (2005). River Deltas - Concepts, Models, and Examples: The Ganges-Brahmaputra Delta. *SEPM Special Publication*, 83:413–434.

Kuehl, S. A., Hariu, T. M., and Moore, W. S. (1989). Shelf sedimentation off the Ganges-Brahmaputra river system. *Marine Geology*, 144:81–96.

Milliman, J. D. and Syvitski, S. P. M. (1992). Geomorphic/tectonic control of sediment discharge to the ocean, the importance of small mountainous rivers. *Geology*, 100:525–544.

Montgomery, D. R., Hallet, B., Yuping, L., Finnegan, N., Anders, A., Gillespie, A., and Greenberg, H. M. (2004). Evidence for Holocene megafloods down the Tsangpo river gorge, southeastern Tibet. *Quaternary Research*, 62:201–207.

Najman, Y. (2006). The detrital record of orogenesis: A review of approaches and techniques used in the Himalayan sedimentary basins. *Earth Science Reviews*, 74:1–72.

Oldfield, F. (1991). Environmental magnetism - A personal perspective. *Quaternary Science Reviews*, 10:73–85.

Palmer, M. R. and Edmond, J. M. (1989). The strontium isotope budget of the modern ocean. *Earth and Planetary Science Letters*, 92:11–26.

Palmer, M. R. and Edmond, J. M. (1992). Controls over the strontium isotope composition of river water. *Geochimica et Cosmochimica Acta*, 56:2099–2011.

Prell, W. L. and Kutzbach, J. E. (1987). Monsoon variability over the past 150,000 years. *Journal of Geophysical Research*, 92:8411–8425.

Prins, M. A. and Postma, G. (2000). Effects of climate, sea level, and tectonics unraveled for last deglaciation turbidite records of the Arabian Sea. *Geology*, 28:375–378.

Richter, F. M., Rowley, D. B., and Depaolo, D. J. (1992). Sr isotope evolution of seawater: The role of tectonics. *Earth and Planetary Science Letters*, 109:11–23.

Sangode, S. J., Sinha, R., Phartiyal, B., Chauhan, O. S., Mazari, R. K., Bagati, T. N., Suresh, N., Mishra, S., Kumar, R., and Bhattacharjee, P. (2007). Environmental magnetic studies on some Quaternary sediments of varied depositional settings on the Indian sub-continent. *Quaternary International*, 159:102–118.

Singh, I. B. (1996). Geological evolution of Ganga Plain - an overview. *Journal of Palaeontological Society of India*, 41:99–137.

Singh, I. B. (2001). Late Quaternary evolution of Ganga Plain and proxy records of climate change, neotectonics, and anthropogenic activity. *Pragdhara, Journal of the U.P. State Archaeological Department (India)*, 12:1–25.

Singh, S. K. and France-Lanord, C. (2002). Tracing the distribution of erosion in the Brahmaputra watershed from isotopic compositions of stream sediments. *Earth and Planetary Science Letters*, 202:645–662.

Singh, S. K., Kumar, A., and France-Lanord, C. (2006). Sr and $^{87}Sr/^{86}Sr$ in waters and sediments of the Brahmaputra river system: Silicate weathering, CO_2 consumption and Sr flux. *Chemical Geology*, 234:308–320.

Singh, S. K., Trivedi, J. R., Pande, K., Ramesh, R., and Krishnaswami, S. (1998). Chemical and Sr, O, C, isotopic compostions of carbonates from the Lesser Himalaya: implications to the Sr isotope composition of the source waters of the Ganga, Ghaghara and the Indus Rivers. *Geochimica et Cosmochimica Acta*, 62:743–755.

Sirocko, F., Sarnthein, M., and Erlenkeuser, H. (1993). Century-scale events in monsoonal climate over the past 24,000 years. *Nature*, 364:322–324.

Stuiver, M. and Polach, H. A. (1977). Discussion: Reporting of ^{14}C data. *Radiocarbon*, 3:353–363.

Sundriyal, Y. P., Tripathi, J. K., Sati, S. P., Rawat, G. S., and Srivastava, P. (2007). Landslide-dammed lakes in the Alaknanda Basin, Lesser Himalaya: Causes and implications. *Current Science*, 93:568–574.

Swain, A. M., Kutzbach, J. E., and Hastenrath, S. (1983). Estimates of Holocene precipitation for Rajasthan, India, based on pollen and lake-level data. *Quaternary Research*, 19:1–17.

Tripathi, J. K., Ghazanfari, P., Rajamani, V., and Tandon, S. K. (2007). Geochemistry of sediments of the Ganges alluvial plains: Evidence of large-scale sediment recycling. *Quaternary International*, 159:119–130.

Turekian, K. K. and Kulp, J. L. (1956). The geochemistry of strontium. *Geochimica et Cosmochimica Acta*, 10:245–296.

van Achterbergh, E., Ryan, C. G., Jackson, S. E., and Griffin, W. L. (1996). Data reduction software for LA-ICPMS: Appendix in: Sylvester, P.J., Editor, 2000. Laser ablation-ICP-mass spectrometry in the earth sciences: Principles and applications: Mineralogical Association of Canada Short Course, Ottawa. 29:241–244.

Van Campo, E. (1986). Monsoon fluctuations in two 20,000-yr B.P. oxygen-isotope/pollen records off southwest India. *Quaternary Research*, 26:376–388.

Van Geen, A., Zheng, Y., Goodbred Jr., S., Horneman, A., Aziz, Z., Cheng, Z., Stute, M., Mailloux, B., Weinman, B., Hoque, M. A., Seddique, A. A., Hossain, M. S., Chowdury, S. H., and Ahmed, K. M. (2008). Flushing history as a hydrogeological control on the regional distribution of arsenic in shallow groundwater of the Bengal Basin. *Environmental Science and Technology*, 42:2283–2288.

Verosub, K. L. and Roberts, A. P. (1995). Environmental magnetism, Past, present, and future. *Journal of Geophysical Research*, 100:2175–2192.

Weber, M. E., Niessen, F., Kuhn, G., and Wiedicke, M. (1997a). Calibration and application of marine sedimentary physical properties using a multi-sensor core logger. *Marine Geology*, 136:151–172.

Weber, M. E., Wiedicke, M. H., Kudrass, H. R., Hubscher, C., and Erlenkeuser, H. (1997b). Active growth of the Bengal fan during sea-level rise and highstand. *Geology*, 25:315–318.